PROBING WEAK COPPER CHAPERONE-WILSON DISEASE PROTEIN INTERACTIONS AT THE SINGLE-MOLECULE LEVEL WITH NANOVESICLE TRAPPING

by Jaime Benitez

PROBING WEAK COPPER CHAPERONE-WILSON DISEASE PROTEIN INTERACTIONS AT THE SINGLE-MOLECULE LEVEL WITH NANOVESICLE TRAPPING

A Dissertation

Presented to the Faculty of the Graduate School

of Cornell University

In Partial Fulfillment of the Requirements for the Degree of

Doctor of Philosophy

by

Jaime Benitez

August 2010

PROBING WEAK COPPER CHAPERONE-WILSON DISEASE PROTEIN INTERACTIONS AT THE SINGLE-MOLECULE LEVEL WITH NANOVESICLE TRAPPING

Jaime Benitez, Ph.D.

Cornell University 2010

Copper is an essential cofactor for many metalloproteins, yet it can also be cytotoxic, therefore, intracellular copper trafficking is tightly regulated. Copper delivery inside cells is mediated by copper chaperones, which bind and deliver copper to their target proteins, preventing adventitious chemical reactions with the metal. Various pathways for copper transport exist; of particular interest to this thesis is the pathway between the copper chaperone Hah1 and Wilson disease protein (WDP).

Limited dynamic information is available on how the copper chaperone Hah1 and the metal binding domains (MBDs) of WDP interact for copper transfer. In this thesis, the interaction dynamics of Hah1 and a single MBD of WDP is investigated. Since these protein-protein interactions are relatively weak in nature, a nanovesicle trapping strategy is used to increase the effective concentration of single molecules (Chapter 2). Individual interaction events are then monitored by single-molecule Förster resonance energy transfer (smFRET).

The interaction dynamics of Hah1 and the fourth MBD (MBD4) of WDP are initially studied in the absence of copper. The protein-protein interaction scheme and associated rate constants for the interaction process are extracted from the FRET efficiency (E_{FRET}) and waiting-time distributions (Chapter 3). The E_{FRET} distributions obtained from interactions in the absence and presence of copper are then used to gain insight on the underlying copper transfer process (Chapter 4).

BIOGRAPHICAL SKETCH

Jaime J. Benítez was born in San Juan, Puerto Rico in 1980. He obtained a Bachelor of Science from the University of Puerto Rico in 2004, majoring in chemistry. As an undergraduate he acquired research experience in biochemistry, electrophysiology, and natural products chemistry. His first research project was at the University of Puerto Rico under the supervision of Prof. Fernando Gonzalez. Research with Prof. Gonzalez focused on the fluorometric measurement of intracellular calcium. His second research project was at Cornell University under the supervision of Prof. George Hess. This research project involved measurement of single cell currents elicited by the dopamine transporter and its inhibition by cocaine. His final undergraduate project and the theme of his undergraduate thesis was at the University of Puerto Rico with Prof. Abimael Rodriguez. This research focused on the purification and characterization of secondary metabolites from the sea plume *Pseudopterogorgia kallos*. During this time he discovered two new minor cembranolides and fully characterized them by various spectroscopic methods. This study earned him a publication in the Journal of Natural Products in 2008.

In 2004, Jaime J. Benítez was admitted to Cornell University to pursue his Ph.D. in Chemistry. Since 2005 he has been doing research with Dr. Peng Chen. Jaime was the first student of the group and led along with Dr. Chen in the initial stages of research. He has contributed to all the bioinorganic research on-going in the laboratory. Jaime has also trained many of the undergraduate and graduate students as well as postdoctoral researchers working on the bioinorganic side of the laboratory. By 2010 he produced this thesis in partial fulfillment to the degree of Doctor in Philosophy in Chemistry and Chemical Biology.

Dedicated to the memory of Victor Melendez (1980-2004)

ACKNOWLEDGMENTS

First off, I thank my mother for her struggle to provide me with the best education that we could not afford, early on in my life. Were it not for her, this thesis would have never been written.

I thank my wife Madeline Martinez for always being there for me when I needed her and putting up with me throughout these past 5 years. My sister Lara Calo also deserves acknowledgement for her support. She is the only family member I have in close proximity.

I would also like to thank my lab mates Derek Klarin, Aaron Keller, Jason Kong and Susanta Sarkar for sharing part of these years in the Chen Lab. They are both colleagues and friends.

Cynthia Kinsland has helped me from the very beginning of the group when I was the first and only member. She trained me in molecular biology and protein chemistry and has always been there to answer any questions. For this I am grateful to her.

I thank my advisor Peng Chen for providing the opportunity to do my doctoral research in his lab and showing a side of research I was not aware of. Thanks are also due to my committee members Barbara Baird and Brian Crane for overseeing my research.

Finally, I would like to thank Kru Kevin Seaman and the Muay Thai Club for providing a space to unleash some violence without having to be arrested for it.

TABLE OF CONTENTS

LIST OF FIGURES

LIST OF TABLES

LIST OF ABBREVIATIONS

Proteins

CCS	Copper chaperone for superoxide dismutase
SOD1	Cu, Zn superoxide dismutase
MNK	Menkes disease protein
WDP	Wilson disease protein
MBD	Metal binding domain
BSA	Bovine serum albumin

Chemicals

Egg PC	~99% of which is L-α-phosphatidylcholine
Biotinyl-cap PE	1,2-Dipalmitoyl-*sn*-Glycero-3-Phosphoethanolamine-N-(Cap Biotinyl)
DPPC	1,2-dipalmitoyl-*sn*-glycero-3-phosphocholine
DMPC	1,2-dimyristoyl-*sn*-glycero-3-phosphocholine
PEG	Polyethylene glycol
IPTG	Isopropyl-beta-D-thiogalactopyranoside
BCA	Bicinchoninic acid
TCEP	Tris(2-carboxyethyl)phosphine
DMSO	Dimethyl sulfoxide
EDTA	Ethylenediaminetetraacetic acid
MES	2-(N-morpholino)ethanesulfonic acid

Techniques

NMR	Nuclear magnetic resonance
SPR	Surface plasmon resonance
FRET	Förster (or Fluorescence) resonance energy transfer
smFRET	Single-molecule Förster resonance energy transfer
FPLC	Fast protein liquid chromatography
SDS-PAGE	Sodium dodecyl sulfate polyacrylamide gel electrophoresis
PCR	Polymerase chain reaction
MS	Mass spectrometry
LC-MS	Liquid chromatography, mass spectrometry
ESI-MS	Electrospray ionization mass spectrometry

MALDI-MS	Matrix assisted laser desorption/ionization mass spectrometry

CHAPTER 1

Introduction

Transition metals, such as copper and iron, are essential as cofactors to a variety of proteins and enzymes.[1] Under physiological conditions, copper can adopt two oxidation states (Cu(I) or Cu(II)), which makes it useful as a catalytic cofactor to many metalloproteins that carry out redox reactions. Despite its usefulness as a catalytic cofactor, copper can also be very toxic to cells. Although the molecular mechanisms that cause this toxicity are not entirely clear, it is well known that copper can catalyze Fenton radical chemistry producing reactive oxygen species (Scheme 1.1):

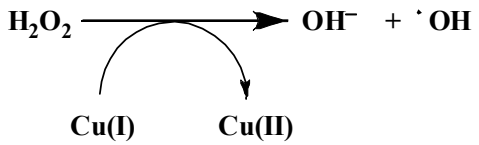

Scheme 1.1. Fenton reaction.

These reactive oxygen species, such as hydroxyl radicals, can cause oxidative damage to lipids, proteins and DNA, as well as many other biomolecules.[2] Therefore, the concentration, availability, and trafficking of copper within cells must be tightly regulated.

Cells have evolved different mechanisms for safe trafficking of copper ions and regulation of copper concentrations.[3,4] A multitude of copper-binding molecules such as glutathione, metallothionein and metallochaperones exist to bind and protect copper from otherwise biologically harmful reactions. Copper chaperones function as a shuttle system for copper. They bind copper with high affinity, thus protecting against adventitious reactions, as well as deliver copper to specific target proteins, thereby ensuring safe metal trafficking. These target proteins, in turn, transport copper to copper-dependent enzymes or mediate copper efflux from the cell.

1.1. Cellular copper trafficking

Copper is imported into eukaryotic cells as Cu(I) by members of the Ctr family of copper transporters (Figure 1.1).[5] Once inside the cytosol, soluble Cu(I)-binding proteins called copper chaperones deliver copper to target proteins via direct protein-protein interactions.[6] It is not clear how the chaperones obtain copper, but it may be through a direct interaction with the Ctr transporters.[7]

The copper chaperone for superoxide dismutase (CCS)[8] delivers copper to the antioxidant enzyme Cu,Zn superoxide dismutase (SOD1) (Figure 1.1).[9] Metallation of SOD1 occurs primarily in the cytosol, but a small amount of SOD1 is also localized to the mitochondrial intermembrane space if CCS is also present there.[10] SOD1 catalyzes the disproportionation of superoxide anion to oxygen and hydrogen peroxide.[11]

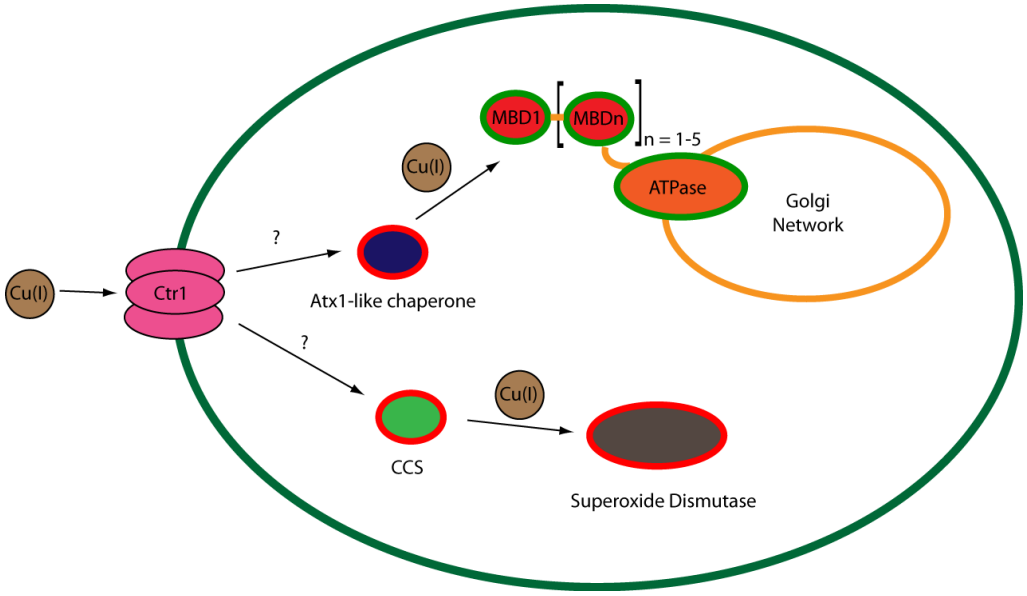

Figure 1.1. Two Intracellular copper transport pathways in eukaryotic cells. The number of MBDs in the ATPases can vary from n = 1 in yeast to n = 5 in humans.

The Atx1-like chaperones transfer Cu(I) to membrane-bound, copper transporting P_{1B}-type ATPases. In yeast, Atx1 delivers Cu(I) to Ccc2 in the *trans*-Golgi network.[12] Ccc2 then translocates copper into secretory vesicles, where it is

loaded into the enzyme Fet3.[13] The human homologue of Atx1, known as Hah1 or Atox1,[14] delivers copper to the Menkes and Wilson disease ATPases (ATP7A and ATP7B, respectively) for ultimate incorporation into copper dependent enzymes such as ceruloplasmin or for copper efflux. Fet3 and ceruloplasmin are multicopper oxidases that play a role in iron metabolism by catalyzing the oxidation of Fe(II) to Fe(III) at the plasma membrane.[15] Ccc2 and the Menkes/Wilson disease proteins all belong to the P-type ATPase superfamily of integral membrane proteins that couple the energy of ATP hydrolysis to cation translocation across membranes.[16,17] The Cu(I) transporting P_{1B}-type ATPases consist of eight transmembrane helices, a cytoplasmic ATP binding (ATPBD: composed of N and P domains) and actuator domains (A domain), and multiple N-terminal soluble metal binding domains (MBDs) (Figure 1.2).[18] The number of MBDs vary, ranging from two in Ccc2 to six in the Menkes/Wilson disease proteins.[19,20]

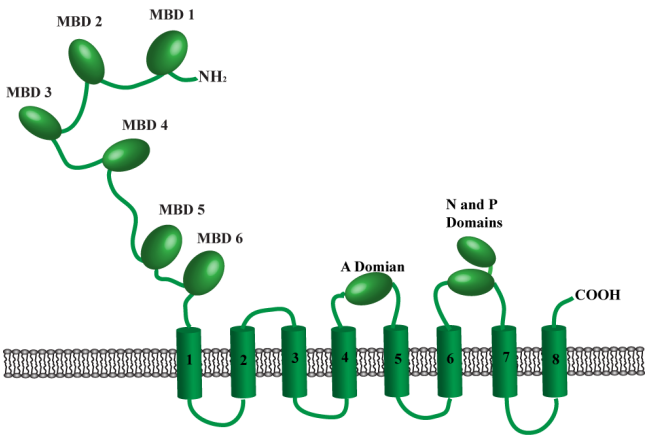

Figure 1.2. Overall structural model for ATP7A and ATP7B P_{1B}-type ATPases. Transmembrane segments are numbered, remaining domains are indicated.

1.2. The Cu(I) ATPase ATP7B and the Hah1 copper chaperone

Mutations on ATP7A or ATP7B can lead to Menkes and Wilson diseases, respectively.[21-23] Both are diseases of copper metabolism associated with copper

absorption and efflux. The main focus of this thesis is on the human copper transport pathway from the intracellular copper chaperone Hah1 to the copper transporting ATPase, ATP7B, the Wilson disease protein (WDP) (Figure 1.3).

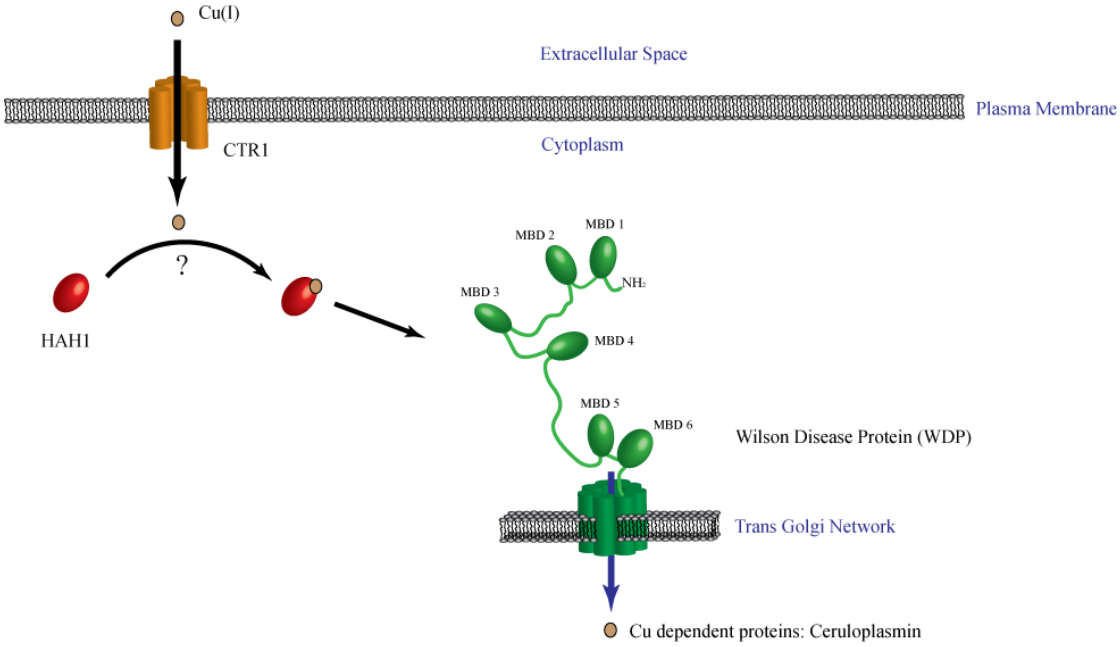

Figure 1.3. Copper transport pathway from the Hah1 copper chaperone to Wilson disease protein.

Hah1 is a soluble, single domain, cytoplasmic protein, belonging to the Atx1-like copper chaperone family.[6, 24-29] WDP is a multidomain protein that is anchored on the *trans*-Golgi membrane and has a soluble N-terminal region consisting of six homologous metal-binding domains (MBDs).[21, 22, 30] WDP mediates the translocation of copper to copper dependent enzymes as well as copper efflux from the cell. Two characteristic features for both the Hah1 chaperone and the WDP MBDs [6, 24-29, 31-34] are a conserved, surface-exposed, MXCXXC motif, where the two cysteines bind copper, and a βαββαβ ferredoxin-like protein fold (Figure 1.4). The similarity in protein fold between the chaperone and WDP MBDs renders their specific interactions

through complementary surface residues.[32, 34, 35] Copper is transferred as Cu(I) from Hah1 to the MBDs of WDP by means of direct and specific protein-protein interactions.[12, 24, 25, 32, 34, 35]

Past studies have shown that the six MBDs of WDP have different functional roles:[32, 36-42] MBDs 1 to 4 are important for interaction with Hah1 to acquire copper and MBDs 5 and 6 are critical for copper translocation through the membrane. Interestingly, NMR studies performed with a full six domain construct of the N-terminal MBDs show that Hah1 can transfer copper to all MBDs, yet only domains 1, 2 and 4 can form detectable adducts with Hah1, and only in the presence of Cu(I).[43]

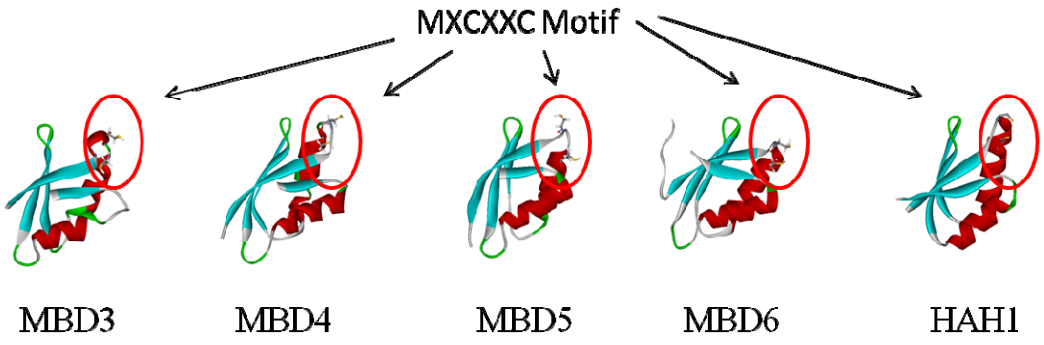

Figure 1.4. Solved WDP MBD structures and Hah1.

1.2.1. Hah1 and MBD structural data

Much structural information has been obtained from NMR and x-ray crystallography studies on the Atx1-like chaperones and the MBDs of their target proteins. The Hah1 structure has been solved in the presence of copper, mercury and cadmium, as well as in its apo form.[44] The structures solved by crystallography are homodimeric, with the metal sandwiched between two protein units. The metal coordination varies between 3 and 4 coordinate depending on the metal.[44] The homodimeric structures have served as a model for interaction with the MBDs for

many years. A recent heterodimeric structure between the first MBD of Menkes disease protein (MNK1) and Hah1 shows this same mode of interaction in which both proteins face each other on their metal binding motif (Figure 1.5).[45]

The structures for the individual MBDs of MNK have also been fully solved by NMR in the presence of Cu(I) or Ag(I) and in the absence of metal. All the domains bind copper in a 2 coordinate fashion. MBDs 1 and 2 of WDP have not been fully solved as of yet, but domains 3 through 6 have. In the WDP case only the apo structures have been solved (Table 1.1). A comprehensive review is available of all solved structures for the atx1-like chaperones and their respective ATPase target MBDs up to the year 2009.[46]

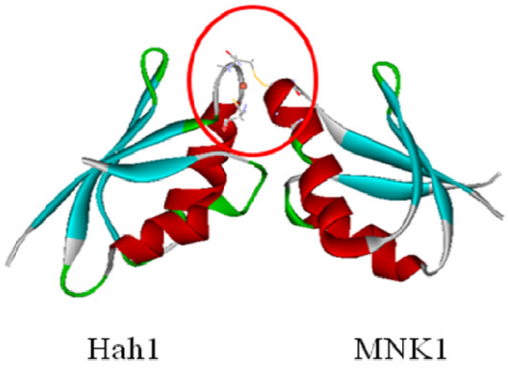

Figure 1.5. Heterodimer structure of Hah1 and the first metal binding domain of Menkes disease protein (MNK1). The red circle indicates the two metal binding motifs facing each other with copper sandwiched in between.

Table 1.1. Known WDP/MNK MBD and Hah1 structures.

Structure	Type	PDB ID	Reference
Hg(II)-Hah1	X-ray	1FE4	[34]
Cd(II)- Hah1	X-ray	1FE0	[34]
Cu(I)- Hah1	X-ray	1FEE	[34]
Cu(I)- Hah1	NMR	1TL4	[47]
Apo- Hah1	NMR	1TL5	[47]
Apo-MNK4	NMR	1AW0	[48]
Ag(I)-MNK4	NMR	2AW0	[48]
Apo-MNK2	NMR	1Q8L	[49]
Apo-MNK2	NMR	1S6O	[50]
Cu(I)-MNK2	NMR	1S6U	[50]
Apo-MNK1	NMR	1KVI	[51]
Cu(I)-MNK1	NMR	1KVJ	[51]
Apo-MNK3	NMR	2G9O	[52]
Cu(I)-MNK3	NMR	2GA7	[52]
A69P apo-MNK6	NMR	1YJR	[53]
A69P Cu(I)-MNK6	NMR	1YJT	[53]
Apo-MNK6	NMR	1YJU	[53]
Cu(I)-MNK6	NMR	1YJV	[53]
Apo-WD56	NMR	2EW9	[36]
Apo-WD34	NMR	2ROP	[54]
WD-N-Domain	NMR	2ARF	[55]

1.2.2. Previous Hah1-MBD interaction studies

Rosenzweig and others showed that all WDP MBDs, as well as Hah1, have similar copper binding affinities.[42, 56] This similarity indicates that the Hah1 to WDP copper transfer is under kinetic control mediated by Hah1-WDP interactions, and that the functional differences among WDP MBDs are not defined by their Cu(I) binding affinities but may be related to how each MBD interacts with Hah1 and other MBDs. Very limited quantitative information is available, however, on how Hah1 and WDP interact, other than the surface plasmon resonance (SPR) studies on the association and dissociation kinetics of related systems by Solioz,[57] Mercer[58] and coworkers. These SPR studies employed nonspecific surface immobilization of proteins, which can influence protein interaction kinetics. Different NMR studies have been performed with different MBD constructs to probe their inter- and intra-molecular interactions. Huffman and coworkers[36 59] showed copper transfer can occur between the MBDs of WDP via MBD-MBD interactions. In particular, the double-domain construct MBD56 construct could not acquire copper from Hah1 but instead from the single-domain construct MBD4, which indicates the interdomain interactions and copper transfer are integral to WDP-mediated copper transport. As mentioned above, experiments performed on the full N-terminal MBD tail of WDP actually show that Hah1 is capable of metallating all of the MBDs.[43] There is still some disagreement on how copper is handled between Hah1 and the MBDs of WDP, which may have a foundation on how the different MBDs and Hah1 interact. In addition, limited kinetic information is available on the interaction processes.

Interdomain interactions will not be addressed in this dissertation, yet the fundamental process of interaction between a single MBD and Hah1 is scrutinized. These may serve as a foundation to a better understanding of how MBDs and Hah1 interact for metal transfer.

1.3. The single-molecule approach to study weak, dynamic protein interactions

In general, weak, dynamic protein interactions, such as those between Hah1 and the MBDs, are difficult to quantify in ensemble experiments for various reasons: (1) They are stochastic, making synchronization of molecular actions necessary. (2) The steady state concentrations of interaction intermediates are often low. (3) The presence of multiple interaction intermediates convolutes ensemble-averaged measurements. In contrast, single-molecule experiments offer several advantages for studying these interactions: (1) No synchronization is needed. (2) Molecular actions are followed in real time, and so are the formation, interconversion, and dissolution of interaction intermediates. (3) Only one molecular state, be it an intermediate, is observed at any given time. For these reasons, the single molecule approach provides a unique means to characterize weak dynamic protein interactions. This dissertation focuses on the single molecule characterization of the interactions between the copper chaperone Hah1 and the fourth metal binding domain of Wilson disease protein (MBD4).

1.3.1. Single-molecule Förster resonance energy transfer (smFRET)

Single molecule Förster (or Fluorescence) Resonance Energy Transfer (smFRET) is the nonradiative transfer of electronic excitation energy from a single donor to a single acceptor dye molecule via a weak dipole-dipole coupling mechanism. The transfer efficiency was predicted by Förster to decrease with the distance between the two dyes, as $[1 + (R/R_0)^6]^{-1}$ (Figure 1.6), where R is the distance between the two dyes and R_0 is the Förster radius.[60] The Förster radius is the distance corresponding to 50% energy transfer and depends on the photophysical properties of the dyes and their relative orientations. Due to its long-range distance dependent behavior, FRET can be used as a spectroscopic ruler to determine relative dye to dye

distances typically in the range of 2 to 8 nm.[61] Past studies have shown that smFRET is well suited for studying conformations and dynamics of biological macromolecules.[62-66] SmFRET has been successfully used in a variety of biological applications from protein and DNA conformational dynamics[62-64, 66-69] to enzyme reactions.[70]

SmFRET measurements can be used not only to probe average distances as in an ensemble experiment but also to observe distributions and the time evolution of conformational properties directly. The FRET efficiency (E_{FRET}) can be expressed in terms of k_D and k_T, the donor-only fluorescence and the energy transfer rate constants, respectively. Because the transfer process results in an excited state for the acceptor, the efficiency of energy transfer can be rewritten in terms of the donor (I_D) and acceptor (I_A) fluorescence intensities as:

$$E_{FRET} = \frac{k_T}{k_D + k_T} = \frac{1}{1 + (k_D / k_T)} = \frac{1}{1 + \gamma (I_D / I_A)} \approx \frac{1}{1 + (I_D / I_A)}$$

where γ (= $\eta_A\varphi_A/\eta_D\varphi_D$) is a correction factor that accounts for the detection efficiencies (η) and fluorescence quantum yields (φ) for the individual dyes.[60, 61, 70] Hence, direct detection of the individual fluorescence intensities of individual dyes affords a direct determination of the efficiency of energy transfer. The correction factor γ can be measured directly by determining the ratio $\Delta I_A / \Delta I_D$, where ΔI_A and ΔI_D are the acceptor and donor intensity changes on acceptor photobleaching. This value was experimentally determined by Ha and coworkers to be ~1 from 45 individual molecules.[70]

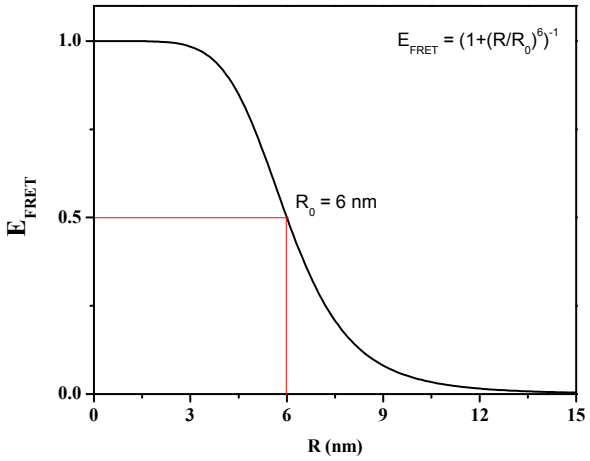

Figure 1.6. FRET efficiency as a function of distance (R).

1.3.2. Protein interaction dynamics studied by smFRET

SmFRET has become a common tool for characterizing protein dynamics at the single molecule level. Previous studies of protein-protein interactions include the chaperonin system GroEL-GroES interactions,[71] Wiskott-Aldrich Syndrome protein and Cdc42 protein interactions for cell signaling,[72] chymotrypsin inhibitor 2 and subtilisin BPN' interactions,[73] and protein-enzyme interactions in energy conversion systems.[74] Individual protein-protein events were followed and the associated protein interaction dynamics were deconvoluted. Further examples can be found in protein-DNA interactions from metalloregulators to enzymes involved in DNA replication.[62, 63, 66, 75, 76]

There are challenges to overcome before single-molecule methods can be applied to probe any *weak* protein-protein interactions. The primary obstacle is the concentration limit. The fore mentioned examples involve relatively strong interactions. Single-molecule experiments are normally performed at low concentrations (10^{-9} to 10^{-12} M) of fluorescent species to separate molecules spatially for optical detection. This low concentration severely limits single-molecule studies to

strongly interacting proteins.[77] Weak protein interactions with dissociation constants in the μM range are much more common in biology and need to be studied at higher concentrations. Nonspecific surface interactions present another challenge.[65] These must be minimized when molecules are immobilized to follow them over time. Therefore, different ways to study weak, dynamic protein interactions at the single molecule level are needed.

In this thesis, I will describe a nanovesicle trapping approach to overcome the above two challenges and enable smFRET study of weak, dynamic protein-protein interactions.

1.4. Thesis outline

In this dissertation the weak, dynamic protein-protein interactions between the Hah1 copper chaperone and the fourth metal binding domain of Wilson disease protein are investigated. Using a combination of nanovesicle trapping and smFRET, the different behaviors of association, dissociation and complex interconversions are characterized under different conditions.

In chapter 2, the nanovesicle trapping strategy is described, detailing all the advantages and disadvantages of this approach as well as possible improvements. The theoretical approach to quantifying bimolecular binding events within the nanovesicle is described.

The following chapters focus on the interaction dynamics between Hah1 and WDP MBD4. In chapter 3 the nanovesicle approach is used to study interactions between both proteins in the absence of any metal. The dynamics of association and dissociation, as well as complex interconversions are exposed from the single molecule data. In chapter 4 Hah1–MBD4 interactions are studied in the presence of varying amounts of copper. The stabilization of different FRET populations and their

possible implications are discussed. These experiments and their results shed light into the fundamental interaction processes that take place between the copper chaperone and the metal binding domains of WDP.

REFERENCES

1.Hazegh-Azam, M. C. L. a. M., Copper Biochemistry and Molecular Biology. *American Journal of Clinical Nutrition* **1996,** *63*, 797S-811S.

2.Gutteridge, B. H. a. J. M. C., Oxygen toxicity, oxygen radicals, transition metals and disease. *Biochem. J.* **1984,** *219*, 1-14.

3.L. Banci, I. B., K.S. McGreevy and A. Rosato, Molecular recognition in copper trafficking. *Natural Product Reports* **2010,** *27* (5), in press.

4.Rosenzweig, A. K. B. a. A. C., Structural Biology of Copper Trafficking. *Chem. Rev.* **2010,** *109* (10), 4760-4779.

5.Kim, B.-E.; Nevitt, T.; Thiele, D. J., Mechanisms for Copper Acqusition, Distribution and Regulation. *Nat. Chem. Biol.* **2008,** *4*, 176-185.

6.Rosenzweig, A. C., Copper Delivery by Metallochaperone Proteins. *Acc. Chem. Res.* **2001,** *34*, 119-128.

7.Xiao, Z.; Loughlin, F.; George, G. N.; Howlett, G. J.; Wedd, A. G., C-Terminal Domain of the Membrane Copper Transporter Ctr1 from Saccharomyces cerevisiae Binds Four Cu(I) Ions as a Cuprous-Thiolate Polynuclear Cluster: Sub-femtomolar Cu(I) Affinity of Three Proteins Involved in Copper Trafficking. *J. Am. Chem. Soc.* **2004,** *126*, 3081-3090.

8.Culotta, V. C.; Yang, M.; O'Halloran, T. V., Activation of superoxide dismutases: Putting the metal to the pedal. *Biochim. Biophys. Acta* **2006,** *1763*, 747-758.

9.Bertini, I.; Mangani, S.; Viezzoli, M. S., Structure and Properties of Copper-Zinc Superoxide Dismutases. *Advances in Inorganic Chemistry* **1998,** *45*, 127-250.

10.Field, L. S.; Furukawa, Y.; O'Halloran, T. V.; Culotta, V. C., Factors controlling the uptake of yeast copper/zinc superoxide dismutase into mitochondria. *J. Biol. Chem.* **2003,** *278*, 28052-28059.

11.McCord, J. M.; Fridovich, I., Superoxide dismutase. An enzymatic function for erythrocuprein (hemocuprein). *J. Biol. Chem.* **1969,** *244*, 6049-6055.

12.Pufahl, R. A.; Singer, C. P.; Peariso, K. L.; Lin, S.-J.; Schmidt, P. J.; Fahrni, C. J.; Culotta, V. C.; Penner-Hahn, J. E.; O'Halloran, T. V., Metal Ion Chaperone Function of the Soluble Cu(I) Receptor Atx1. *Science* **1997,** *278*, 853-856.

13.Yuan, D. S.; Stearman, R.; Dancis, A.; Dunn, T.; Beeler, T.; Klausner, R. D., The Menkes/Wilson disease gene homologue in yeast provides copper to a ceruloplasmin-like oxidase required for iron uptake. *Proc. Nat. Acad. Sci.* **1995,** *92*, 2632-2636.

14.Hung, I. H.; Casareno, R. L. B.; Gilles, L.; Mathews, F. S.; Gitlin, J. D., Hah1 Is A Copper-Binding Protein with Distinct Amino acid Residues Mediating Copper Homeostasis and Antioxidant Defense. *J. Biol. Chem.* **1998,** *273*, 1749-1754.

15.Hellman, N. E.; Gitlin, J. D., Ceruloplasmin metabolism and function. *Annu. Rev. Nutr.* **2002,** *22*, 439-458.

16.Axelsen, K. B.; Palmgren, M. G., Evolution of Substrate Specificities in the P-Type ATPase Superfamily. *Journal of Molecular Evolution* **1998,** *46*, 84-101.

17.Lutsenko, S.; Kaplan, J. H., Organization of P-type ATPases: significance of structural diversity. *Biochemistry* **1995,** *34* (48), 15607-15613.

18.Argüello, J. M.; Eren, E.; González-Guerrero, M., The structure and function of heavy metal transport P_{1B}-ATPases. *BioMetals* **2007,** *20*, 233-248.

19.Solioz, M.; Vulpe, C., CPx-type ATPases: a class of P-type ATPases that pump heavy metals. *Trends Biochem. Sci.* **1996,** *21* (7), 237-241.

20.Arnesano, F.; Banci, L.; Bertini, I.; Ciofi-Baffoni, S.; Molteni, E.; Huffman, D. L.; O'Halloran, T. V., Metallochaperones and Metal-Transporting ATPases: A Comparative Analysis of Sequences and Structures. *Genome Research* **2002,** *12*, 255-271.

21.Bieganowska, K.; Czlonkowska, A., Diagnosis of Wilson Disease by Methods of Molecular Genetics. *Neurol. Neurochir. Pol.* **1994,** *28*, 577-583.

22.Sarkar, B., Treatment of Wilson and Menkes Disease. *Chem. Rev.* **1999,** *99*, 2535-2544.

23.Vulpe, C.; Levinson, B.; Whitney, S.; Packman, S.; Gitschier, J., Isolation of A Candidate Gene for Menkes Disease and Evidence That It Encodes A Copper-Transporting ATPase. *Nature Genet.* **1993,** *3*, 7-13.

24.Huffman, D. L.; O'Halloran, T. V., Function, Structure, and Mechanism of Intracellular Copper Trafficking Proteins. *Ann. Rev. Biochem.* **2001,** *70*, 677-701.

25.O'Halloran, T. V.; Culotta, V. C., Metallochaperones, An Intracellular Shuttle Service for Metal Ions. *J. Biol. Chem.* **2000,** *275*, 25057-25060.

26.Poulos, T. L., Helping Copper Find A Home. *Nat. Struct. Biol.* **1999,** *6*, 709-711.

27.Rosenzweig, A. C., Metallochaperones: Bind and Deliver. *Chem. Biol.* **2002,** *9*, 673-677.

28.Rosenzweig, A. C.; O'Halloran, T. V., Structure and Chemistry of the Copper Chaperone Proteins. *Curr. Opin. Chem. Biol.* **2000,** *4*, 140-147.

29.Valentine, J. S.; Gralla, E. B., Delivering Copper Inside Yeast and Human Cells. *Science* **1997,** *278*, 817-818.

30.Bull, P. C.; Thomas, G. R.; Rommens, J. M.; Forbes, J. R.; Cox, D. W., The Wilson Disease Gene Is A Putative Copper Transporting ATPase Similar to the Menkes Gene. *Nature Genet.* **1993,** *5*, 327-337.

31.Arnesano, F.; Banci, L.; Bertini, I.; Ciofi-Baffoni, S.; Molteni, E.; Huffman, D. L.; O'Halloran, T. V., Metalloschaperones and Metal-Transporting ATPases: A Comparative Analysis of Sequences and Structures. *Genome Research* **2002,** *12*, 255-271.

32.Larin, D.; Mekios, C.; Das, K.; Ross, B.; Yang, A.-S.; Gilliam, T. C., Characterization of the Interaction between the Wilson and Menkes Disease Proteins and the Cytoplasmic Copper Chaperone, Hah1p. *J. Biol. Chem.* **1999,** *274*, 28497-28504.

33.Lutsenko, S.; Petrukhin, K.; Cooper, M. J.; Gilliam, T. C.; Kaplan, J. H., N-terminal Domains of Human Copper-transporting Adenosine Triphosphatases (the Wilson's and Menkes Disease Proteins) Bind Copper Selectively in vivo and in vitro with Stoichiometry of One Copper per Metal-Binding Repeat. *J. Biol. Chem.* **1997,** *272*, 18939-18944.

34.Wernimont, A. K.; Huffman, D. L.; Lamb, A. L.; O'Halloran, T. V.; Rosenzweig, A. C., Structural Basis for Copper Transfer by the Metallochaperone for the Menkes/Wilson Disease Proteins. *Nat. Struct. Biol.* **2000,** *7*, 766-771.

35.Arnesano, F.; Banci, L.; Bertini, I.; Bonvin, M. J. J., A Docking Approach to the Study of Copper Trafficking Proteins: Interactions between Metallochaperones and Soluble Domains of Copper ATPases. *Structure* **2004,** *12*, 669-676.

36.Achila, D.; Banci, L.; Bertini, I.; Bunce, J.; Ciofi-Baffoni, S.; Huffman, D. L., Structure of human Wilson protein domains 5 and 6 and their interplay with domain 4 and the copper chaperone HAH1 in copper uptake. *Proc. Natl. Acad. Sci. U.S.A.* **2006,** *103*, 5729-5734.

37.Banci, L.; Bertini, I.; Cantini, F.; Chasapis, C. T.; Hadjiliadis, N.; Rosato, A., A NMR Study of the Interactions of a Three-Domain Construct of ATP7A with

Copper(I) and Copper(I)-Hah1: The Interplay of Domains. *J. Biol. Chem.* **2005,** *280*, 38259-38263.

38.Huster, D.; Lutsenko, S., The Distinct Roles of the N-Terminal Copper-Binding Sites in Regulation of Catalytic Activity of the Wilson's Disease Protein. *J. Biol. Chem.* **2003,** *278*, 32212-32218.

39.Lutsenko, S.; LeShane, E. S.; Shinde, U., Biochemical Basis of Regulation of Human Copper-Transporting ATPase. *Arch. Biochem. Biophys.* **2007,** *463*, 134-148.

40.van Dongen, E. M. W. M.; Klomp, L. W. J.; Merkx, M., Copper-Dependent Protein-Protein Interactions Studied by Yeast Two-Hybrid Analysis. *Biochem. Biophys. Res. Commun.* **2004,** *323*, 789-795.

41.Walker, J. M.; Huster, D.; Ralle, M.; Morgan, C. T.; Blackburn, N. J.; Lutsenko, S., The N-Terminal Metal-Binding Site 2 of the Wilson's Disease Protein Play a Key Role in the Transfer of Copper from Atox1. *J. Biol. Chem.* **2004,** *279*, 15376-15384.

42.Yatsunyk, L. A.; Rosenzweig, A. C., Copper(I) Binding and Transfer by the N-terminus of the Wilson Disease Protein. *J. Biol. Chem.* **2007,** *282*, 8622-8631.

43.Banci, L.; Bertini, I.; Cantini, F.; Massagni, C.; Migliardi, M.; Rosato, A., An NMR Study of the Interaction of N-terminal Cytoplasmic Tail of the Wilson Disease Protein with Copper(I)-Hah1. *J. Biol. Chem.* **2009,** *284*, 9354-9360.

44.Rosenzweig, A. C.; Boal, A. K., Structural Biology of Copper Trafficking. *Chem. Rev.* **2009,** *109* (10), 4760-4779.

45.Banci, L.; Bertini, I.; Calderone, V.; Della-Malva, N.; Felli, I. C.; Neri, S.; Pavelkova, A.; Rosato, A., Copper(I)-mediated protein-protein interactions result from suboptimal interaction surfaces. *Biochem. J.* **2009,** *422*, 37-42.

46.Boal, A. K.; Rosenzweig, A. C., Structural Biology of Copper Trafficking. *Chem. Rev.* **2009,** *109*, 4760–4779.

47.Anastassopoulou, I.; Banci, L.; Bertini, I.; Cantini, F.; Katsari, E.; Rosato, A., Solution Structure of the Apo and Copper(I)-Loaded Human Metallochaperone HAH1. *Biochemistry* **2004,** *43*, 13046-13053.

48.Gitschier, J.; Moffat, B.; Reilly, D.; Wood, W. I.; Fairbrother, W. J., Solution Structure of the Fourth Metal-Binding Domain from the Menkes Copper-Transporting ATPase. *Nat. Struct. Biol.* **1998,** *5*, 47-54.

49.Jones, C. E.; Daly, N. L.; Cobine, P. A.; Craik, D. J.; Dameron, C. T., Structure and metal binding studies of the second copper binding domain of the Menkes ATPase. *J. Struct. Biol.* **2003,** *143* (3), 209-218.

50.Banci, L.; Bertini, I.; Del Conte, R.; D'Onofrio, M.; Rosato, A., Solution Structure and backbone Dynamics of the Cu(I) and Apo Forms of the Second Metal-Binding Domain of the Menkes Protein ATP7A. *Biochemistry* **2004,** *43*, 3396-3403.

51.DeSilva, T. M.; Veglia, G.; Opella, S. J., Solution structures of the reduced and Cu(I) bound forms of the first metal binding sequence of ATP7A associated with Menkes disease. *Proteins* **2005,** *61* (4), 1038-1049.

52.Banci, L.; Bertini, I.; Cantini, F.; Della-Malva, N.; Herrmann, T.; Rosato, A.; Wüthrich, K., Solution Structure and Intermolecular Interactions of the Third Metal-binding Domain of ATP7A, the Menkes Disease Protein *J. Biol. Chem.* **2006,** *281*, 29141-29147.

53.Banci, L.; Bertini, I.; Cantini, F.; Migliardi, M.; Rosato, A.; Wang, S., An Atomic-level Investigation of the Disease-causing A629P Mutant of the Menkes Protein, ATP7A. *J. Mol. Biol.* **2005,** *352*, 409-417.

54.Banci, L.; Bertini, I.; Francesca, C.; Rosenzweig, A. C.; Yatsunyk, L. A., Metal Binding Domains 3 and 4 of the Wilson Disease Protein: Solution Structure and Interaction with the Copper(I) Chaperone Hah1. *Biochemistry* **2008,** *47*, 7423-7429.

55.Dmitriev, O.; Tsivkovskii, R.; Abildgaard, F.; Morgan, C. T.; Markley, J. T.; Lutsenko, S., Solution structure of the N-domain of Wilson disease protein: Distinct nucleotide-binding environment and effects of disease mutations *Proc. Nat. Acad. Sci.* **2006,** *103* (14), 5302-5307.

56.Huffman, D. L.; O'Halloran, T. V., Energetics of Copper Trafficking between the Atx1 Metallochaperone and the Intracellular Copper Transporter Ccc2. *J. Biol. Chem.* **2000,** *275*, 18611-18614.

57.Multhaup, G.; Strausak, D.; Bissig, K.-D.; Solioz, M., Interaction of the CopZ Copper Chaperone with the CopA Copper ATPase of *Enterococcus hirae* Assessed by Surface Plasmon Resonance. *Biochem. Biophys. Res. Commun.* **2001,** *288*, 172-177.

58.Strausak, D.; Howies, M. K.; Firth, S. D.; Schlicksupp, A.; Pipkorn, R.; Multhaup, G.; Mercer, J. F. B., Kinetic Analysis of the Interaction of the Copper Chaperone Atox1 with the Metal Binding Sites of the Menkes Protein. *J. Biol. Chem.* **2003,** *278*, 20821-20827.

59.Bunce, J.; Achila, D.; Hetrick, E.; Lesley, L.; Huffman, D. L., Copper Transfer Studies between the N-terminal Copper Binding Domains One and Four of Human Wilson Protein. *Biochim. Biophys. Acta* **2006,** *1760*, 907-912.

60.Lakowicz, J. R., *Principles of Fluorescence Spectroscopy*. 2nd ed.; Kluwer Academic/Plenum Publishers: New York, 1999.

61.Deniz, A. A.; Laurence, T. A.; Dahan, M.; Chemla, D. S.; Schultz, P. G.; Weiss, S., Ratiometric single-molecule studies of freely diffusing biomolecules. *Annu. Rev. Phys. Chem.* **2001,** *52*, 233-253.

62.Andoy, N. M.; Sarkar, S. K.; Wang, Q.; Panda, D.; Benitez, J. J.; Kalininskiy, A.; Chen, P., Single-Molecule Study of Metalloregulator CueR-DNA Interactions Using Engineered Holliday Junctions. *Biophys. J.* **2009,** *97*, 97, 844-852.

63.Benitez, J. J.; Keller, A. M.; Ochieng, P.; Yatsunyk, L. A.; Huffman, D. L.; Rosenzweig, A. C.; Chen, P., Probing Real-time Transient Metallochaperone-Target Protein Interactions at the Single-Molecule Level with Nanovesicle Trapping. *J. Am. Chem. Soc.* **2008,** *130*, 2446-2447.

64.Ha, T.; Enderle, T.; Ogletree, D. F.; Chemla, D. S.; Selvin, P. R.; Weiss, S., Probing the interaction between two single molecules: Fluorescence resonance energy transfer between a single donor and a single acceptor. *Proc. Natl. Acad. Sci. U.S.A.* **1996,** *93* (13), 6264-6268.

65.Rasnik, I.; McKinney, S. A.; Ha, T., Surfaces and Orientations: Much to FRET about? *Acc. Chem. Res.* **2005,** *38*, 542-548.

66.Sarkar, S. K.; Andoy, N. M.; Benitez, J. J.; Chen, P. R.; Kong, J. S.; He, C.; Chen, P., Engineered Holliday Junctions as Single-Molecule Reporters for Protein-DNA Interactions with Application to a MerR-Family Regulator. *J. Am. Chem. Soc.* **2007,** *129*, 12461-12467.

67.Deniz, A. A.; Dahan, M.; Grunwell, J. R.; Ha, T.; Faulhaber, A. E.; Chemla, D. S.; Weiss, S., Single-Pair Fluorescence Resonance Energy Transfer on Freely Diffusing Molecules. *Proc. Natl. Acad. Sci. U.S.A.* **1999,** *96*, 3670-3675.

68.Ishii, Y.; Yoshida, T.; Funatsu, T.; Wazawa, T.; Yanagida, T., Fluorescence resonance energy transfer between single fluorophores attached to a coiled-coil protein in aqueous solution. *Chem. Phys.* **1999,** *247* (1), 163-173.

69.Jia, Y. W.; Talaga, D. S.; Lau, W. L.; Lu, H. S. M.; DeGrado, W. F.; Hochastrasser, R. M., Folding dynamics of single GCN-4 peptides by fluorescence resonant energy transfer confocal microscopy. *Chem. Phys.* **1999,** *247* (1), 69-83.

70.Ha, T. J.; Ting, A. Y.; Liang, J.; Caldwell, W. B.; Deniz, A. A.; Chemla, D. S.; Schultz, P. G.; Weiss, S., Single-Molecule Fluorescence Spectroscopy of Enzyme Conformational Dynamics and Cleavage Mechanism. *Proc. Natl. Acad. Sci. U.S.A.* **1999,** *96*, 893-898.

71.Taguchi, H.; Ueno, T.; Tadakuma, H.; Yoshida, M.; Funatsu, T., Single-Molecule Observation of Protein-Protein Interactions in the Chaperonin System. *Nature Biotechnol.* **2001,** *19*, 861-865.

72.Tan, X.; Nalbant, P.; Toutchkine, A.; Hu, D.; Vorpagel, E. R.; Hahn, K. M.; Lu, H. P., Single-Molecule Study of Protein-Protein Interaction Dynamics in a Cell Signaling System. *J. Phys. Chem. B* **2004,** *108*, 737-744.

73.Jager, M.; Michalet, X.; Weiss, S., Protein–protein interactions as a tool for site-specific labeling of proteins. *Protein Sci.* **2005,** *14*, 2059-2068.

74.Yokota, H.; Kaseda, K.; Matsuura, H.; Arai, Y.; Iwane, A.; Ishii, Y.; Kodama, T.; Yanagida, T., Single-Molecule Imaging of the Dynamic Interactions between Macromolecules. *J. Nanosci. Nanotechnol.* **2004,** *4*, 616-621.

75.Benitez, J. J.; Keller, A. M.; Ochieng, P.; Yatsunyk, L. A.; Huffman, D. L.; Rosenzweig, A. C.; Chen, P., Correction/Addition: Probing Real-time Transient Metallochaperone-Target Protein Interactions at the Single-Molecule Level with Nanovesicle Trapping. *J. Am. Chem. Soc.* **2009,** *131*, 871.

76.Joo, C.; Balci, H.; Ishitsuka, Y.; Buranachai, C.; Ha, T., Advances in Single-Molecule Fluorescence Methods for Molecular Biology. *Annu. Rev. Biochem.* **2008,** *77*.

77.Laurence, T. A.; Weiss, S., How to Detect Weak Pairs. *Science* **2003,** *299*, 667-668.

CHAPTER 2

Nanovesicle trapping for studying weak protein interactions by single-molecule FRET*

***** Benitez, J. J.; Keller, A. M.; Chen, P., Nanovesicle Trapping for Studying Weak Protein Interactions by Single-Molecule FRET. *Meth. Enzymol.* **2010**, 472, 41-60. Reproduced with permission from *Methods in Enzymology,* Elsevier press.

2.1. Abstract

Protein–protein interactions are fundamental biological processes. While strong protein interactions are amenable to many characterization techniques including crystallography, weak protein interactions are challenging to study due to their dynamic nature. Single-molecule FRET can monitor dynamic protein interactions in real time, but are generally limited to strong interacting pairs because of the low concentrations needed for single-molecule detection. Here we describe a nanovesicle trapping approach to enable single-molecule FRET study of weak protein interactions at high effective concentrations. We describe the experimental procedures, summarize the application in studying the weak interactions between intracellular copper transporters, and detail the single-molecule kinetic analysis of bimolecular interactions involving three states. Both the experimental approach and the theoretical analysis are generally applicable for studying many other biological processes at the single-molecule level.

2.2. Introduction

Protein–protein interactions are essential for cellular functions including protein folding, cell signaling, and metal trafficking [1-3]. The strength of protein–protein interactions can vary widely depending on the proteins involved. Strong protein interactions can have equilibrium dissociation constants (K_D) of a few picomolar (10^{-12} M), for example antigen–antibody interactions, for which tight binding is crucial [4]. Weak protein interactions can have K_D's of a few micromolar to millimolar (10^{-6} – 10^{-3} M), for example interactions between metallochaperones and their target proteins, for which dynamic binding and unbinding are necessary to have many interaction turnovers [3, 5-10].

For understanding their fundamental properties, strong protein interactions are amenable to characterization by ensemble measurements, as stable interaction complexes can form even at dilute solution conditions. Stable protein complexes can further be crystallized for structural determination down to atomic resolution. In contrast, weak protein interactions are challenging to characterize in ensemble measurements for several reasons: (1) They are dynamic and stochastic, making synchronization of molecular actions often necessary. (2) The steady-state concentrations of interaction intermediates are often low, making detection difficult. (3) The presence of multiple interaction intermediates can complicate ensemble-averaged measurements. To study these weak protein interactions, single-molecule measurements offer several advantages: (1) No synchronization of molecular reactions is necessary. (2) The molecular reactions, including the formation, interconversion, and dissolution of interaction intermediates, are followed in real time. (3) Only one molecular state, be it an intermediate, is observed at any time point, enabling the resolution of complex reaction kinetics.

Single-molecule fluorescence resonance energy transfer (smFRET), with its inherent distance dependence in the nanometer scale, is particularly suited for probing dynamic protein–protein interactions, which is accompanied by changes in protein–protein distances. There are challenges to overcome, however, before smFRET can be applied to study weak protein interactions. The primary challenge is the concentration limit. Single-molecule fluorescence measurements are generally done at low concentrations ($<10^{-9}$ M) to spatially separate fluorophores so that there is less than one fluorophore (or one pair of fluorophores) on average in the detection volume (about 10^{-16} – 10^{-15} L) monitored in confocal microscopy or total internal reflection microscopy. This low concentration range limits single-molecule protein

interaction studies to strong interacting pairs, whereas weak protein interactions need to be studied at much higher concentrations (> 10^{-6} M) to favor complex formation.

To overcome this concentration limit, one needs to decrease the effective detection volume to ~10^{-19}–10^{-21} L, so that at concentrations up to 10^{-6} – 10^{-4} M there is no more than one fluorophore on average found in it [11]. This can be done by reducing the laser excitation volume or by confining molecules in space.

For reducing the excitation volume, Webb, Craighead and coworkers have fabricated zero-mode waveguides made of metal-clad wells on top of a silica substrate [12]. The diameter of these wells is much smaller than the wavelength of the excitation light, and therefore, light shining at the silica substrate cannot propagate through the wells. This blockage of light propagation reduces the light excitation to an evanescent electromagnetic field close to the silica substrate surface, leading to reduction of the laser excitation volume to ~10^{-21} L. Using this approach, Webb, Craighead and coworkers have studied the reactions of individual DNA polymerase molecules that have substrate binding affinity in the micromolar range. As these zero-mode waveguides are open reaction containers, a big advantage is easy exchange of solutions for changing reaction conditions. A disadvantage is the proximity of a metal surface to the fluorophore; the metal surface can influence the fluorophore's fluorescence properties, such as its intensity and fluorescence lifetime. To follow individual molecules over time, the molecules also have to be immobilized on the silica surface at the bottom of the wells, which can introduce nonspecific surface interactions.

For confining molecules spatially, trapping with nanometer-sized lipid vesicles is an effective approach (Figure 2.1), which was initially used in single-molecule studies of enzyme reactions [13], protein folding [14-17], and nucleic acid conformation dynamics [18, 19]. Because of the confined volume, the effective concentration of a single

molecule inside a nanovesicle can be as high as tens of micromolar, while the overall concentration of the nanovesicles can be kept low to maintain the single-molecule detection condition. Using this nanovesicle trapping approach combined with smFRET measurements, Ha and coworkers have studied dynamic protein–nucleic acid interactions [20], and we have studied weak protein–protein interactions at high effective concentrations [21, 22]. In this article we describe in detail how nanovesicle trapping, combined with smFRET measurements, can be used to characterize weak, dynamic protein interactions at the single-molecule level. We also detail the single-molecule kinetic analysis of bimolecular interactions that show three FRET states.

2.3. Nanovesicle trapping approach

Nanovesicle trapping is an effective approach in reducing the effective detection volume to enable high concentration studies at the single-molecule level. This approach also offers several other advantages: (1) The lipid membrane enclosure mimics biological environments inside cells or organelles. (2) The membrane prevents nonspecific interactions between the protein and the glass surface because molecule immobilization is done via tethering the nanovesicle (Figure 2.1). Nevertheless, nonspecific interactions with the lipid membrane may occur; control experiments must be performed to check this possibility (see below). (3) The diameter of vesicles can be varied from a few hundred nanometers down to ~50 nm, covering effective concentrations up to ~24 μM for a single molecule inside (Figure 2.2). (4) For protein–protein interaction studies, interactions between molecules of the same type, if occurring, can be selectively discarded in the data analysis stage by examining only the nanovesicles that contain molecules of different types.

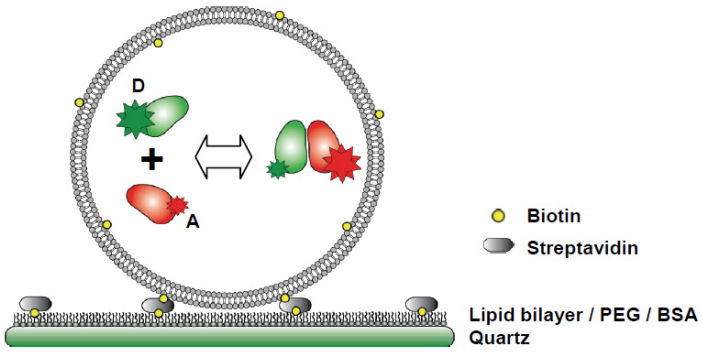

Figure 2.1. Schematics of nanovesicle trapping of two proteins labeled with a FRET donor-acceptor pair for smFRET studies.

In this section, we describe the experimental details of preparing nanovesicles to trap two different proteins for protein interaction studies. The procedures largely follow those of Haran and Ha [14, 18].

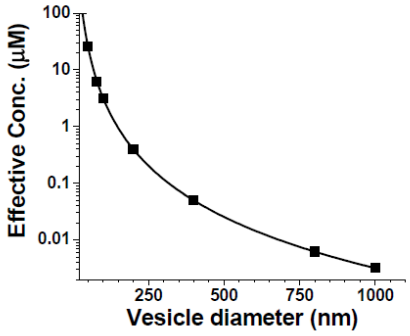

Figure 2.2. Dependence of the effective concentration of a single molecule on the diameter of the nanovesicle. The solid symbols indicate a few commercial available membrane pore sizes for preparing nanovesicles.

2.3.1. Lipid selection

The lipids for forming the membrane bilayer of the nanovesicles contain two components: one major lipid (~99%) that dominates the behavior of the membrane bilayer and the other minor lipid (~1%) that contains a biotin group for surface immobilization. The chemical nature and the gel-to-liquid phase transition temperature (T_m) of the major lipid are important here. The lipid must not significantly interact

with the proteins and perturb the protein interactions. A lipid with a net zero charge is preferred, as it is less likely to interact with soluble, largely hydrophilic proteins [14]. Usually the T_m of the major lipid should be much lower than the temperature for the single-molecule experiments, so the lipid bilayer stays in the fluidic liquid phase. A common major lipid used in single-molecule applications is Egg PC, extracted from egg yolk and ~99% of which is L-α-phosphatidylcholine. Its T_m is about –2°C [23], so its bilayer is in the liquid phase at room temperature. Many other lipids with different T_m and charge properties are available and can be used for preparing vesicles [23]. For the biotinylated minor lipid, Biotinyl-cap PE (1,2-Dipalmitoyl-*sn*-Glycero-3-Phosphoethanolamine-N-(Cap Biotinyl)) is commonly used.

2.3.2. Lipid nanovesicle preparation and protein trapping

The procedure consists of two major steps: (1) Preparation of dry lipid film and hydration of the lipid film with buffer containing fluorescently labeled proteins to form vesicles and trap proteins inside. (2) Extrusion of the formed vesicles through a polycarbonate membrane with well-defined pore diameters to make unilamellar vesicles of defined size. Using 100-nm pore-size membranes for extrusion, the multilamellar vesicles were estimated to be less than 2% [24].

2.3.2.1. Lipid film preparation and hydration

1. Prepare lipid stock solutions in chloroform at 100 mg mL^{-1} and store at –20 °C in a desiccator. The biotinylated lipid stock solution is prepared at 1 mg mL^{-1}.
2. Transfer aliquots of lipid solutions into a clean glass test tube, forming a solution of ~99% major lipid and ~1% biotinylated minor lipid. Use enough amounts for a final total lipid concentration of 5 mg mL^{-1} upon hydration. Dry under a nitrogen flow until a thin lipid film is formed on the wall of the test

tube. The lipid film can be further put under vacuum for 1 – 2 h to remove residual chloroform.

3. Hydrate the lipid film with the solution containing a mixture of the two labeled proteins under study. The concentration of each of the fluorescently labeled proteins should be close to the targeted effective concentration when the protein is trapped inside the nanovesicle. For example, for trapping a pair of protein molecules in 100 nm diameter nanovesicles, the concentration of each protein should be ~3 μM, whereas for trapping in 200 nm diameter nanovesicles, use ~400 nM concentration. The efficiency of co-trapping a pair of molecules can be increased if the hydration and trapping are done under conditions where the protein pair has maximum binding affinity to each other.
4. Briefly vortex the hydrated solution to detach the lipid film from the wall of the test tube. Incubate the solution for 10 min to 1 h at a temperature of at least 10°C above the T_m of the major lipid. The hydrated lipids will spontaneously form large multilamellar vesicles. Further freeze-thaw cycles (5–10 times) of the vesicle solution using liquid nitrogen and warm water can induce cracks in the membrane, which can improve entrapment of small molecules. Here care must be taken that the freeze-thaw cycles do not denature the proteins; circular dichroism spectroscopy can be used to check the folding state of the protein.

2.3.2.2. Preparation of unilamellar nanovesicles via extrusion

Unilamellar nanovesicles are formed by extrusion of the above vesicle solution through a polycarbonate membrane with nanometer-sized pores [24-26]. Extrusion should be performed at a temperature of at least 10°C above the T_m of the major lipid. The Avanti mini extruder (Avanti Polar Lipids, Inc.) is handy for this purpose. Polycarbonate membranes of different pore diameters are available, ranging from 50

nm to a micron. The nanovesicle diameter obtained after extrusion follows a Gaussian distribution, the width of which is dependent on the number of passes through the extruder; the more passes, the narrower the distribution [24, 26]. The diameter distribution can be checked using dynamic light scattering measurements. We normally perform tens of passes, significantly more than what is suggested by Avanti. The number of molecules trapped within the nanovesicles follows a Poisson distribution, with the average occupation number depending on the protein/lipid ratio in the hydration step[14]. The exact occupancy of each nanovesicle can be determined by single-molecule fluorescence imaging (see Section 3.2).

2.4. SmFRET measurements of weak protein–protein interactions

The smFRET experiments consist of: (1) immobilization of nanovesicles in a flow cell, and (2) real-time imaging using total internal reflection fluorescence microscopy. The microscope is equipped with two-color detection for imaging the fluorescence of the FRET donor and acceptor simultaneously.

2.4.1. Surface immobilization of nanovesicles

To follow the protein–protein interactions inside each nanovesicle over time, the nanovesicles need to be immobilized on a surface. A biotin-avidin linkage is most frequently used. Biotinylated lipids in the nanovesicle membrane are used to bind avidins (e.g., streptavidin or neutravidin), which in turn are bound to a biotin-modified surface. We have used three different schemes to modify the surface with biotins, all of which yield similar results: (1) coating the surface with a lipid bilayer containing biotinylated lipids, (2) coating with biotinylated bovine serum albumin (BSA), and (3) coating with partially biotinylated polyethylene glycol (PEG).

2.4.1.1. Lipid bilayer coating

This surface modification scheme takes advantage of the spontaneous fusion of lipid vesicles onto clean quartz surfaces to form a lipid bilayer [27, 28], over which the nanovesicles can be attached. The lipids used for this bilayer can be the same as those used for the nanovesicles, e.g., 99% Egg PC and 1% Biotinyl-cap PE.

1. The procedure for lipid preparation is the same as described earlier. The lipid film is prepared first and then hydrated with buffer in the absence of proteins.
2. The hydrated solution is sonicated for 30 min to 1 h until clarity. The sonication here breaks large multilamellar vesicles to form small unilamellar vesicles, which can spontaneously fuse to clean quartz surfaces. The distribution of vesicle sizes is not important here.
3. Incubate the quartz substrate with the solution containing small unilamellar vesicles at a total lipid concentration of 1 – 5 mg mL^{-1} for 1 h. Wash out excess lipids from the quartz surface with buffer.
4. Vesicle preparation, surface coating and washing should all be performed at a temperature of at least 10°C above the T_m of the major lipid.

One problem using Egg PC for the supported bilayer is that at room temperature the bilayer exists in the liquid phase, so the attached nanovesicles are mobile. The nanovesicle mobility can be reduced by increasing the percentage of biotinylated lipid so that each nanovesicle is anchored to the supported bilayer by multiple biotin-avidin linkages [18]. Nevertheless, many nanovesicles still remain mobile as we observed in our experiments. To alleviate this mobility problem, we have used another lipid, DPPC (1,2-dipalmitoyl-*sn*-glycero-3-phosphocholine), which has a T_m of ~41°C. Because of its high T_m, DPPC exists in the gel phase at room temperature, resulting in a mostly immobile lipid support.

2.4.1.2. BSA coating

BSA can bind to quartz surfaces strongly via nonspecific interactions [29], and therefore, biotinylated BSA can be used to coat the quartz surface to immobilize nanovesicles:

1. Prepare 1 mg mL^{-1} biotinylated BSA solution and incubate on the quartz substrate for 30 min to 1 h.
2. Wash out excess biotinylated BSA with buffer.

The BSA coating is easy to perform and can prevent rupture and fusion of nanovesicles to the quartz surface. (In case some bare patches on the glass surface exist due to incomplete coating with BSA, vesicle fusion to the glass surface can form patches of lipid bilayer to fill them up.)

2.4.1.3. PEG coating

Covalent functionalization of a quartz surface with partially biotinylated PEG is another scheme for immobilizing nanovesicles. The quartz surface is first covalently functionalized with amine groups, which are then covalently linked to PEG via succinimidyl ester chemistry.

For amine modification:

1. Prepare a fresh solution of 1.5-2% amino silane reagent (Vectabond, Vector Laboratories) in acetone. (Other types of amino silane reagents work too, for example, 3-aminopropyltriethoxysilane.)
2. Drop 200 μL of the amino silane solution onto the quartz slide.
3. Incubate for 5 minutes and then wash extensively with ultra-filtered, deionized water for 1 min. Dry slides with nitrogen and store under a dry environment.

For PEG modification:

1. Prepare a solution of 98~99% m-PEG-SPA-5000 and 1~2% biotin-PEG-NHS-3400 (Nektar Therapeutics, JenKem Technology Inc., or SunBio USA) in 100 mM $NaHCO_3$, pH 8.2.
2. Drop 200 μL of the PEG solution onto an amine-functionalized slide and sandwich it with another slide. Place parafilm spacers in between to prevent squeezing out the solution. Incubate for 4 h in the dark.
3. Wash slides thoroughly with nanopure water and dry with nitrogen for usage.

2.4.2. Control experiments

2.4.2.1. Lipid–protein interactions

To check if the fluorescently labeled proteins have nonspecific interactions with the lipid membrane, one can coat the quartz surface with a lipid bilayer and flow in solutions containing high concentrations (e.g., 100 nM) of labeled proteins. After washing the flow cell with fresh buffer and imaging the single-molecule fluorescence, the number of molecules that are immobilized on the lipid bilayer by nonspecific interactions can be counted. Comparing the number of nonspecifically bound molecules to the number of molecules detected using specific biotin-avidin immobilization of nanovesicles provides an estimate of the extent of nonspecific interactions between the protein and the lipid membrane.[18, 21, 22]

2.4.2.2. Occupancy of nanovesicles

The nanovesicle trapping procedure will result in a distribution of occupancy of individual nanovesicles. The nanovesicle occupation is important to verify when using smFRET to study weakly interacting pairs. Under normal smFRET

measurements, only the FRET donor is continuously excited and emitting fluorescence. The FRET acceptor is emitting ideally only when it is close to the donor labeled protein (e.g., upon protein–protein interaction) and is excited via energy transfer. The possible presence of multiple acceptor-labeled proteins within a nanovesicle can adversely affect quantitative determination of protein–protein interaction kinetics. Control experiments are necessary to determine the distribution of occupancy of nanovesicles under the trapping conditions.

To do so, one can use two different lasers to excite the FRET donor and acceptor separately. For example, for the Cy3–Cy5 FRET pair, the Cy3 fluorescence can be directly imaged by excitation with a 532-nm laser and Cy5 fluorescence with a 637-nm laser. With the nanovesicles already loaded with fluorescent proteins and immobilized on the surface, the control experiments follow:

1. Directly excite the donor dye and record a movie of fluorescence intensity.
2. Switch to the second laser to excite the acceptor dye in the same area and record a fluorescence movie.
3. Analyze both movies to obtain fluorescence trajectories and positions of individual molecules. Use the number of photobleaching steps in the fluorescence intensity trajectory to determine the number of donor (or acceptor) molecules in the nanovesicle.
4. Check the position colocalization if the donor and acceptor dyes belong to the same nanovesicle. In our experience, incidental vesicle colocalization due to limited spatial resolution is minimal when the surface density of protein containing vesicles is smaller than 0.2 μm^{-2}.

For weakly interacting protein pairs, such as Hah1 and MBD4 (see Section 3.3), the co-trapping efficiency is low. Among 340 nanovesicles containing either Hah1-Cy5 or MBD4-Cy3, only 21 of them contain a Hah1-Cy5 and a MBD4-Cy3.

The number of acceptor molecules can also be checked during normal smFRET measurements. One can first use the donor-exciting laser for smFRET while recording a fluorescence movie. In the later part of the movie, the acceptor-exciting laser is turned on to excite the acceptor dye until the acceptor photobleaches. The photobleaching events in the acceptor intensity will indicate the number of acceptor molecules in the nanovesicle. In this way one is sure to only examine single pairs of protein molecules.

2.4.2.3. FRET differentiation of acceptor blinked/bleached states from the dissociated state of protein interactions

Organic fluorescent dyes show blinking behavior, i.e., the fluorescence intensity sometimes switches off temporarily. Although fluorescence blinking can be suppressed significantly by using an oxygen scavenging system and triplet quenchers (e.g., Trolox) [30], occasional blinking of the FRET acceptor is problematic, as it would result in an apparently low FRET efficiency ($E_{FRET} = I_A/(I_A+I_D)$, where I_A and I_D are the acceptor and donor fluorescence intensities), which could be mistaken as that of the dissociated state of protein–protein interactions. Fortunately, using nanovesicle trapping and Cy3–Cy5 as the FRET pair, the Cy5-blinked state has clearly lower E_{FRET} than that of the dissociated state from control experiments [21, 22].

As far as the apparent E_{FRET} is concerned, the acceptor blinked state is effectively the same as that in the absence of the acceptor and that of the acceptor photobleached state. Therefore, the apparent E_{FRET} from nanovesicles that merely contain a donor molecule serves as a control for signal from the acceptor blinked state (Figure 2.3A). The determined apparent E_{FRET} with one Cy3 only is 0.04 ± 0.05, which is the same as Cy5-blinked/bleached state of a Cy3–Cy5 pair (Figure 2.3C).

The dissociated state can be mimicked by a nanovesicle containing a free donor and a free acceptor (Figure 2.3B), as the free dyes do not interact with each other. Here the existence of both a donor and an acceptor must be confirmed by separate laser excitations (Figure 2.3B). Under 532-nm excitation, the apparent E_{FRET} is 0.15 ± 0.14 (Figure 2.3C); the larger value here compared with that of Cy5-blinked state is likely due to the residual direct excitation of Cy5 fluorescence by the 532-nm laser and some energy transfer of Cy3 to Cy5 due to their confined coexistence inside the nanovesicle.

2.4.3. Application to weak interactions between intracellular copper transporters

We applied the nanovesicle trapping approach to enable smFRET studies of the weak, dynamic interactions between the human intracellular copper chaperone Hah1 and the fourth metal-binding domain (MBD4) of the copper transporting ATPase Wilson disease protein (WDP) [21, 22]. The interactions between Hah1 and WDP mediate the copper transfer from Hah1 to the MBDs of WDP, an essential process for safe trafficking of copper ions in human cells [3, 5-10]. Because of the low affinity of the Hah1−WDP interaction ($K_D \sim 10^{-6}$ M), their interaction dynamics have been challenging to quantify in ensemble measurements. Nanovesicle trapping offers an ideal platform to examine their interactions at the single-molecule level using smFRET.

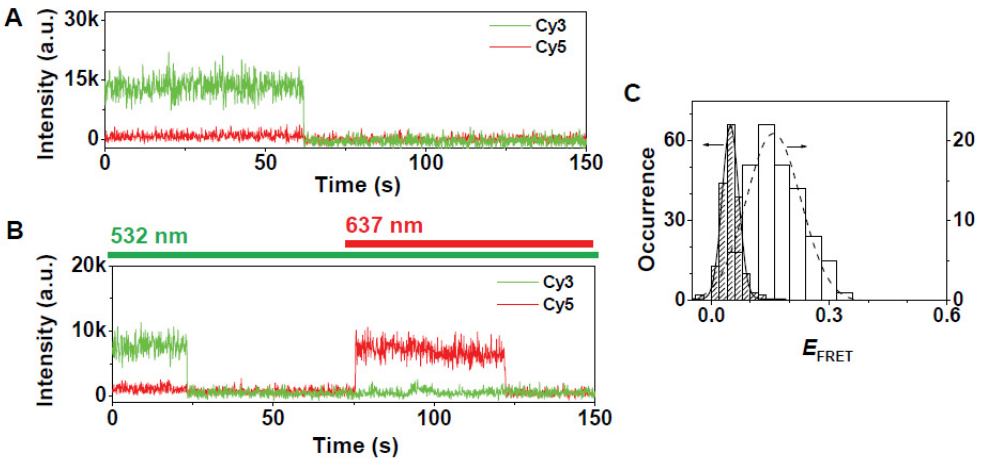

Figure 2.3. SmFRET control experiments for acceptor blinked/bleached states and the dissociated state. (A) Two-color fluorescence intensity trajectories of a nanovesicle containing a single Cy3 molecule using 532-nm laser excitation. The Cy3 molecule photobleaches at the ~62th second. (B) Two-color fluorescence intensity trajectories of a nanovesicle containing a single Cy3 and a single Cy5. The 532-nm laser is on throughout; the 637-nm laser was turned on at the ~75th second. The Cy3 photobleaches at the ~25th second; the Cy5 molecule photobleaches at ~125th second. The first 25 seconds mimics the dissociated state of a Cy3-Cy5 pair. (C) Histograms of the apparent E_{FRET} (=I_A/(I_A+I_D); I_D and I_A are the fluorescence intensities of the donor and acceptor, respectively) for nanovesicles containing a single Cy3 (line patterned columns) and for nanovesicles containing a free Cy3 and a free Cy5 molecule (clear columns).

We labeled Hah1 with the acceptor dye Cy5 and MBD4 with the donor dye Cy3 using maleimide chemistry at specific cysteine residues, and co-trapped them in 100-nm diameter nanovesicles. SmFRET trajectories reveal their dynamic interactions (Figure 2.4A). These trajectories show three different E_{FRET} states: E_0 (~0.2) is the dissociated state, and E_1 (~0.5) and E_2 (~0.8) are two different interaction complexes. Transitions between E_0 and E_1 and between E_0 and E_2 correspond to the binding/unbinding processes for forming complex 1 and 2. The transitions between E_1 and E_2 correspond to the interconversions between the two complexes. Figure 2.4B gives the interaction scheme between Hah1 and MBD4. The kinetic constants of all interaction processes can be extracted by analyzing the distributions of dwell times in

each FRET state (Figure 2.4C–H, Section 4). The direct observation of the interconversion dynamics between the two interaction complexes is particularly exciting here, as it enables determination of both the forward and the reverse interconversion rate constants (see Section 4) — ensemble characterization often can only determine the sum of the forward and reverse rates for intermediate interconversion dynamics, as the interconversion dynamics are generally non-synchronizable.

2.5. Single-molecule kinetic analysis of three-state protein–protein interactions

The interaction scheme between Hah1 and MBD4 can be generalized to that in Figure 2.5A. An idealized E_{FRET} trajectory showing three FRET states is given in Figure 2.5B with different types of dwell times denoted. In this section, we derive the probability density functions of the dwell times involved in this three-state interactions using single-molecule kinetic analysis [21, 22, 31, 32].

We first consider the binding processes that occur during the dwell time τ_0 in the E_0 state. Based on the interaction scheme in Figure 2.5A, the processes occurring during τ_0 are summarized in Scheme 2.1. The ensemble rate equations for these kinetic processes are:

$$-\frac{\mathrm{d[A]}}{\mathrm{d}t} = -\frac{\mathrm{d[A']}}{\mathrm{d}t} = (k_1 + k_2)[\mathrm{A}][\mathrm{A'}] \qquad \text{(Eq. 2.1a)}$$

$$\frac{\mathrm{d[B]}}{\mathrm{d}t} = k_1[\mathrm{A}][\mathrm{A'}] \qquad \text{(Eq. 2.1b)}$$

$$\frac{\mathrm{d[C]}}{\mathrm{d}t} = k_2[\mathrm{A}][\mathrm{A'}] \qquad \text{(Eq. 2.1c)}$$

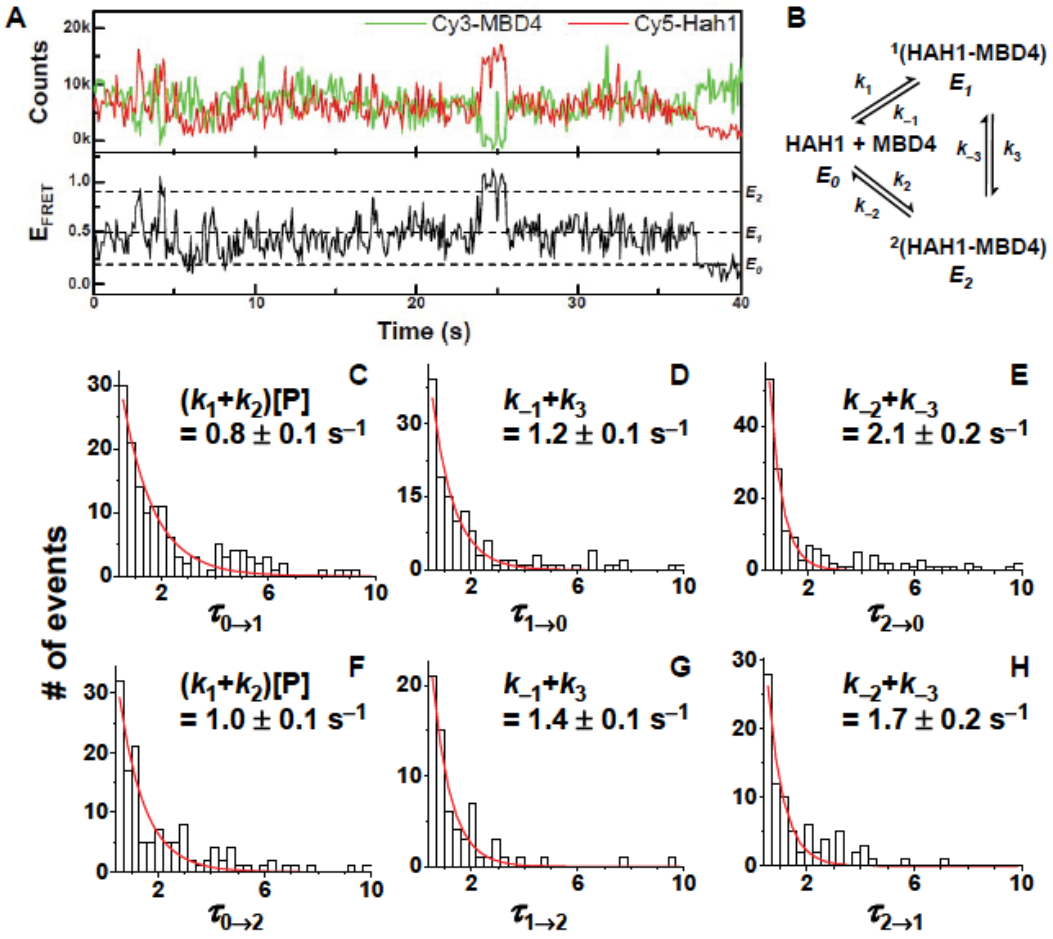

Figure 2.4. SmFRET measurements of weak protein interaction dynamics in a nanovesicle. (A) Two-color fluorescence intensity (upper) and corresponding apparent E_{FRET} (lower) trajectories of a Cy5-Hah1 and a Cy3-MBD4 trapped in a 100-nm nanovesicle. (B) Interaction scheme between Hah1 and MBD4. (C-H) Distributions of the six types of dwell times from the E_{FRET} trajectories of Hah1−MBD4 interactions. Solid lines are exponential fits; insets give the exponential decay constants and their relations to the protein interaction rate constants in (B). [P] is the effective concentration (~3 μM) of a single molecule in a 100-nm vesicle. The individual rate constants are: $k_1 = (1.6 \pm 0.2) \times 10^5$ $M^{-1}s^{-1}$, $k_{-1} = 0.88 \pm 0.04$ s^{-1}, $k_2 = (1.4 \pm 0.2) \times 10^5$ $M^{-1}s^{-1}$, $k_{-2} = 1.3 \pm 0.1$ s^{-1}, $k_3 = 0.42 \pm 0.04$ s^{-1}, and $k_{-3} = 0.7 \pm 0.1$ s^{-1}. Data in (A, C-H) adapted with permission from reference [21, 22]; Copyright 2008 American Chemical Society.

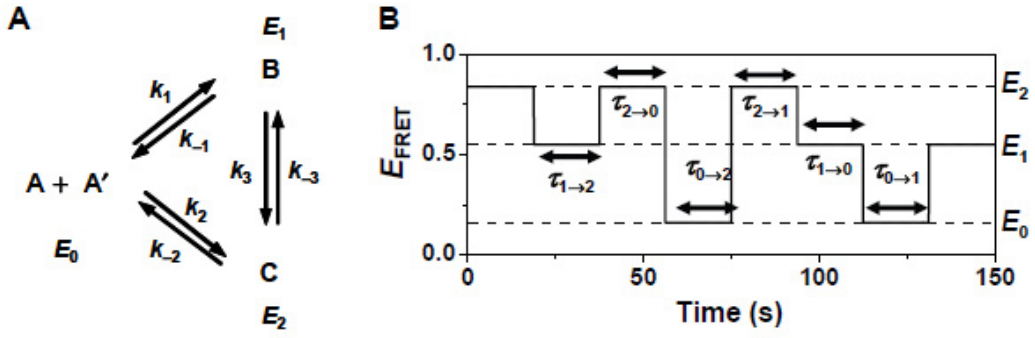

Figure 2.5. Generic kinetic scheme of protein interactions and corresponding E_{FRET} trajectories. (A) Generalized kinetic scheme of a single interacting pair with three FRET states: one dissociated state, **A** + **A′**, with a FRET value of E_0; and two interaction complexes, **B** and **C**, with FRET values of E_1 and E_2, respectively. (B) Idealized three-state E_{FRET} trajectories of an interacting pair; all six types of dwell times are denoted.

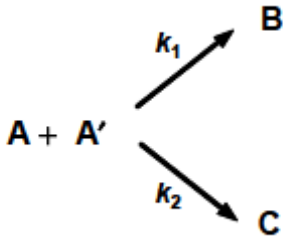

Scheme 2.1. Kinetic processes occurring during the dwell time τ_0 at the E_0 state.

For the single-molecule reactions occurring in a nanovesicle, we have to consider the molecules in terms of their probabilities at time t, $P(t)$. The above rate equations then become:

$$-\frac{dP_A(t)}{dt} = -\frac{dP_{A'}(t)}{dt} = (k_1 + k_2)P_A(t)P_{v,A',A}(t) \qquad \text{(Eq. 2.2a)}$$

$$\frac{dP_B(t)}{dt} = k_1 P_A(t)P_{v,A',A}(t) \qquad \text{(Eq. 2.2b)}$$

$$\frac{dP_C(t)}{dt} = k_2 P_A(t) P_{v,A',A}(t) \qquad \text{(Eq. 2.2c)}$$

Here $P_A(t)$ is the probability of finding A at time t; $P_{A'}(t)$, $P_B(t)$, and $P_C(t)$ are defined similarly; and $P_A(t) + P_B(t) + P_C(t) = 1$. $P_{v,A',A}(t)$ is the *conditional* probability at time t of finding A′ within the same infinitesimal volume v where A is located, provided that A is found. $P_{v,A',A}(t)$ is then

$$P_{v,A',A}(t) = \frac{P_{A',A}(t)}{V} \qquad \text{(Eq. 2.3)}$$

Here $P_{A',A}(t)$ is the *conditional* probability at time t of finding A′ within the entire space of the nanovesicle, provided that A is found; and V is the volume of the nanovesicle. Because whenever A is present, A′ is found, $P_{A',A}(t) = 1$. Therefore, $P_{v,A',A}(t) = 1/V$, which is the effective concentration (c_{eff}) of one molecule inside the nanovesicle. We then have:

$$-\frac{dP_A(t)}{dt} = -\frac{dP_{A'}(t)}{dt} = (k_1 + k_2) c_{eff} P_A(t) \qquad \text{(Eq. 2.4a)}$$

$$\frac{dP_B(t)}{dt} = k_1 c_{eff} P_A(t) \qquad \text{(Eq. 2.4b)}$$

$$\frac{dP_C(t)}{dt} = k_2 c_{eff} P_A(t) \qquad \text{(Eq. 2.4c)}$$

The initial conditions for solving these equations are $P_A(0) = P_{A'}(0) = 1$, $P_B(0) = 0$, and $P_C(0) = 0$ with $t = 0$ being the onset of each binding reaction.

We can then evaluate the probability density $f_0(\tau)$ of the dwell time τ_0. The probability of finding a particular τ_0 is $f_0(\tau)\Delta\tau$, and $f_0(\tau)\Delta\tau$ is equal to the sum of two probabilities: (1) the probability of molecule A and A′ to form B between $t = \tau$ and $\tau +$

$\Delta\tau$, which is $\Delta P_B(\tau) = k_1 c_{eff} P_A(\tau)\Delta\tau$, and (2) the probability of molecule A and A′ to form C between $t = \tau$ and $\tau + \Delta\tau$, which is $\Delta P_C(\tau) = k_2 c_{eff} P_A(\tau)\Delta\tau$. In the limit of infinitesimal $\Delta\tau$,

$$f_0(\tau) = \frac{\mathrm{d}(P_B(\tau) + P_C(\tau))}{\mathrm{d}\tau} = (k_1 + k_2) c_{eff} P_A(\tau) \qquad \text{(Eq. 2.5)}$$

Using the initial conditions to solve Eqs. 2.4a-c for $P_A(\tau)$, we get:

$$f_0(\tau) = (k_1 + k_2) c_{eff} \exp\left[-(k_1 + k_2) c_{eff} \tau\right] \qquad \text{(Eq. 2.6a)}$$

Clearly, $\int_0^\infty f_0(\tau)\mathrm{d}\tau = 1$, as expected.

The dwell time τ_0 can be further separated into two types: one $\tau_{0\to1}$ that ends with a transition to the E_1 state, and the other $\tau_{0\to2}$ that ends with a transition to the E_2 state. We can also evaluate the corresponding probability densities $f_{0\to1}(\tau)$ and $f_{0\to2}(\tau)$ of the dwell times $\tau_{0\to1}$ and $\tau_{0\to2}$. The probability of finding a particular $\tau_{0\to1}$ is $f_{0\to1}(\tau)\Delta\tau$, and $f_{0\to1}(\tau)\Delta\tau$ is equal to the probability for A and A′ to form B between $t = \tau$ and $\tau + \Delta\tau$, which is $\Delta P_B(\tau) = k_1 c_{eff} P_A(\tau)\Delta\tau$. The probability of finding a particular $\tau_{0\to2}$ is $f_{0\to2}(\tau)\Delta\tau$, and $f_{0\to2}(\tau)\Delta\tau$ is equal to the probability for A and A′ to form C between $t = \tau$ and $\tau + \Delta\tau$, which is $\Delta P_C(\tau) = k_2 c_{eff} P_A(\tau)\Delta\tau$. In the limit of infinitesimal $\Delta\tau$.

$$f_{0\to1}(\tau) = \frac{\mathrm{d}P_B(\tau)}{\mathrm{d}\tau} = k_1 c_{eff} \exp\left[-(k_1 + k_2) c_{eff} \tau\right] \qquad \text{(Eq. 2.6b)}$$

$$f_{0\to2}(\tau) = \frac{\mathrm{d}P_C(\tau)}{\mathrm{d}\tau} = k_2 c_{eff} \exp\left[-(k_1 + k_2) c_{eff} \tau\right] \qquad \text{(Eq. 2.6c)}$$

Expectedly, $f_{0\to1}(\tau) + f_{0\to2}(\tau) = f_0(\tau)$. Note the exponential decay constants of $f_{0\to1}(\tau)$ and $f_{0\to2}(\tau)$ are the same as that of $f_0(\tau)$, all equal to $(k_1+k_2)c_{eff}$, the sum of the two

parallel kinetic processes in Scheme 2.1. The ratio between the total occurrence $N_{0\to1}$ of dwell time $\tau_{0\to1}$ and the total occurrence $N_{0\to2}$ of dwell time $\tau_{0\to2}$ in the smFRET trajectories also carries important information:

$$\frac{N_{0\to1}}{N_{0\to2}} = \frac{\int_0^\infty f_{0\to1}(\tau)\mathrm{d}\tau}{\int_0^\infty f_{0\to2}(\tau)\mathrm{d}\tau} = \frac{k_1}{k_2} \qquad \text{(Eq. 2.6d)}$$

Similarly, we can derive the probability density function of the dwell time τ_1 on the E_1 state, which can be separated into two types: $\tau_{1\to0}$ and $\tau_{1\to2}$, and that of the dwell time τ_2 on the E_2 state, which can be separated into $\tau_{2\to0}$ and $\tau_{2\to1}$. The results are:

$$f_1(\tau) = (k_{-1} + k_3)\exp\left[-(k_{-1} + k_3)\tau\right] \qquad \text{(Eq. 2.7a)}$$

$$f_{1\to0}(\tau) = k_{-1}\exp\left[-(k_{-1} + k_3)\tau\right] \qquad \text{(Eq. 2.7b)}$$

$$f_{1\to2}(\tau) = k_3\exp\left[-(k_{-1} + k_3)\tau\right] \qquad \text{(Eq. 2.7c)}$$

$$\frac{N_{1\to0}}{N_{1\to2}} = \frac{k_{-1}}{k_3} \qquad \text{(Eq. 2.7d)}$$

$$f_2(\tau) = (k_{-2} + k_{-3})\exp\left[-(k_{-2} + k_{-3})\tau\right] \qquad \text{(Eq. 2.8a)}$$

$$f_{2\to0}(\tau) = k_{-2}\exp\left[-(k_{-2} + k_{-3})\tau\right] \qquad \text{(Eq. 2.8b)}$$

$$f_{2\to1}(\tau) = k_{-3}\exp\left[-(k_{-2} + k_{-3})\tau\right] \qquad \text{(Eq. 2.8c)}$$

$$\frac{N_{2\to0}}{N_{2\to1}} = \frac{k_{-2}}{k_{-3}} \qquad \text{(Eq. 2.8d)}$$

Equations (Eq. 2.6a-d), (Eq. 2.7a-d), and (Eq. 2.8a-d) can be used to fit the corresponding experimental results to obtain the rate constants. The Figure 2.4C caption gives the determined rate constants for each of the kinetic steps in the Hah1-

MBD4 interaction, from which the K_D's of the interaction complexes can be calculated. In ensemble-averaged measurements, if the two interaction complexes cannot be differentiated but are detectable, the measured effective dissociation constant ($K_{D,eff}$) is related to the K_D's of the two complexes as $1/K_{D,eff} = 1/K_{D1} + 1/K_{D2}$.

2.6. Further developments

A limitation of using Egg PC for forming nanovesicles is the enclosed environment that prevents facile exchange of solution. Being able to change the solution condition and introduce additional chemical reagents is highly desired, however. Ha and coworkers have developed two strategies to make the nanovesicles porous to allow exchange of solution into the nanovesicles [20]: (1) Using a lipid with a higher T_m and performing experiments at its T_m, which induces defects in the lipid membrane. (2) Incorporating into the bilayer membrane the bacterial toxin α-hemolysin that forms pores.

The first strategy is based on the fact that lipid bilayer membranes form packing defects at T_m, making the membrane permeable to small molecules [33, 34]. Ha and coworkers used the lipid DMPC (1,2-dimyristoyl-*sn*-glycero-3-phosphocholine), which has a T_m of ~23°C. They showed that at ~23°C, the nanovesicles made of DMPC lipid membranes are permeable to molecules as large as ATP, but not to macromolecules such as proteins and DNA. The second strategy uses the natural pore-forming ability of the membrane protein α-hemolysin, a heptameric transmembrane channel from *Staphylococcus aureus*. The monomers of α-hemolysin self-assemble into the heptameric channel structure in a lipid bilayer, forming a stable pore of 1.4 – 2.4 nm diameter and allowing exchange of most solution components [35].

The lipid membrane of the nanovesicles also provides a natural platform for studying protein interactions that involve membrane-bound or membrane-anchored

proteins. To do so, one can incorporate or anchor one protein to the lipid membrane of the nanovesicle and trap the other protein inside. SmFRET measurements can then be employed to monitor their interactions at high effective concentrations.

The confined volume of the nanovesicles can also be exploited to probe the crowding effects on protein interactions by co-trapping a larger number of different types of unlabeled macromolecules inside, for example polysaccharides. This crowding effect arguably mimics the intracellular environment, offering an opportunity to study biomacromolecule dynamics in a controlled and confined environment in vitro.

2.7. Concluding remarks

Nanovesicle trapping is a convenient approach to enable single-molecule studies at high effective concentrations. This approach also offers easy surface immobilization and minimization of nonspecific interactions with glass surfaces. Coupled with smFRET measurements, dynamic events of protein interactions with weak affinity can be monitored in real-time at the single-molecule level. Single-molecule kinetic analysis allows extraction of quantitative kinetics of the protein interactions, some of which are challenging to quantify with ensemble techniques. The lipid membrane also mimics the cellular environment, as well as provides a natural platform for studying membrane-bound or membrane–anchored proteins. The confined volume can further be exploited to study crowding effects on macromolecule dynamics at the single-molecule level. With porous vesicles allowing solution exchange, many biological processes can be studied at high effective concentrations in situ. We expect that more biological studies using the nanovesicle trapping approach will emerge.

2.8. Acknowledgements

Thanks are due to Profs. D. L. Huffman and A. R. Rosenzweig for their collaboration. Professor Huffman's group provided the MBD4 expression plasmid and the size exclusion column used in the purification of the labeled proteins. Professor Rosenzweig's group provided the Hah1 expression plasmid. Aaron M. Keller from the Chen Group at Cornell University provided the control experiment to differentiate the dissociated state from the photobleached state. This research is supported by the National Science Foundation (CHE0645392), National Institute of Health (GM082939), the Wilson Disease Association, a Camille and Henry Dreyfus New Faculty Award, an Alfred P. Sloan Fellowship, and Cornell University. J.J.B. and A.M.K. are supported by Molecular Biophysics Traineeships from the National Institute of Health.

REFERENCES

1.Gragerov, A.; Nudler, E.; Komissarova, N.; Gaitanaris, G. A.; Gottesman, M. E.; Nikiforov, V., Cooperation of GroEL/GroES and DnaK/DnaJ heat shock proteins in preventing protein misfolding in *Escherichia coli*. *Proc. Natl. Acad. Sci. U.S.A.* **1992,** *89*, 10341-10344.

2.Hall, A., Ras-related GTPases and the Cytoskeleton. *Mol. Biol. Cell* **1992,** *3*, 475-479.

3.Huffman, D. L.; O'Halloran, T. V., Function, Structure, and Mechanism of Intracellular Copper Trafficking Proteins. *Ann. Rev. Biochem.* **2001,** *70*, 677-701.

4.Nooren, I. M. A.; Thornton, J. M., Diversity of protein-protein interactions. *EMBO J.* **2003,** *22*, 3486-3492.

5.Cobine, P. A.; Pierrel, F.; Winge, D. R., Copper trafficking to the mitochondrion and assembly of copper metalloenzymes. *Biochim. Biophys. Acta* **2006,** *1763*, 759-772.

6.Rosenzweig, A. C., Copper Delivery by Metallochaperone Proteins. *Acc. Chem. Res.* **2001,** *34*, 119-128.

7.Banci, L.; Rosato, A., Structural genomics of proteins involved in copper homeostasis. *Acc. Chem. Res.* **2003,** *36*, 215-221.

8.Lutsenko, S.; LeShane, E. S.; Shinde, U., Biochemical Basis of Regulation of Human Copper-Transporting ATPase. *Arch. Biochem. Biophys.* **2007,** *463*, 134-148.

9.Strausak, D.; Howies, M. K.; Firth, S. D.; Schlicksupp, A.; Pipkorn, R.; Multhaup, G.; Mercer, J. F. B., Kinetic Analysis of the Interaction of the Copper Chaperone Atox1 with the Metal Binding Sites of the Menkes Protein. *J. Biol. Chem.* **2003,** *278*, 20821-20827.

10.Kim, B.-E.; Nevitt, T.; Thiele, D. J., Mechanisms for Copper Acqusition, Distribution and Regulation. *Nat. Chem. Biol.* **2008,** *4*, 176-185.

11.Laurence, T. A.; Weiss, S., How to Detect Weak Pairs. *Science* **2003,** *299*, 667-668.

12.Levene, M. J.; Korlach, J.; Turner, S. W.; Foquet, M.; Craighead, H. G.; Webb, W. W., Zero-Mode Waveguide for Single-Molecule Analysis at High Concentration. *Science* **2003,** *299*, 682-686.

13.Chiu, D. T.; Wilson, C. F.; Karlsson, A.; Danielsson, A.; Lundqvist, A.; Strömberg, A.; Ryttsén, F.; Davidson, M.; Nordholm, S.; Orwar, O.; Zare, R. N., Manipulating the biochemical nanoenvironment around single molecules contained within vesicles. *Chem. Phys.* **1999,** *247*, 133-139.

14.Boukobza, E.; Sonnenfeld, A.; Haran, G., Immobilization in Surface-Tethered Lipid Vesicles as a New Tool for Single Biomolecule Spectroscopy. *J. Phys. Chem. B.* **2001,** *105*, 12165-12170.

15.Rhoades, E.; Gussakovsky, E.; Haran, G., Watching proteins fold one molecule at a time. *Proc. Natl. Acad. Sci. U.S.A.* **2003,** *100*, 3197-3202.

16.Haran, G., Single-molecule fluorescence spectroscopy of biomolecular folding. *J. Phys.: Condens. Matter* **2003,** *15*, R1291-R1317.

17.Rhoades, E.; Cohen, M.; Schuler, B.; Haran, G., Two-State Folding Observed in Individual Protein Molecules. *J. Am. Chem. Soc.* **2004,** *126*, 14686-14687.

18.Okumus, B.; Wilson, T. J.; Lilley, D. M. J.; Ha, T., Vesicle Encapsulation Studies Reveal that Single Molecule Ribozyme Heterogeneities Are Intrinsic. *Biophys. J.* **2004,** *87*, 2798-2806.

19.Lee, J. Y.; Okumus, B.; Kim, D. S.; Ha, T., Extreme Conformational Diversity in Human Telomeric DNA. *Proc. Natl. Acad. Sci. U.S.A.* **2005,** *102*, 18938-18943.

20.Cisse, I.; Okumus, B.; Joo, C.; Ha, T., Fueling Protein-DNA Interactions inside Porous Nanocontainers. *Proc. Natl. Acad. Sci. U.S.A.* **2007,** *104*, 12646-12650.

21.Benitez, J. J.; Keller, A. M.; Ochieng, P.; Yatsunyk, L. A.; Huffman, D. L.; Rosenzweig, A. C.; Chen, P., Probing Real-time Transient Metallochaperone-Target Protein Interactions at the Single-Molecule Level with Nanovesicle Trapping. *J. Am. Chem. Soc.* **2008,** *130*, 2446-2447.

22.Benitez, J. J.; Keller, A. M.; Ochieng, P.; Yatsunyk, L. A.; Huffman, D. L.; Rosenzweig, A. C.; Chen, P., Correction/Addition: Probing Real-time Transient Metallochaperone-Target Protein Interactions at the Single-Molecule Level with Nanovesicle Trapping. *J. Am. Chem. Soc.* **2009,** *131*, 871.

23.Silvius, J. R., Thermotropic Phase Transition of Pure Lipids in Model Membranes and Their Modification by Membrane Proteins. In *Lipid-Protein Interactions*, Jost, P. C.; Griffish, O. H., Eds. Wiley Press: New York, 1983; pp 239-281.

24.Hope, M. J.; Bally, M. B.; Webb, G.; Cullis, P. R., Production of large unilamellar vesicles by a rapid extrusion procedure. Characterization of size distribution, trapped

volume and ability to maintain a membrane potential. *Biochim. Biophys. Acta* **1985,** *812*, 55-65.

25.Johnson, J. M.; Ha, T.; Chu, S.; Boxer, S. G., Early Steps of supported Bilayer Formation Probed by Single Vesicle Fluorescence Assays. *Biophys J.* **2002,** *83*, 3371-3379.

26.MacDonald, R. C.; MacDonald, R. I.; Menco, B. E.; Takeshita, K.; Subbarao, N. K.; Hu., L. R., Small-volume extrusion apparatus for preparation of large, unilamellar vesicles. *Biochim. Biophys. Acta* **1991,** *1061*, 297-303.

27.Boxer, S. G., Molecular Transport and Organization in Supported Lipid Membranes. *Curr. Opin. Cell. Biol.* **2000,** *4*, 704-709.

28.Brian, A. A.; McConnell, H. M., Allogeneic Stimulation of Cytotoxic T Cells by Supported Planar Mambranes. *Proc. Natl. Acad. Sci. USA* **1984,** *81*, 6159-6163.

29.Rasnik, I.; McKinney, S. A.; Ha, T., Surfaces and Orientations: Much to FRET about? *Acc. Chem. Res.* **2005,** *38*, 542-548.

30.Rasnik, I.; McKinney, S. A.; Ha, T., Nonblinking and Long-lasting Single Molecule Fluorescence Imaging. *Nature Methods* **2006,** *3*, 891-893.

31.Xie, X. S., Single-Molecule Approach to Enzymology. *Single Mol.* **2001,** *2*, 229-236.

32.Xu, W.; Kong, J. S.; Chen, P., Single-Molecule Kinetic Theory of Heterogeneous and Enzyme Catalysis. *J. Phys. Chem. C* **2009,** *113*, 2393-2404.

33.Chakrabarti, A. C.; Deamer, D. W., Permeability of Lipid Bilayers to Amino Acids and Phosphate. *Biochim. Biophys. Acta* **1992,** *1111*, 171-177.

34.Monnard, P.-A., Liposome-Entrapped Polymerases as Models for Microscale/Nanoscale Bioreactors. *J. Membrane Biol.* **2003,** *191*, 87-97.

35.Song, L.; Hobaugh, M. R.; Shustak, C.; Cheley, S.; Bayley, H.; Gouaux, J. E., Structure of staphylococcal -hemolysin a heptameric transmembrane pore. *Science* **1996,** *274*, 1859-1865.

CHAPTER 3

Probing transient copper chaperone-Wilson disease protein interactions at the single-molecule level with nanovesicle trapping [*]

***** Benitez, J. J.; Keller, A. M.; Ochieng, P.; Yatsunyk, L. A.; Huffman, D. L.; Rosenzweig, A. C.; Chen, P., Probing Transient Copper chaperone-Wilson Disease Protein Interactions at the Single-Molecule Level with Nanovesicle Trapping. *J. Am. Chem. Soc.* **2008,** *130*, 2446-2447. Benitez, J. J.; Keller, A. M.; Ochieng, P.; Yatsunyk, L. A.; Huffman, D. L.; Rosenzweig, A. C.; Chen, P., Correction/Addition: Probing Real-time Transient Metallochaperone-Target Protein Interactions at the Single-Molecule Level with Nanovesicle Trapping. *J. Am. Chem. Soc.* **2009,** *131*, 871. Reproduced with permission from the *Journal of the American Chemical Society*

3.1. Abstract

Transient metallochaperone-target protein interactions are essential for intracellular metal trafficking, but challenging to study at both the ensemble and the single-molecule level. Here we report using nanovesicle trapping to enable single-molecule fluorescence resonance energy transfer (smFRET) studies of transient interactions between the copper chaperone Hah1 and the fourth metal-binding domain of its target protein, the Wilson disease protein (WDP). We were able to monitor their interactions in real time one event at a time, capture distinct protein interaction intermediates, resolve intermediate interconversion dynamics, and quantify both the interaction kinetics and thermodynamics in the absence of copper. The study exemplifies the ability of nanovesicle trapping in combination with smFRET for studying weak protein interactions, and provides insight into how Hah1 and WDP may collaborate to mediate copper transfer inside cells.

3.2. Introduction

Metals are essential nutrients that can also be toxic. Safe trafficking of metal ions is necessary inside cells, and specific metal transport pathways exist to deliver them to their destinations.[1-4] In human cells, the copper chaperone Hah1 and the Wilson disease protein (WDP) constitute a copper transport pathway—Hah1 is a single-domain cytoplasmic protein; WDP is a multidomain protein anchored on organelle membranes and has a cytosolic N-terminal region consisting of six homologous metal-binding domains (MBDs). All WDP MBDs and Hah1 contain a conserved CXXC motif that binds Cu^{1+}, and Cu^{1+} is transferred from Hah1 to a WDP MBD via *direct and specific* Hah1-MBD interactions.[1, 2, 5, 6]

Although the MBDs of WDP have different functional roles,[6-9] all of them, as well as Hah1, have similar Cu^{1+} binding affinities.[5] This similarity indicates that the Hah1 to WDP Cu^{1+} transfer is under kinetic control mediated by Hah1-WDP interactions, and that the functional differences among WDP MBDs are not defined by their Cu^{1+} binding abilities but may be related to *how* each MBD interacts with Hah1. Very limited quantitative information is available, however, on the Hah1-WDP interaction dynamics. This is partly because the Hah1-WDP interactions are transient, and transient interactions are difficult to quantify in ensemble-averaged experiments.

Here we report using nanovesicle trapping and single-molecule fluorescence resonance energy transfer (smFRET) measurements to probe the transient interactions between Hah1 and the fourth MBD (MBD4) of WDP in real time. We chose MBD4 as a representative WDP MBD because it is known to interact with Hah1 directly for Cu^{1+} transfer.[6, 10, 11] Quantification of Hah1-MBD4 interaction dynamics will help understand how Hah1 and the full length WDP interact for Cu^{1+} transfer.

3.3. Experimental

3.3.1. Protein engineering, expression, purification, and quantitation

The Hah1 gene, cloned into a pET21b vector (Novagen),[12] was modified via site directed mutagenesis to produce a Cys41 → Ser mutation (forward primer: 5'-CCC AAC AAG AAG GTC **TCA** ATT GAA TCT GAG CAC-3'; reverse primer: 5'-GTG CTC AGA TTC AAT **TGA** GAC CTT CTT GTT GGG-3'. The mutations are indicated in bold face.) The resulting gene was amplified by PCR using primers containing a cysteine inserted at the C-terminal (Cys69) (forward primer: 5'-TAA TAC GAC TCA CTA TAG GG-3'; reverse primer: 5'-GGA GCT CGA ATT CTA **GCA** CTC AAG GCC AAG GTA GG-3'. The insertion is indicated in bold face. Underlined is the EcoRI restriction site.) and reinserted into an empty pET21b

between the restriction sites of EcoRI and NdeI to generate the final Hah1 mutant. Cloning was performed in the cell strain NovaBlue or DH5α. All mutations were confirmed by DNA sequencing (Biotechnology Resource Center, Cornell University).

The mutant Hah1 was expressed in BL21(DE3) cells,[12] which were grown to a optical density of 0.8 – 1.1 at 600 nm and induced with 1 mM IPTG. Cells were lysed via freeze/thaw cycles, and proteins were purified from the lysate via anion exchange (HiTrap Q HP), cation exchange (HiTrap SP HP), and gel filtration (HiLoad 26/60 Superdex 200 prep grade) chromatography using a GE FPLC system. The protein purity was determined by SDS-PAGE and the identity was confirmed by mass spectrometry. The protein was stored in 20 mM MES, pH 6.0, 150 mM NaCl, 20% Glycerol.

The wild type MBD4 gene in pET24d[6] was amplified by PCR using primers containing Cys4 → Ser mutation and a C-terminal cysteine insertion (Cys76) (Forward primer: 5'-TAG TAG GGC GCG CCA ATG GGC ACA **TCG** AGT ACC ACT C-3'; reverse primer: 5'-ATT TGA GGC TTC AGT CGT TTC TGA ATG CTG AAG CTT TAG TAG-3'. The insertion is indicated in bold face. AscI and HindIII sites are underlined.) The mutant gene was then cloned between the AscI and HindIII restriction sites of a pET24b vector bearing a 15-residue AviTag!^{TM} sequence (Avidity)[13] inserted between NdeI and HindIII sites, resulting an AviTag fused to the N-terminal of the mutant MBD4. This peptide sequence renders the expression of the mutant MBD4 gene, which does not express well alone, and can also be biotinylated specifically for immobilization if needed. All mutations were confirmed by DNA sequencing.

The mutant MBD4 was expressed in Rosetta(DE3) cells as described.[6] Briefly, cells were grown to an optical density of 0.6 at 600 nm and induced with 0.5 mM IPTG. Cells were lysed via freeze/thaw cycles and proteins were purified from the

lysate through anion exchange and gel filtration chromatography. The protein purity was checked by SDS-PAGE and the identity was confirmed by mass spectrometry. The protein was stored in 20 mM MES, pH 6.0, 150 mM NaCl, 20% Glycerol.

Protein concentrations were quantified using BCA and Bradford protein assays using BSA as a standard (Pierce), and the thiol quantitation method (Molecular Probes). Copper concentrations were quantified using a BCA-based method by Brenner and Harris and with $[Cu(CH_3CN)_4]PF_6$ (Aldrich) or copper atomic absorption standard solution (Acros Organics) as the standard.[14]

The copper transfer assay was done according to the literature procedures.[5, 15, 16] Briefly, the Cu^{1+}–loaded Cy5-Hah1 was mixed with the apo Cy3-MBD4 and incubated at room temperature for 30 minutes. Then the proteins were separated using anion-exchange chromatography (Amersham Tricorn Mono Q 5/50 GL). We then quantitated the protein concentrations by measuring the absorbance of the Cy3 and Cy5 labels and using their extinction coefficients. The extinction coefficients of Cy3 (113,400 ± 800 $M^{-1}cm^{-1}$ at 549 nm) and Cy5 (171,000 ± 2000 $M^{-1}cm^{-1}$ at 646 nm) were determined in the same buffer solution (20 mM MES, 150 mM NaCl, pH 6.0) as that for protein samples.

3.3.2. Protein labeling and purification

Mutant Hah1, at a concentration of 500 μM, was initially treated with 5 mM TCEP in 100 mM pH 7.0 phosphate buffer for 30 minutes to fully reduce all disulfide bonds. $[Cu^{I}(CH_3CN)_4]PF_6$ was then added to a final concentration of 1 mM and incubated for 30 minutes to bind to the metal binding cysteines in the CXXC motif to protect these cysteines from labeling. Cy5 maleimide mono reactive dye (Amersham Biosciences), in DMSO, was then added to a final concentration of 2 mM (4 equivalents) and the reaction was incubated for 4 hours at room temperature followed

by gentle rocking overnight at 4°C. The reaction was then quenched by adding an excess of β-mercaptoethanol (Sigma) and incubated for one hour to ensure all unreacted dye was quenched. The reaction mixture was then treated with a ten-fold excess of KCN (J.T. Baker) over copper concentration to chelate out most of the Cu^{1+} bound to Hah1. Free dye and CN^- chelated Cu^{1+} were removed by size exclusion chromatography (Superdex Peptide HR 10/30, Amersham Biosciences). Labeled and unlabeled protein species were then separated by anion exchange chromatography (Tricorn Mono Q 5/50 GL, Amersham Biosciences). The labeled protein was further treated with three cycles of incubation with 200 equivalents of BCA and membrane centrifugation filtration to remove the residual protein bound Cu^{1+}.

Labeling procedure of the mutant MBD4 with Cy3 was parallel to that for the mutant Hah1 with a few exceptions. Instead of protecting the metal binding cysteines in the CXXC motif with Cu^{1+}, Hg^{2+} ($Hg(NO_3)_2$) was used. In addition, 12 equivalents of Cy3 (6 mM) were added to the protein in small aliquots. We removed Hg^{2+} bound to MBD4 after labeling using three cleaning cycles; each cycle includes incubation with 5 equivalents of EDTA followed by membrane centrifugation filtration to removed EDTA-Hg^{2+}.

3.3.3. Labeling specificity confirmation

Labeling specificity was determined by trypsin digestion of the modified proteins. The proteins to be digested were mixed in equal amounts with 1:1 tert-butanol:H_2O and heat-denatured for 10 minutes at 65 °C. The solution was then diluted 6 times with 50 mM NH_4HCO_3 pH 7.6. Trypsin (0.1μg/μL) (Roche) was subsequently added and incubated for 24 hours at 37 °C. Peptide fragments were then buffer exchanged to 70% acetonitrile, 4% acetic acid and 26% H_2O for MS analysis. The peptide fragments of mutant Hah1 were analyzed by LC-MS (LCMS-QP8000α,

Shimadzu). Peptide fragments of mutant MBD4 were analyzed using MALDI mass spectrometry at the Protein Structure Facility at University of Michigan.

3.3.4. Nanovesicle trapping

Nanovesicle trapping was performed following literature procedures.[17-19] A mixture of L-α-phosphatidylcholine (eggPC) and 1% 1,2-dipalmitoyl-*sn*-glycero3-phosphoethanolamine-N-(cap biotinyl) (16:0 biotinyl cap PE) (Avanti Lipids) in chloroform was dried under a constant flow of nitrogen. For preparing the bilayer support, lipids were hydrated with standard lipid buffer (10 mM Tris-HCl, pH 7.4, 150 mM NaCl, 1 mM EDTA) to form multilamellar vesicles at a concentration of 5 mg/mL total lipids. Protein loaded vesicles were prepared by hydrating the lipid film with solutions containing 3 μM Cy5-Hah1, 3 μM Cy3-MBD4, 1 mM Trolox (Sigma), and 1 mM TCEP (Sigma) in 20 mM MES, 150 mM NaCl, pH 6.0 buffer, followed by seven freeze-thaw cycles to increase the encapsulation efficiency. Protein integrity after freeze-thaw cycles was confirmed by circular dichroism spectroscopy. The solution was then repeatedly extruded through a polycarbonate membrane with 100 nm pores (Avanti Mini Extruder) to form 100-nm diameter unilamellar vesicles encapsulating proteins. Loaded vesicles were used for experiments immediately or within 48 hours from preparation.

3.3.5. Single-molecule experiments

Single-molecule fluorescence measurements were performed on a homebuilt prism-type total internal reflection microscope based on an Olympus IX71 inverted microscope. A continuous wave circularly polarized 532 nm laser beam (CrystaLaser, GCL-025-L-0.5%) of 1-5 mW was focused onto an area of ~150 × 75 μm^2 on the sample to directly excite the Cy3 probe. To directly excite Cy5 fluorescence, a linearly

polarized 637 nm laser (CrystaLaser) was used. The fluorescence of Cy3 and Cy5 was collected by a 60X NA1.2 water-immersion objective (UPLSAPO60XW, Olympus), filtered to reject laser light (HQ550LP), and split by a dichroic mirror (635DCXR) into two channels using a Dual-View® system (Optical Insights, Inc). Each channel of fluorescence was further filtered (HQ580-60m or HQ660LP) and projected onto half of the imaging area of a camera (Andor iXon EMCCD, DV887DCS-BV), controlled by an Andor IQ software. All optical filters are from Chroma Technology Corp. Single-molecule fluorescence images and movies were taken with the Andor-IQ software.

A flow cell, formed by double-sided tape placed between a quartz slide (Technical Glass or Finkenbeiner) and a boronsilicate coverslip (Gold Seal®), was used to hold aqueous sample solutions for single-molecule fluorescence measurements. All samples were in 20 mM MES, pH 6.0, 150 mM NaCl unless indicated otherwise. To form the bilayer support, unloaded vesicles were flowed in at 5 mg/mL (500 μL) and incubated for 1 to 2 hours. Excess lipids were washed away with standard lipid buffer. Alternatively, the slides were first amine-functionalized (Vectabond, Vector Laboratories) and then coated with PEG polymers (100 mg/mL m-PEG-SPA-5000 and 1 mg/mL biotin-PEG-NHS-3400, Nektar Therapeutics).[20, 21] 1% of the PEG polymers contain a biotin terminal group to form biotin-streptavidin (Molecular Probes) linkages. 500 μL of streptavidin at a concentration of 0.2 mg/mL was then flowed in and incubated for 10 minutes. Unbound streptavidin was then washed out with buffer containing 0.1 mg/mL BSA, which help to block nonspecific binding sites.[22] Protein-loaded vesicles were flowed in at a total protein concentration of 30 pM and unbound vesicles were then washed out before single-molecule imaging experiments. An oxygen scavenging system (0.1 mg/mL glucose oxidase (Sigma), 0.025 mg/mL catalase (Roche), 4% glucose (Aldrich)) and 1 mM Trolox (Sigma)[23]

was added into the sample solution just before each experiment to prolong the lifetime of the fluorescence probes, and was refreshed during experiments every half an hour.

3.4. Results and analysis

A primary obstacle in single-molecule experiments to probe transient protein interactions is the low concentrations (10^{-12}-10^{-9} M) commonly used to spatially separate molecules for detection, which limits the experiments to strong protein interactions. Weak protein interactions, including Hah1-WDP interactions, need to be studied at higher concentrations. Nonspecific protein-glass surface interactions during molecule immobilization present another challenge, and must be minimized.

To overcome these challenges, we adapted a nanovesicle trapping strategy, which was used to study protein and RNA folding and DNA-protein interactions at the single-molecule level.[19, 24] We trapped the two interacting molecules in a 100-nm-diameter lipid vesicle. Because of the confined volume (~5×10^{-19} L), the effective concentration is ~3 μM for each protein inside. Low concentrations of vesicles are then immobilized on a lipid bilayer or polymer coated glass surface so protein-glass interactions are eliminated.

To report Hah1-MBD4 interactions by smFRET, we introduced a C-terminal cysteine in both Hah1 and MBD4 and labeled this cysteine of Hah1 with Cy5 and that of MBD4 with Cy3. Cy3-Cy5 form a FRET pair with a Förster radius of ~6 nm. The cysteines in the CXXC motifs were protected specifically from labeling. We purified the labeled proteins and confirmed their Cu^{1+} binding and transfer functions (see Supporting Information (SI)).

We used total internal reflection fluorescence microscopy with 532-nm laser excitation to measure smFRET of single interacting pairs of Cy5-Hah1 and Cy3-MBD4 trapped in nanovesicles. We only analyzed data from vesicles containing one

Cy5-Hah1 and one Cy3-MBD4 (see SI). This way we also eliminated the complication of dimeric or multimeric interactions between molecules of the same type, which are unavoidable in ensemble experiments and complicate protein-interaction studies. This is particularly relevant in studying Hah1-WDP interactions, as Hah1 could form homodimers.[12]

The fluorescence and the corresponding FRET efficiency (E_{FRET}) trajectories of two interacting pairs of Hah1 and MBD4 molecules are shown in Figure 3.1A and 3.1B. The Cy3 and Cy5 fluorescence of each pair show anticorrelated intensity fluctuations, reporting transient Hah1-MBD4 interactions. Three E_{FRET} states are clear in the E_{FRET} trajectories at E_{FRET} ~0.2, 0.5, and 0.9, denoted as E_0, E_1 and E_2, respectively. E_0 is clearly different from that (<0.1) of the acceptor photobleached or blinked state. Considering the small dimensions of Hah1 and MBD4 (2~3 nm),[6, 12, 25] the small value of E_0 indicates Hah1 and MBD4 are distant from each other; we thus associated E_0 with their dissociated state (see section 3.4.1). The values of E_1 and E_2 indicate the two proteins are within a few nanometers in these two states; we thus associated E_1 and E_2 with two transient Hah1-MBD4 interaction complexes (see section 3.4.1 and Figure 3.3). The significant difference between E_1 and E_2 indicate the Cy3-Cy5 distances differ by nanometers between the two complexes, which can arise from their differences in overall interaction geometries or in the conformation of one or both proteins. The latter is less likely as NMR studies showed Hah1 only has angstrom-scale conformational flexibilities,[26] which should not result in significant

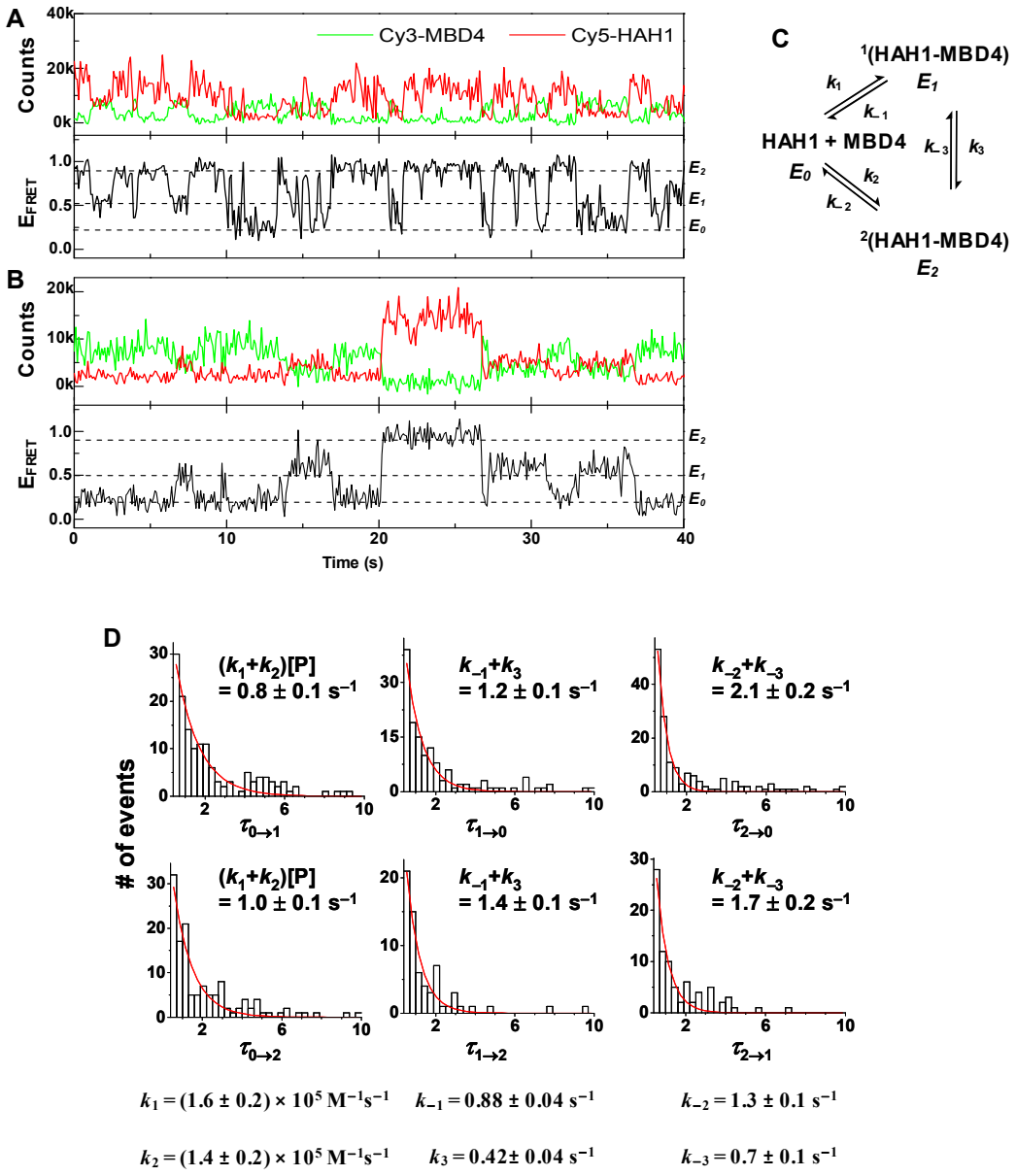

Figure 3.1. Single-molecule trajectories, interaction scheme and dwell-time distributions. (A), (B) Fluorescence and E_{FRET} (= $I_{Cy5}/(I_{Cy3}+I_{Cy5})$) trajectories of two interacting Cy5-Hah1 and Cy3-MBD4 pairs. (C) Hah1-MBD4 interaction scheme. (D) Waiting time (τ) distributions for the six kinetic steps in (C). Data compiled from 163 Hah1-MBD4 interacting pairs and total 1101 transitions. Solid lines are exponential fits.

difference in E_{FRET} that is sensitive only at the nanometer scale. The NMR structure of the fourth MBD of the Wilson protein has only angstrom–scale conformational flexibility as well.[27] The direct resolution of two distinct interaction complexes here is the first evidence that multiple interaction intermediates exist for metallochaperone-target protein interactions and that Hah1 can form complexes with WDP without Cu^{1+}. We have further confirmed that nonspecific interactions between the proteins and the lipids are minimal and the protein interactions are not induced by the labeling (see SI).

In the E_{FRET} trajectories, the transitions between E_0 and E_1 and between E_0 and E_2 reflect the Hah1-MBD4 association and dissociation events, while those between E_1 and E_2 are the interconversions between the two interaction complexes. Figure 3.1C shows the Hah1-MBD4 interaction scheme deduced from the smFRET data. The six rate constants in the scheme are obtainable from the statistical distributions of the six types of waiting times before each E_{FRET} transition (Figure 3.1D; see SI). All waiting time distributions can be fitted with single-exponential decays. For Hah1-MBD4 complex dissociations and interconversions, which are unimolecular reactions, the rate constants can be obtained from the decay constants of the E_1 and E_2 dwell-time distributions. For protein association, the effective concentration (~3 μM) of a molecule in a nanovesicle needs to be factored out from the decay constants to obtain the combination of rate constants. The determined rate constants are $\sim 10^0$ s^{-1} for complex dissociations and interconversions, and $\sim 10^5$ $M^{-1}s^{-1}$ for protein associations (Figure 3.1D). Particularly, we have directly resolved the interconversion dynamics between the two interaction complexes and quantified the rate constants of both the forward and the reverse reactions—ensemble studies of intermediate interconversion dynamics typically only obtain the sum of the forward and reverse rate constants. The rate constants also enabled determination of separate dissociation constants for the two interaction complexes with $K_1 = 5.6 \pm 0.6$ μM and $K_2 = 9 \pm 1$ μM (see also Figure 3.2).

Figure 3.2 shows the compiled histograms of E_{FRET} trajectories of many interaction pairs of Cy3-MBD4 and Cy5-Hah1. The histogram shows three peaks at ~0.2, 0.5, and 0.9, corresponding to E_0, E_1, and E_2, respectively. The relative areas of these three peaks represent the relative stability of the dissociated state, complex 1, and complex 2; the calculated dissociated constants are K_1 ~5 ± 1 μM and K_2 = 8 ± 2 μM, consistent with those calculated from the kinetic constants (Figure 3.1D).

3.5. Discussion

The ability of Hah1 and MBD4 to form multiple interaction complexes with different interaction geometries has functional significance. First, it increases the probability of complex formation when Hah1 and WDP encounter through diffusion inside cells. The formed complex may proceed to accomplish Cu^{1+} transfer, or, if unproductive, convert to another complex for Cu^{1+} transfer. Second, it raises the possibility of Hah1 interacting with two WDP MBDs simultaneously and hence cooperative effects among WDP MBDs for Cu^{1+} transfer. The interactions of Hah1 with different combinations of MBDs may also play a role in the functional differences of these MBDs.

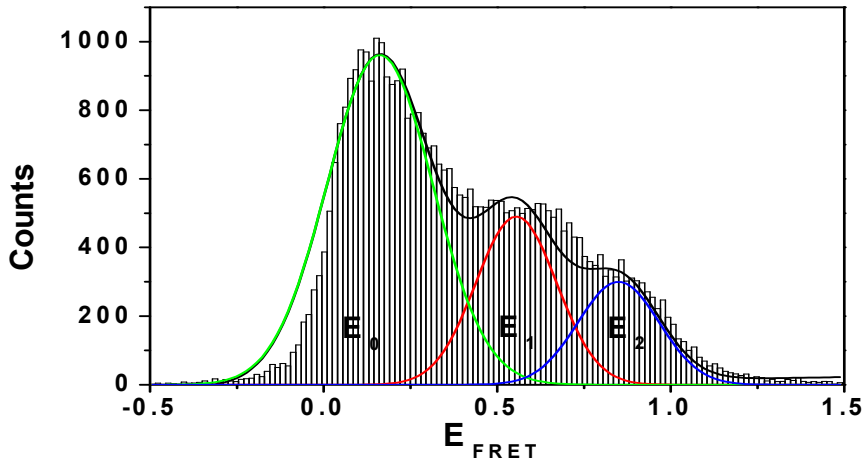

Figure 3.2. Compiled histogram of E_{FRET} trajectories of Hah1-MBD4 interacting pairs (163 trajectories), showing three peaks corresponding to E_0, E_1, and E_2 states. The solid lines are fits with three Gaussian functions centered at ~0.16 ± 0.15, 0.55 ± 0.12, 0.84 ± 0.12 (the errors here are standard deviations). The relative areas of these three peaks represent the relative stabilities of the dissociated state, complex 1, and complex 2; the calculated dissociation constants are K_1 ~5 ± 1 μM and K_2 = 8 ± 2 μM, consistent with those calculated from the kinetic constants. The trajectories are truncated at the photobleaching step of either label.

3.5.1. Further discussions of the E_{FRET} states for Hah1-MBD4 interactions

The control experiments using Cy5-Hah1 with free Cy3 and using Cy3-MBD4 with free Cy5 co-trapped in a nanovesicle also provide references for the Hah1 and MBD4 dissociated state. For both control experiments, the E_{FRET} values obtained from the fluorescence trajectories are ~0.17, same as E_0 (see Figure 3.2 above). This confirms that E_0 is the dissociated state of Hah1 and MBD4.

As further controls and to calibrate the apparent E_{FRET} values (approximated as $I_{Cy5}/(I_{Cy5}+I_{Cy3})$), we used the data from our single-molecule FRET studies of a DNA Holliday junction.[28] This DNA Holliday junction has two stacked conformations at dynamic equilibrium with each other. With Cy3 and Cy5 labeled at specific locations, these two stacked conformations give rise to two E_{FRET} states due to their different Cy3-Cy5 distances.[28] Using a crystal structure of Holliday junction[29] and standard

DNA structural parameters, we obtained the distances between the attachment points of Cy3 and Cy5 for both conformations. The obtained E_{FRET} versus Cy3-Cy5 distances are plotted in Figure 3.3, and fitted with the scaled E_{FRET} equation $E_{FRET} = c/[1+(r_{D-A}/r_0)^6]$ used by Meller and coworkers for calibrating single-molecule FRET studies with Cy3-Cy5 probes.[30] Here c is a scaling factor accounting for the contributions to the apparent E_{FRET} by non-FRET processes, including detection channel cross-talks, residual direct excitation of the acceptor, and detection efficiencies of the two channels. r_{D-A} here is the distance between the attachment points of the Cy3 and Cy5 labels.

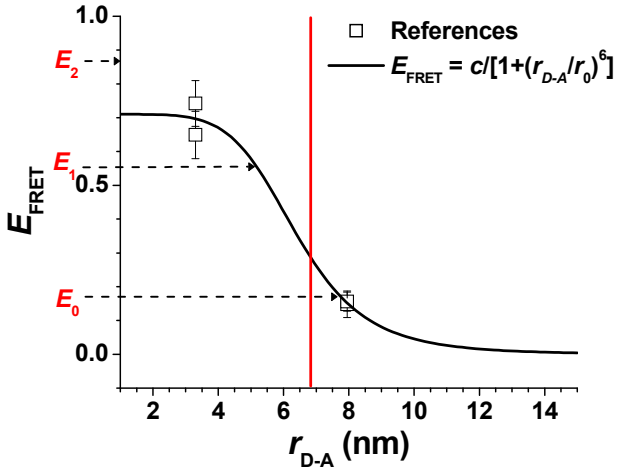

Figure 3.3. E_{FRET} calibration. The reference data points are taken from reference.[28] Black solid line is a fit with the equation $E_{FRET} = c/[1+(r_{D-A}/r_0)^6]$ (c = 0.71 and r_0 = 6.4 nm). The vertical red line marks the maximum possible D-A distance in an Hah1-MBD4 complex.

Based on this calibration (Figure 3.3), E_0 (~0.17) corresponds to r_{D-A} ~7.8 nm, significantly larger than the maximum dimension possible for a Hah1-MBD4 complex. (Using the crystal structure of Hah1 and a homology model of MBD4 (Figure S1),[12, 25] the maximum edge-to-edge distance of a possible Hah1-MBD4 complex is ~6.8 nm.) This further supports that E_0 is the dissociated state of Hah1 and MBD4. Similarly, E_1 (~0.55) corresponds to r_{D-A} ~5.2 nm. For E_2 (~0.87), as its value

is outside the bounds of our reference points and the FRET technique is known to not be sensitive in the short distance regime, determination of its corresponding r_{D-A} is unreliable; instead, we obtained an upper bound, i.e., $r_{D-A} < 3.3$ nm ($r_{D-A} \sim 3.3$ nm corresponds to $E_{FRET} \sim 0.7$). The small r_{D-A}'s of E_1 and E_2 are consistent with the assignment that they are two Hah1-MBD4 interaction complexes. Moreover, the difference between the r_{D-A} of E_1 and that of E_2 is >19 Å. This difference is less likely from mere conformational differences of Hah1 or MBD4 in these two complexes, as Hah1 and MBD4 only have conformational flexibility of a few angstroms from NMR studies[25, 26] We thus suggest that E_1 and E_2 are two Hah1-MBD4 complexes with different interaction geometries.

3.6. Summary

In summary, this study represents the first application of nanovesicle trapping to study weak protein-protein interactions on a single-molecule basis. We observed transient copper chaperone-target protein interactions one event at a time, captured distinct protein interaction intermediates, and resolved intermediate interconversion dynamics. The quantitative dynamic information will help understand how metallochaperones and their target proteins collaborate for metal transfer. By studying the Cu^{1+} dependence of the interaction kinetics, this single-molecule approach also offers a means to probe the Cu^{1+} transfer process and identify the productive interaction complex. Moreover, we expect that the nanovesicle trapping strategy coupled with smFRET is applicable for studying many other weak protein interactions at the single-molecule level

3.7. Acknowledgements

Thanks are due to our collaborators Patrick Ochieng and Profeessor David L. Huffman from Western Michigan University, Liliya A. Yatsunyk and Amy C. Rosenzweig from Northwestern University. Patrick Ochieng purified part of the MBD4 protein batch used in experiments. Liliya A. Yatsunyk provided the Hah1 expression plasmid. Thanks are also due to Aaron M. Keller from Cornell University for the copper binding and transfer experiments as well as quantization of Hg binding to MBD4. We thank NSF (CHE0645392, P.C.; CHE0645518, D.L.H), Dreyfus Foundation (P.C.), NIH traineeship (J.J.B., A. M. K.), Wilson Disease Association (P.C., D.L.H.), and NIH GM58518 (A.C.R.).

SUPPORTING INFORMATION

S.1. Protein mutations

Both Hah1 and MBD4 have three cysteines: two in the conserved CXXC motifs that bind Cu^{1+} and a nonessential third. We mutated the nonessential cysteine to serine and introduced a C-terminal cysteine in both proteins for specific labeling. The mutation sites and the labeling locations are distant from the Cu^{1+} binding CXXC motifs in both proteins, and they thus should not interfere with the Cu^{1+} binding of the proteins (Figure S1). The identities of the mutant proteins were confirmed by mass spectrometry (Figure S2).

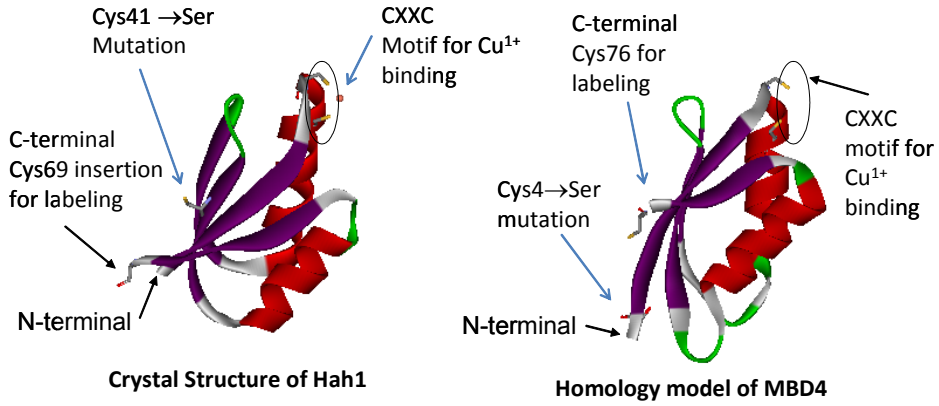

Figure S1. Protein models. (A) Crystal structure of wild type Hah1.[12] (B) A homology model of WDP MBD4 structure based on the NMR structure of the fourth metal binding domain of the Menkes protein.[25] The engineering locations, labeling sites, and the conserved Cu^{1+} binding CXXC motif are marked.

S.2. Protein labeling and labeling specificity confirmation

We labeled the mutant Hah1 and MBD4 at the C-terminal cysteines with Cy5 and Cy3 respectively, using maleimide chemistry. We protected the metal binding cysteines in the CXXC motif of Hah1 from labeling by addition of Cu^{1+}, and those of MBD4 by addition of Hg^{2+}. We then removed Cu^{1+} using CN^{-} and BCA as chelators, and removed Hg^{2+} using EDTA. The complete removal of Cu^{1+} from Hah1 was

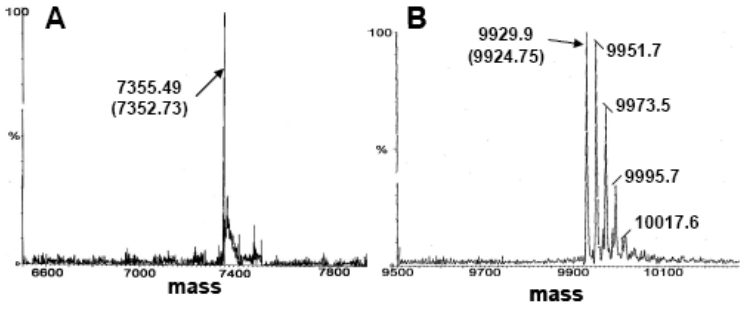

Figure S2. Mass spectra of mutant Hah1 (A) and MBD4 (B). The numbers in the parentheses are expected values. The side peaks in B are due to sodium adducts.

verified by the BCA copper quantitation assay (lower than the detection limit, corresponding to less than 1% copper content), and the complete removal of Hg^{2+} from MBD4 was confirmed (less than 1%) by the absence of the thiolate $\rightarrow$ Hg^{2+} charge transfer transition at 250 nm in the UV-Vis spectra (Figure S3).[31, 32]

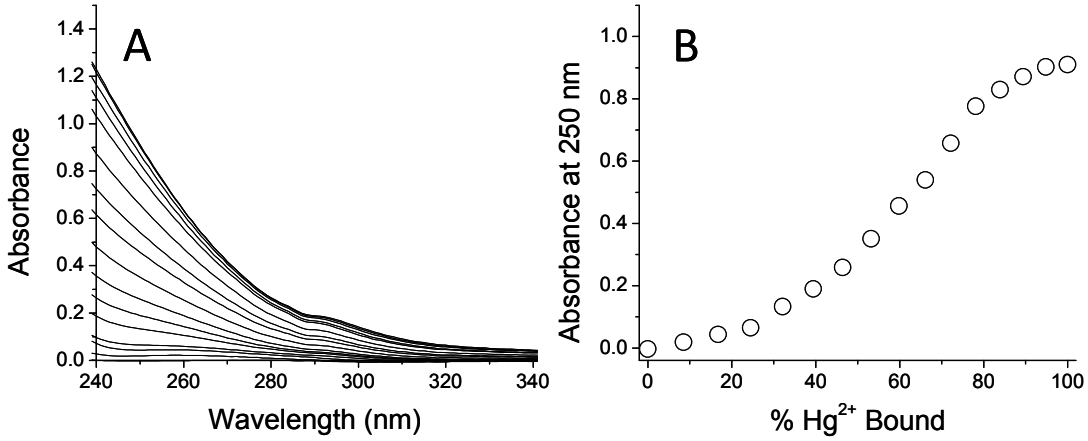

Figure S3. Hg^{2+} binding. (A) UV-Visible spectra monitoring the appearance of the thiolate $\rightarrow$ Hg^{2+} charge transfer band upon titrating 40 μM MBD4 with excess $Hg(NO_3)_2$. The absorbance of the free protein, free $Hg(NO_3)_2$, and buffer were subtracted from the spectra. (B) The absorbance (at 250 nm) titration curve derived from (A). This titration curve was used to calculate the percentage of protein-bound Hg^{2+} and confirm Hg^{2+} removal by EDTA.

The singly labeled proteins were separated cleanly from the unlabeled proteins using anion-exchange chromatography (Figure S4). The total masses of Cy5-Hah1 and Cy3-MBD4 suggest the presence of a single label (Figure S5A and C). We confirmed their labeling specificity at the C-terminal cysteines using trypsin digestion and mass spectrometry. The masses of their C-terminal fragments indicate the addition of the Cy5/Cy3, as expected (Figure S5B and D).

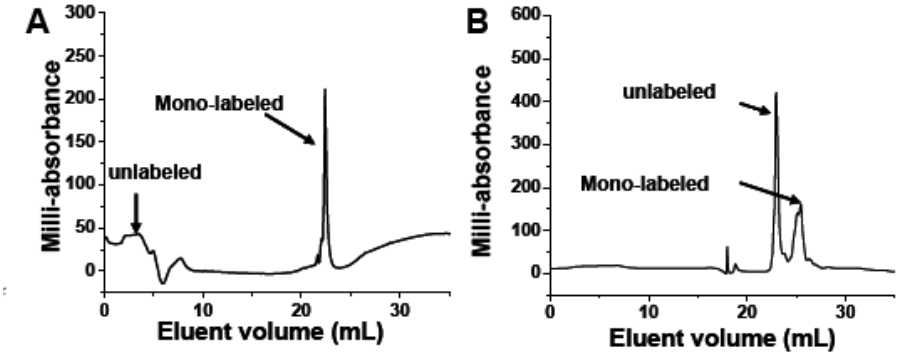

Figure S4. Anion exchange chromatography of purification of Cy5-Hah1 (A) and Cy3-MBD4 (B).

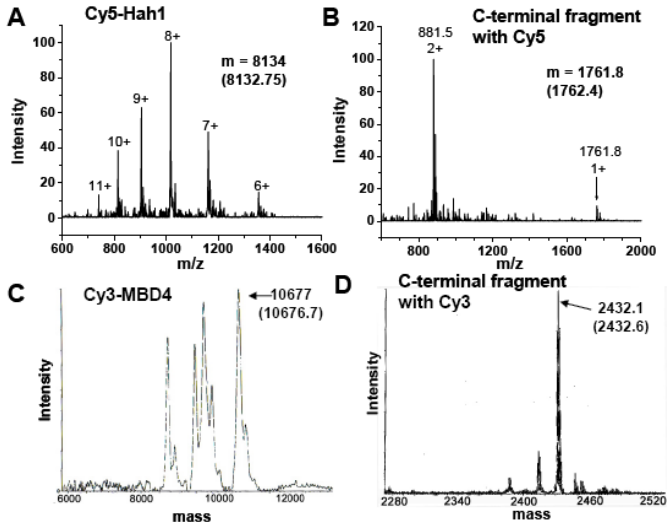

Figure S5. MS spectra. ESI-MS spectra of Cy5-Hah1 (A), and its trypsin digested C-terminal fragment with Cy5 (B). Multiply charged ions are indicated. MALDI spectra of Cy3-MBD4 (C) and its trypsin digested C-terminal fragment with Cy3 (D). Expected masses in parentheses.

S.3. Confirmation of Cu^{1+} binding and transfer function of labeled Hah1 and MBD4

We confirmed the Cu^{1+} binding and transfer capabilities of the labeled Hah1 and MBD4 (see Materials and Methods). The copper-to-protein ratio of a Cu^{1+}-loaded Cy5-Hah1 was found to be 0.92 ± 0.08, slightly higher than the reported literature values of 0.85 ± 0.10 and 0.68 ± 0.12,[5, 33] and that of Cy3-MBD4 was 1.28 ± 0.16, also slightly higher than the reported literature value of 0.84.[15] The equilibrium constant for Cu^{1+} transfer from Cy5-Hah1 to Cy3-MBD4, K_{ex}, was found to be 2 ± 1, slightly lower than the 5.4 ± 0.3 value of Cu^{1+} transfer between wild type Hah1 and the fourth MBD within a six-domain construct of WDP.[5]

S.4. Single-molecule control experiments

In preparation of the nanovesicles encapsulating proteins, we adjusted the protein/lipid ratio to ensure statistically that most of the vesicles contain only one protein molecule and only a small percentage of vesicles contain two protein molecules. We used 532-nm excitation to directly image the Cy3-MBD4 and 637-nm excitation to directly image Cy5-Hah1. By counting the photobeaching steps in Cy3 or Cy5 fluorescence signal, we confirmed that the number of vesicles containing more than two molecules (either Cy3-MBD4 or Cy5-Hah1) is negligible. In our smFRET measurements, we only use 532-nm excitation, and we select out vesicles that only contain one Cy3-MBD4 and that there is a simultaneous Cy5-Hah1 signal from FRET—because of the average vesicle occupation number, the probability that there is another Cy5-Hah1 in the same vesicle is negligible.

We performed control experiments to check if Cy5-Hah1 and Cy3-MBD4 have nonspecific interactions with the lipid membrane. We coated the glass surface with a lipid bilayer in the sample cell and flowed in solutions containing up to 100 nM free

Cy5-Hah1 or Cy3-MBD4. We then washed the sample cell with fresh buffer and imaged the Cy5 and Cy3 fluorescence with 637 nm and 532 nm excitations respectively. The number of single Cy5-Hah1 or Cy3-MBD4 molecules that are immobilized on the lipid bilayer by nonspecific interactions is less than 10 in a typical experiment. In contrast, the number of immobilized single molecules of Cy5-Hah1/Cy3-MBD4 is about 150-250, using the nanovesicle trapping and immobilization via biotin-streptavidin linkages at a total protein concentration of only 30 pM. We thus concluded the nonspecific interactions between Cy5-Hah1/Cy3-MBD4 and the lipid membrane is insignificant.

To check if the observed dynamic interactions between Cy5-Hah1 and Cy3-MBD4 are induced by the fluorescent labels, we trapped Cy5-Hah1 with free Cy3 or Cy3-MBD4 with free Cy5 in nanovesicles in the same way as we co-trapped Cy5-Hah1 and Cy3-MBD4 in the nanovesicles. In either case, we did not observe anti-correlated Cy3-Cy5 fluorescence intensity fluctuations like those of Cy5-Hah1 and Cy3-MBD4 interactions, and the dynamic Hah1-MBD4 interactions observed in our single-molecule experiments are thus not due to dye-dye interactions.

REFERENCES

1.Huffman, D. L.; O'Halloran, T. V., Function, Structure, and Mechanism of Intracellular Copper Trafficking Proteins. *Ann. Rev. Biochem.* **2001,** *70*, 677-701.

2.Rosenzweig, A. C., Copper Delivery by Metallochaperone Proteins. *Acc. Chem. Res.* **2001,** *34*, 119-128.

3.Cobine, P. A.; Pierrel, F.; Winge, D. R., Copper trafficking to the mitochondrion and assembly of copper metalloenzymes. *Biochim. Biophys. Acta* **2006,** *1763*, 759-772.

4.Donnelly, P. S.; Xiao, Z.; Wedd, A. G., Copper and Alzheimer's disease. *Curr. Opin. Chem. Biol.* **2007,** *11*, 128-133.

5.Yatsunyk, L. A.; Rosenzweig, A. C., Copper(I) Binding and Transfer by the N-terminus of the Wilson Disease Protein. *J. Biol. Chem.* **2007,** *282*, 8622-8631.

6.Achila, D.; Banci, L.; Bertini, I.; Bunce, J.; Ciofi-Baffoni, S.; Huffman, D. L., Structure of human Wilson protein domains 5 and 6 and their interplay with domain 4 and the copper chaperone HAH1 in copper uptake. *Proc. Natl. Acad. Sci. U.S.A.* **2006,** *103*, 5729-5734.

7.Walker, J. M.; Huster, D.; Ralle, M.; Morgan, C. T.; Blackburn, N. J.; Lutsenko, S., The N-Terminal Metal-Binding Site 2 of the Wilson's Disease Protein Play a Key Role in the Transfer of Copper from Atox1. *J. Biol. Chem.* **2004,** *279*, 15376-15384.

8.Cater, M. A.; Forbes, J.; Fontaine, S. L.; Cox, D.; Mercer, J. F. B., Intracellular trafficking of the human Wilson protein: the role of the six N-terminal metal-binding sites. *Biochem. J.* **2004,** *380*, 805-813.

9.Banci, L.; Bertini, I.; Cantini, F.; Della-Malva, N.; Migliardi, M.; Rosato, A., The Different Intermolecular Interactions of the Soluble Copper-Binding Domains of the Menkes Protein, ATP7A. *J. Biol. Chem.* **2007,** *282*, 23140-23146.

10.Larin, D.; Mekios, C.; Das, K.; Ross, B.; Yang, A.-S.; Gilliam, T. C., Characterization of the Interaction between the Wilson and Menkes Disease Proteins and the Cytoplasmic Copper Chaperone, Hah1p. *J. Biol. Chem.* **1999,** *274*, 28497-28504.

11.van Dongen, E. M. W. M.; Klomp, L. W. J.; Merkx, M., Copper-Dependent Protein-Protein Interactions Studied by Yeast Two-Hybrid Analysis. *Biochem. Biophys. Res. Commun.* **2004,** *323*, 789-795.

12.Wernimont, A. K.; Huffman, D. L.; Lamb, A. L.; O'Halloran, T. V.; Rosenzweig, A. C., Structural Basis for Copper Transfer by the Metallochaperone for the Menkes/Wilson Disease Proteins. *Nat. Struct. Biol.* **2000,** *7*, 766-771.

13.Schatz, P. J., Use of peptide libraries to map the substrate specificity of a peptide-modifying enzyme: a 13 residue consensus peptide specifies biotinylation in Escherichia coli. *Biotechnology* **1993,** *11* (10), 1138-1143.

14.Brenner, A. J.; Harris, E. D., A Quantitative Test for Copper Using Bicinchoninic Acid. *Anal. Biochem.* **1995,** *226*, 80-84.

15.Bunce, J.; Achila, D.; Hetrick, E.; Lesley, L.; Huffman, D. L., Copper Transfer Studies between the N-terminal Copper Binding Domains One and Four of Human Wilson Protein. *Biochim. Biophys. Acta* **2006,** *1760*, 907-912.

16.Huffman, D. L.; O'Halloran, T. V., Energetics of Copper Trafficking between the Atx1 Metallochaperone and the Intracellular Copper Transporter Ccc2. *J. Biol. Chem.* **2000,** *275*, 18611-18614.

17.Boukobza, E.; Sonnenfeld, A.; Haran, G., Immobilization in Surface-Tethered Lipid Vesicles as a New Tool for Single Biomolecule Spectroscopy. *J. Phys. Chem. B.* **2001,** *105*, 12165-12170.

18.Okumus, B.; Wilson, T. J.; Lilley, D. M. J.; Ha, T., Vesicle Encapsulation Studies Reveal that Single Molecule Ribozyme Heterogeneities Are Intrinsic. *Biophys. J.* **2004,** *87*, 2798-2806.

19.Rhoades, E.; Gussakovsky, E.; Haran, G., Watching proteins fold one molecule at a time. *Proc. Natl. Acad. Sci. U.S.A.* **2003,** *100*, 3197-3202.

20.Rasnik, I.; McKinney, S. A.; Ha, T., Surfaces and Orientations: Much to FRET about? *Acc. Chem. Res.* **2005,** *38*, 542-548.

21.Rasnik, I.; Myong, S.; Cheng, W.; Lohman, T. M.; Ha, T., DNA-Binding Orientation and Domain Conformation of the E. coli Rep Helicase Monomer bound to a Partial Duplex Junction: Single -Molecule Studies of Fluorescently Labeled Enzymes. *J. Mol. Biol.* **2004,** *336*, 395-408.

22.Ha, T., Single-Molecule Fluorescence Resonance Energy Transfer. *Methods* **2001,** *25*, 78-86.

23.Rasnik, I.; McKinney, S. A.; Ha, T., Nonblinking and Long-lasting Single Molecule Fluorescence Imaging. *Nature Methods* **2006,** *3*, 891-893.

24.Cisse, I.; Okumus, B.; Joo, C.; Ha, T., Fueling Protein-DNA Interactions inside Porous Nanocontainers. *Proc. Natl. Acad. Sci. U.S.A.* **2007,** *104*, 12646-12650.

25.Gitschier, J.; Moffat, B.; Reilly, D.; Wood, W. I.; Fairbrother, W. J., Solution Structure of the Fourth Metal-Binding Domain from the Menkes Copper-Transporting ATPase. *Nat. Struct. Biol.* **1998,** *5*, 47-54.

26.Anastassopoulou, I.; Banci, L.; Bertini, I.; Cantini, F.; Katsari, E.; Rosato, A., Solution Structure of the Apo and Copper(I)-Loaded Human Metallochaperone HAH1. *Biochemistry* **2004,** *43*, 13046-13053.

27.Banci, L.; Bertini, I.; Francesca, C.; Rosenzweig, A. C.; Yatsunyk, L. A., Metal Binding Domains 3 and 4 of the Wilson Disease Protein: Solution Structure and Interaction with the Copper(I) Chaperone Hah1. *Biochemistry* **2008,** *47*, 7423-7429.

28.Sarkar, S. K.; Andoy, N. M.; Benitez, J. J.; Chen, P. R.; Kong, J. S.; He, C.; Chen, P., Engineered Holliday Junctions as Single-Molecule Reporters for Protein-DNA Interactions with Application to a MerR-Family Regulator. *J. Am. Chem. Soc.* **2007,** *129*, 12461-12467.

29.Eichman, B. F.; Vargason, J. M.; Mooers, B. H. M.; Ho, P. S., The Holliday junction in an inverted repeat DNA sequence: sequence effects on the structure of four-way junctions. *Proc. Natl. Acad. Sci. USA* **2000,** *97*, 3971-3976.

30.Sabanayagam, C. R.; Eid, J. S.; Meller, A., Using fluorescence resonance energy transfer to measure distances along individual DNA molecules: Corrections due to nonideal transfer. *J. Chem. Phys.* **2005,** *122* (6), 061103.

31.Vasak, M.; Kagi, J. H. R.; Hill, H. A. O., Zinc(II), Cadmium(II), and Mercury(II) Thiolate Transitions in Metallothioneint. *Biochemistry* **1981,** *20*, 2852-2856.

32.Watton, S. P.; Wright, J. G.; MacDonnell, F. M.; bryson, J. W.; Sabat, M.; O'Halloran, T. V., Trigonal Mercuric complex of an Aliphatic Thiolate: A Spectroscopic and Structural Model for the Receptor Site in the Hg(II) Biosensor MerR. *J. Am. Chem. Soc.* **1990,** *112*, 2824-2826.

33.Walker, J. M.; Tsivkovskii, R.; Lutsenko, S., Metallochaperone Atox1 Transfers Copper to the NH2-Terminal Domain of the Wilson's Disease Protein and Regulates Its Catalytic Activity. *J. Biol. Chem.* **2002,** *277*, 27953-27959.

34.Xie, X. S., Single-Molecule Approach to Enzymology. *Single Mol.* **2001,** *2*, 229-236.

CHAPTER 4

Relating dynamic protein interactions of metallochaperones with metal transfer at the single-molecule level [*]

* Benitez, J. J.; Keller, A. M.; Huffman, D. L.; Yatsunyk, L. A.; Rosenzweig, A. C.; Chen, P., Relating Dynamic Protein Interactions of Metallochaperones with Metal Transfer at the Single-Molecule Level. *Faraday Disscusions* **2010,** DOI: 10.1039/c004913a. Reproduced with permission from The Royal Society of Chemistry.

4.1. Abstract

Metallochaperones undertake specific interactions with their target proteins to deliver metal ions inside cells. Understanding how these protein interactions are coupled with the underlying metal transfer process is important, but challenging because they are weak and dynamic. Here we use a nanovesicle trapping scheme to enable single-molecule FRET measurements of the weak, dynamic interactions between the copper chaperone Hah1 and the fourth metal binding domain (MBD4) of WDP. By monitoring the behaviors of single interacting pairs, we visualize their interactions in real time in both the absence and the presence of various equivalents of Cu^{1+}. Regardless of the proteins' metallation state, we observe multiple, interconverting interaction complexes between Hah1 and MBD4. Within our experimental limit, the overall interaction geometries of these complexes appear invariable, but their stabilities are dependent on the proteins' metallation state. In apo–holo Hah1–MBD4 interactions, the complexes are stabilized relative to that observed in the apo–apo interactions. This stabilization is undiscernible when Hah1's Cu^{1+}-binding is eliminated or when both proteins have Cu^{1+} loaded. The nature of this Cu^{1+}-induced complex stabilization and of the interaction complexes are discussed. These Cu^{1+}-induced effects on the Hah1–MBD4 interactions provide a step toward understanding how the dynamic protein interactions of copper chaperones are coupled with their metal transfer function.

4.2. Introduction

Metals are essential for life processes, such as oxygen transport, electron transport, and hormone production.[1] They can also be toxic, however, especially at high concentrations. To maintain normal metabolism, a variety of protein machineries control the concentrations and availability of metal ions inside cells.[2-4] One type of

such protein machineries mediate intracellular metal trafficking, so the metal ions can reach their functional locations while avoiding adventitious binding by many other possible molecules inside cells.[2, 4-8] Intracellular copper trafficking is mediated by copper chaperones; they bind and deliver copper to their target proteins through specific and dynamic protein–protein interactions.[5, 6, 8-10] In human cells, the copper chaperone Hah1 (also called Atox1) delivers Cu^{1+} to the Wilson disease protein (WDP, also called ATP7B) or the Menkes disease protein (MNK, also called ATP7A), for subsequent incorporation into copper-requiring enzymes or for efflux under copper stress.[11-14]

Hah1 is a small single-domain cytoplasmic protein;[6] WDP and MNK are large, multidomain proteins anchored on organelle membranes.[13, 15-18] The cytosolic N-termini of WDP and MNK both have six metal-binding domains (MBDs). All these MBDs, as well as Hah1, share the same βαββαβ protein fold and all have the surface exposed, conserved CXXC motif, where the two cysteines bind Cu^{1+}. Upon Hah1–MBD interaction, Cu^{1+} can be transferred via a thiol ligand exchange mechanism at the protein interaction interface.[5, 9, 13, 19-21]

Past studies have shown that the N-terminal MBDs of WDP and MNK have different functional roles,[13, 22-32] even though all these MBDs, as well as Hah1, have similar Cu^{1+} binding affinities.[17, 27, 33-35] This similarity indicates that the Cu^{1+} transfer between them is under *kinetic* control mediated by protein interactions and that the functional differences among WDP (or MNK) MBDs are not defined by their Cu^{1+} binding affinity but may be related to *how* each MBD interacts with Hah1. Quantifying how Hah1 and WDP/MNK MBDs interact is thus crucial for understanding their interaction mediated copper transfer process.

Yet few quantitative measurements are available, especially on the dynamics of protein interactions of copper chaperones.[36] This scarcity comes mainly from the

difficulty of conventional ensemble measurements of weak protein interactions. These weak interactions are dynamic and stochastic, making synchronization of molecular actions necessary. Often the steady-state concentrations of interaction intermediates are low, making detection difficult. Furthermore, multiple interaction intermediates, if present, convolute the ensemble-averaged measurements.

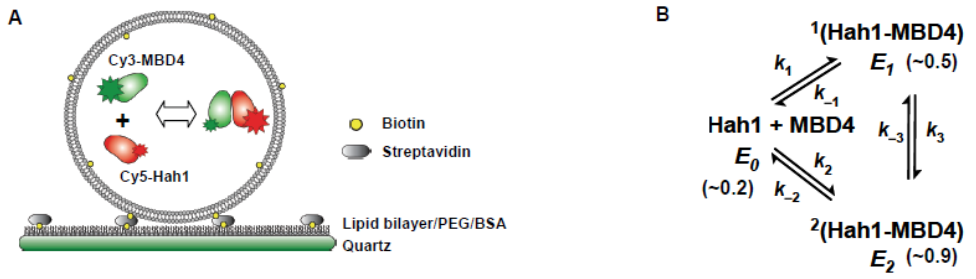

Figure 4.1. Protein-protein interactions within a nanovesicle. (A) Schematic of nanovesicle trapping of Cy5-Hah1 and Cy3-MBD4 for smFRET studies. The inner diameter of the nanovesicle is 80 ± 20 nm. The glass surface is coated with biotinylated lipid bilayer, PEG, or BSA to prevent vesicle rupture. (B) Interaction scheme between apo-forms of Hah1 and MBD4. Besides the dissociated state, there are two interaction complexes that interconvert dynamically. k's are rate constants. k_1 and k_2: ~10^5 $M^{-1}s^{-1}$; k_{-1}, k_{-2}, k_3, and k_{-3}: ~10^0 s^{-1}.[37, 38]

Our group has used single-molecule fluorescence resonance energy transfer (smFRET) to study the dynamic interactions of copper chaperones (Figure 4.1A).[36-39] At the single-molecule level, no synchronization of molecular actions is necessary; molecular actions are followed in real time, including the formation and dissociation of interaction intermediates; and at any time point, only one molecular state is observed. We have initially focused on the interactions between Hah1 and a single MBD of WDP (the fourth MBD, MBD4). We label the two interacting proteins with a FRET donor–acceptor pair and excite the donor directly with a laser while monitoring the fluorescence intensities of both the donor (I_D) and the acceptor (I_A) simultaneously. The donor-to-acceptor FRET efficiency can be determined ($E_{FRET} \approx I_A/(I_A+I_D)$), which

is directly correlated with the donor–acceptor interdistance, r, as $E_{FRET} = 1/[1+(r/r_0)^6]$, where r_0 is the Förster radius of the donor–acceptor pair. Changes in E_{FRET} thus directly reflect the changes in the donor–acceptor interdistances and thus the protein interactions that cause these interdistance changes.

There are still technical challenges to overcome before smFRET can be applied to follow *weak* protein interactions *in real time*. The primary challenge is the concentration limit: single-molecule measurements are typically performed at pM–nM concentrations of fluorescently labeled species to separate them spatially. Weak protein interactions, including those of copper chaperones with $K_D \sim \mu M$, need to be studied at much higher concentrations (> μM) to favor complex formation. Moreover, to follow the same protein molecules interacting in real time, they need to be surface immobilized, where their nonspecific interactions with surfaces must be minimized.

We have used a nanovesicle trapping scheme[40-42] to overcome the above two challenges (Figure 4.1A).[37-39] Because of the confined volume (~10^{-19} L) of a nanovesicle, each molecule of an interacting pair inside has an effective concentration of a few μM (see Experimental Section). The overall number of nanovesicles is kept low to separate them spatially to ensure single-nanovesicle (i.e., single-pair) detection. The nanovesicles are then immobilized on the surface, where possible nonspecific interactions of the proteins with the glass surface are eliminated. Although we cannot ensure that every nanovesicle will contain two different protein molecules, we can control the statistical distribution of molecules in nanovesicles, and for each nanovesicle, the number and type of molecules inside can be determined from their photobleaching events.[37, 39] By examining only the nanovesicles containing two different molecules, we can eliminate interactions between molecules of the same type, which is not possible in ensemble experiments and significantly complicates protein

interaction studies. This complication is particularly relevant for copper chaperones, as they can form dimers in solution.[43]

Using the nanovesicle trapping scheme combined with smFRET measurements, we have observed real-time interaction events between a single pair of Hah1 and WDP MBD4.[37, 38, 44] More important, we have identified that even in the absence of Cu^{1+}, Hah1 and MBD4 can form two interaction complexes, which interconvert dynamically (Figure 4.1B). One complex has an E_{FRET} value of ~0.5 (E_1), the other of ~0.8 (E_2), besides their dissociated state (E_0 ~0.2). The significant difference in the E_{FRET} values of these two complexes further suggests that they likely have different overall interaction geometries. The results have also enabled us to quantify the kinetics of association, dissociation, and interconversion of the two interaction complexes, as well as their dissociation constants.

The existence of multiple interaction complexes between Hah1 and a WDP MBD has functional implications. Inside cells, copper chaperones encounter their target proteins through diffusion. The initial encounter pair often rapidly returns to the dissociated form. The ability to form multiple interaction complexes with different geometries increases the probability of complex formation. The formed complex, if productive, may proceed to accomplish Cu^{1+} transfer, or, if unproductive, can convert to the other complex for Cu^{1+} transfer. The interconversion kinetics of Hah1–MBD4 complexes are comparable to their dissociation kinetics (k_3 and k_{-3} versus k_{-1} and k_{-2}, Figure 4.1B), further supporting this possible mechanism of operation.

Still, many questions remain. For example, how are the Hah1–MBD interactions coupled with the Cu^{1+} transfer process? Of the two interaction complexes, which one is productive for metal transfer, or are both so? Do Hah1 and a WDP MBD still form multiple complexes in the presence of Cu^{1+}? To address these questions, observing Cu^{1+} transfer directly during protein interaction would be ideal, but is

challenging because the d^{10} electron configuration of Cu^{1+} makes it magnetically silent and optically invisible except for x-ray-based techniques. Our smFRET measurements cannot directly observe Cu^{1+} transfer, either. Nevertheless, as we are able to study the protein interactions in real time and quantitatively, we can examine the effects of Cu^{1+} on the interaction dynamics between Hah1 and a WDP MBD. Changes in the protein interaction dynamics should inform how the copper chaperone interactions are coupled with the underlying Cu^{1+} transfer process. Here we report our initial results along this line. We show how Cu^{1+} affects the formation and stability of Hah1–MBD4 interaction complexes and how the effects are related to the Cu^{1+} binding ability of Hah1.

4.3. Experimental

4.3.1. Protein expression, purification, labeling, and mutation.

Hah1 and WDP MBD4 were expressed, purified, and labeled as previously described.[37] Both proteins have a C-terminal cysteine introduced via site-directed mutagenesis for labeling with a fluorescent probe using maleimide chemistry. Hah1 is labeled with the FRET acceptor Cy5 at Cys69, and MBD4 is labeled with the FRET donor Cy3 at Cys76. The Cu^{1+}-binding cysteines in Hah1 and MBD4 are protected from labeling by coordinating to Cu^{1+} or Hg^{2+}, which can be removed afterwards using BCA or CN^- (for Cu^{1+}) and EDTA (for Hg^{2+}) as chelators.

The mutant Hah1, mHah1, has the two Cu^{1+}-binding cysteines in its CXXC motif (Cys12 and Cys15) mutated to serines to eliminate its Cu^{1+} binding. The mutation was confirmed by DNA sequencing and MALDI mass spectrometry of the purified protein product (MW: calculated,7325.3 Da; observed, 7325.0 Da).

Protein concentrations were quantified using the BCA and Bradford assays with BSA as a standard (Pierce), and the thiol quantitation method (Molecular Probes).

Copper concentrations were quantified using a BCA-based method by Brenner and Harris[45] and a copper atomic absorption standard solution (Acros Organics).

4.3.2. Nanovesicle trapping.

Nanovesicle trapping was performed as previously described.[37, 39] A mixture of L-α-phosphatidylcholine (eggPC) and 1% 1,2-dipalmitoyl *sn*-glycero3-phosphoethanolamine-N-(cap biotinyl) (16:0 biotinyl cap PE) (Avanti Lipids) in chloroform was dried under a constant flow of nitrogen. Protein-loaded vesicles were prepared by hydrating the lipid film with solutions containing 3 μM Cy5-Hah1, 3 μM Cy3-MBD4, 1 mM Trolox (Sigma), and 15–20 μM TCEP (Sigma) in 60 mM MES, 110 mM NaCl, pH 6.0 buffer, followed by seven freeze-thaw cycles to increase the encapsulation efficiency. Protein integrity after freeze-thaw cycles was confirmed by circular dichroism spectroscopy. The solution was then repeatedly extruded through a polycarbonate membrane with 100 nm pores (Avanti Mini Extruder) to form approximately 100-nm diameter unilamellar vesicles encapsulating proteins. Loaded vesicles were used for experiments immediately or within 48 hrs from preparation.

To prepare the copper-loaded proteins, the proteins were first incubated for 30 min with 15–20 μM TCEP to reduce the proteins, followed by 1 hr incubation with appropriate equivalents of Cu^{1+} ($[Cu(CH_3CN)_4]PF_6$ (Aldrich) in 50% acetonitrile). The solution was then used to hydrate the dry lipid film and incubated for 1 hr for nanovesicle encapsulation.

The size of the nanovesicles was measured to be 90 ± 20 nm by dynamic light scattering (Malvern Zetasizer Nano-ZS; the error bar here is the standard deviation). Taking into account the lipid bilayer thickness of ~5 nm,[46] the resulting nanovesicles have an inner diameter of 80 ± 20 nm. The corresponding effective concentration for a single molecule trapped inside is thus 6 ± 5 μM.

4.3.3. Single-molecule FRET measurements.

Single-molecule FRET measurements were performed on a homebuilt prism-type total internal reflection microscope as described previously.[38] Briefly, a continuous wave circularly polarized 532 nm laser beam was used to directly excite the Cy3 probe. The fluorescence of Cy3 and Cy5 was collected, filtered to reject laser light, and split into two wavelength channels. Each channel of fluorescence was further filtered and projected onto half of the imaging area of a camera, operating at 50-200 ms frame rate. At 30 seconds prior to the end of data collection, the sample was illuminated with a 637 nm laser to directly excite the Cy5 fluorescence for determining its number within nanovesicles.[39] Single-molecule fluorescence intensity trajectories were extracted from the recorded movie, from which the E_{FRET} trajectories were calculated. Only the portions of the trajectories during 532 nm laser illumination and before the photobleaching events of the probes were analyzed.

A flow cell, formed by double-sided tape placed between a quartz slide and a coverslip, was used to hold aqueous sample solutions for single-molecule fluorescence measurements. All samples were in 60 mM MES, pH 6.0, 110 mM NaCl, 15–20 μM TCEP unless indicated otherwise. The TCEP was present to ensure a reducing environment to prevent air oxidation of Cu^{1+}. To form the bilayer support,[37, 39] unloaded vesicles were flowed in at 5 mg/mL (500 μL) and incubated for 1 to 2 hours. Excess lipids were washed away with standard lipid buffer. Alternatively, the slides were first amine-functionalized (Vectabond, Vector Laboratories) and then coated with PEG polymers (100 mg/mL m-PEG-SPA-5000 and 1 mg/mL biotin-PEG-NHS-3400, Nektar Therapeutics).[39, 47] 1% of the PEG polymers contain a biotin terminal group to form biotin-streptavidin (Molecular Probes) linkages. We also used biotinylated BSA to coat the quartz surface:[39] a solution of 1 mg/mL biotinylated BSA was incubated on the quartz slide for 30 min to 1 hr. Excess biotinylated BSA was then washed out with

buffer. 500 μL of streptavidin at a concentration of 0.2 mg/mL was then flowed in and incubated for 10 minutes. Unbound streptavidin was then washed out with buffer containing 0.1 mg/mL BSA, which help to block nonspecific binding sites.[48] Protein-loaded vesicles were flowed in at a total protein concentration of 30 pM and unbound vesicles were then washed out before single-molecule imaging experiments. An oxygen scavenging system (0.1 mg/mL glucose oxidase (Sigma), 0.025 mg/mL catalase (Roche), 4% glucose (Aldrich) and 1 mM Trolox (Sigma)[49] was added into the sample solution just before each experiment to prolong the lifetime of the fluorescence probes, and was refreshed during experiments every hour.

4.4. Results and analysis

4.4.1. Observation of Hah1–MBD4 interactions in the presence of Cu^{1+} and identification of interaction complexes.

We applied nanovesicle trapping in combination with smFRET to study Hah1–MBD4 interactions in the presence of Cu^{1+}. We first added one equivalent of Cu^{1+} per Hah1–MBD4 pair in preparing nanovesicle trapped molecules. As Hah1 and MBD4 have similar Cu^{1+} binding affinities and their Cu^{1+} transfer is reversible,[23, 27] approximately half of the molecules of each protein have a Cu^{1+} bound at their CXXC sites at this condition. Therefore, among a population of Hah1–MBD4 pairs trapped inside vesicles, there are pairs of apo–apo, apo–holo (i.e., either Hah1 or MBD4 has a Cu^{1+} bound), and holo–holo proteins; and for a particular Hah1–MBD4 pair, it can be in either one of these three Cu^{1+}-loading states.

Figure 4.2A shows an exemplary E_{FRET} trajectory of a single Hah1–MBD4 pair inside a nanovesicle in the presence of one equivalent of Cu^{1+}. The temporal E_{FRET} fluctuations report the dynamic interactions between Hah1 and MBD4. Three distinct E_{FRET} states are observed in this trajectory at E_{FRET} ~0.2, ~0.5, and ~0.8, similar to the

dissociated state (E_0 ~0.2) and the two interaction complexes (E_1 ~0.5 and E_2 ~0.8) observed for Hah1–MBD4 interactions in the absence of Cu^{1+}.[37, 38]

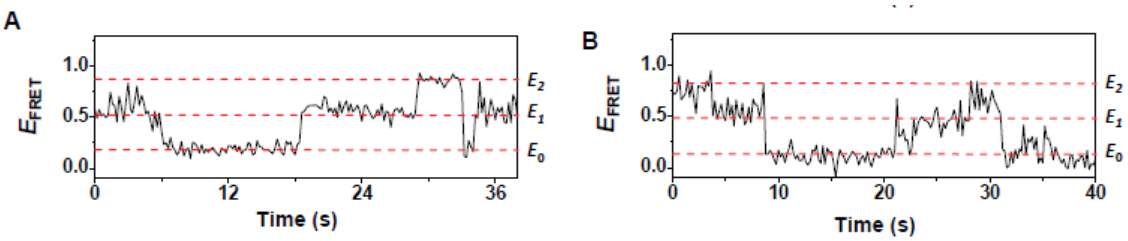

Figure 4.2. Exemplary E_{FRET} trajectories of a Cy5-Hah1 and a Cy3-MBD4 inside a nanovesicle in the presence of one equivalent (A) and four equivalents of Cu^{1+} (B). Trajectories are at 200 ms time resolution.

Owing to the finite trajectory length (up to 1–2 min) limited by the photobleaching of the fluorescent probes, many E_{FRET} trajectories only show two E_{FRET} states within their time span. For the same reason, it is difficult to determine reliably the E_{FRET} values of all three states from a *single* E_{FRET} trajectory. To distinguish these three states and determine their E_{FRET} values with statistical reliability, we used a 2-dimensional histogram analysis of E_{FRET} values. For each of the E_{FRET} trajectories that show merely two states, we calculated the average E_{FRET} value of each state and assigned the smaller value as E_{low} and the larger value as E_{high}. We then plotted the 2-dimensional histogram of these two E_{FRET} values from many trajectories (Figure 4.3B). For those E_{FRET} trajectories that have three states and thus three E_{FRET} values, we used any two out of the three values (there are three possible combinations of selecting two values out of three), assigned them as E_{low} and E_{high} based on their relative magnitudes, and added them onto the 2-dimensional histogram. Combining results from hundreds of single Hah1–MBD4 pairs, the resulting 2-dimensional histogram shows three distinct populations (Figure 4.3B), definitively indicating the presence of three E_{FRET} states in Hah1–MBD4 interactions in the

presence of one equivalent of Cu^{1+}. These three populations are centered at the positions of (E_0, E_1), (E_0, E_2), and (E_1, E_2) in the 2-dimensional histogram (Figure 4.3B). Projecting this 2-dimensional histogram onto the *x,y* axes and Gaussian-fitting the projections give the reliable E_{FRET} values for the three states: $E_0 = 0.13 \pm 0.06$, $E_1 = 0.50 \pm 0.08$, and $E_2 = 0.8 \pm 0.1$. For reference, the 2-dimensional histogram from single-pair apo–Hah1 ↔ apo–MBD4 interactions is shown in Figure 4.3A, from which the determined E_{FRET} values are $E_0 = 0.14 \pm 0.07$, $E_1 = 0.50 \pm 0.08$, and $E_2 = 0.8 \pm 0.1$, consistent with what we reported previously.[37]

At one equivalent of Cu^{1+}, there is a mixture of apo–apo, apo–holo, and holo–holo pairs of Hah1–MBD4. Consequently, the observed E_1 and E_2 states here could just be the two complexes from apo–apo interactions in the population, and it is not yet clear if apo–holo and holo–holo interactions will also form multiple complexes.

To probe pure holo–holo interactions, we added four equivalents of Cu^{1+} per Hah1–MBD4 pair. The extra equivalents of Cu^{1+} are to ensure full occupation of the proteins' copper binding sites. Further increasing the Cu^{1+} equivalents to six does not cause any significant changes in the Hah1–MBD4 interactions (such as the histogram of the E_{FRET} trajectories; see below), indicating that both proteins are already metallated in the presence of four equivalents of Cu^{1+}.

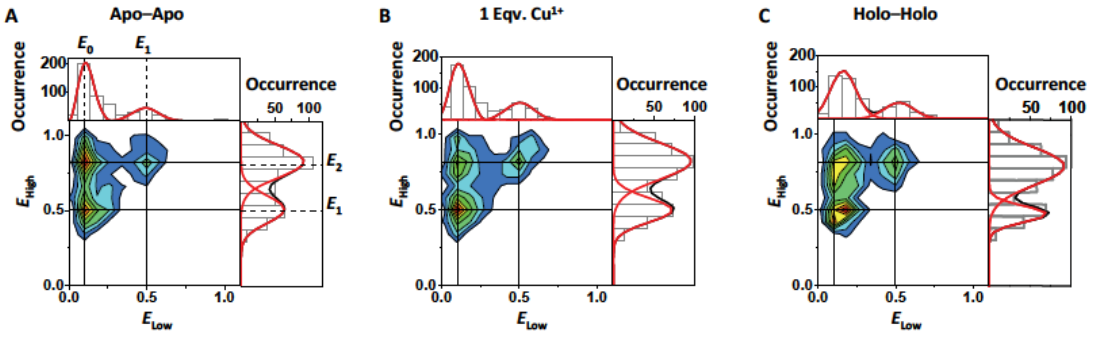

Figure 4.3. 2-dimensional histograms of E_{FRET} values of Hah1 ↔ MBD4 interaction states. (A) apo–apo interactions. (B) In the presence of one equivalent of Cu^{1+}. (C) In the presence of four equivalents of Cu^{1+}. E_{low}, the E_{FRET} value of the lower FRET state; E_{high}, the E_{FRET} value of the higher FRET state in an E_{FRET} trajectory. The projections of the histograms on the x,y axes are Gaussian resolved to determine the E_{FRET} values of the three states: (A) $E_0 = 0.14 \pm 0.07$, $E_1 = 0.50 \pm 0.08$, $E_2 = 0.8 \pm 0.1$; (B) $E_0 = 0.13 \pm 0.06$, $E_1 = 0.50 \pm 0.08$, $E_2 = 0.8 \pm 0.1$; (C) $E_0 = 0.15 \pm 0.08$, $E_1 = 0.48 \pm 0.07$, $E_2 = 0.8 \pm 0.1$. Data compiled from 309 (A), 420 (B), and 249 (C) Hah1–MBD4 interacting pairs.

Figure 4.2B shows an exemplary E_{FRET} trajectory of a single holo–holo pair. Again, three states are observed at E_{FRET} ~0.2, ~0.5, and ~0.8, corresponding to the dissociated state and the two interaction complexes, respectively. The 2-dimensional histogram of E_{FRET} values definitively shows the three-state behavior of holo–holo Hah1–MBD4 interactions (Figure 4.3C). Therefore, the presence of multiple interaction complexes is general for both holo–holo and apo–apo interactions between Hah1 and MBD4. Furthermore, the E_{FRET} values of the two holo–holo interaction complexes are the same within experimental error as those of apo–apo interactions (Figure 4.3C versus A), indicating that the overall interaction geometries of the complexes are unperturbed by Cu^{1+} binding in both proteins. Similarly, apo–holo interactions between Hah1 and MBD4 also form two complexes, as will be shown below.

4.4.2. Cu^{1+}-induced stabilization of apo–holo interaction complexes.

The real-time E_{FRET} trajectories of single-pair Hah1–MBD4 interactions also contain information about the stabilities of their complexes. Figures 4.4A–C show the histograms of the E_{FRET} trajectories of Hah1–MBD4 interactions when they are in their apo-forms, in the presence of one equivalent of Cu^{1+}, and in their holo-forms, respectively. All three histograms can be fitted by three Gaussian peaks, centered at E_0, E_1 and E_2, corresponding to the dissociated state and the two interaction complexes, respectively. As the three peaks are not clearly resolved in these histograms, the peak locations were constrained to improve the reliability of the Gaussian fits, using the E_{FRET} values determined from the analyses of the 2-dimensional E_{FRET} histograms (Figure 4.3). The relative areas of the three peaks in each histogram represent the relative stabilities of the relevant states. For the apo–apo Hah1–MBD4 interactions (Figure 4.4A), the calculated dissociation constants of the two complexes are K_{D1}~ 3 ± 6 μM and K_{D2} ~ 5 ± 9 μM (the large error bars here mainly result from the size dispersion of the nanovesicles (inner diameter 80 ± 20 nm; see Experimental Section), from which the effective concentration of a single molecule inside is calculated).[37, 38]

For holo–holo Hah1–MBD4 interactions, the relative areas of the three peaks in the histogram of E_{FRET} trajectories are similar to those of apo–apo interactions (Figure 4.4C versus 4A, and 4D). Therefore, there is no change in stability for both the E_1 and the E_2 complex when both proteins are loaded with Cu^{1+}.

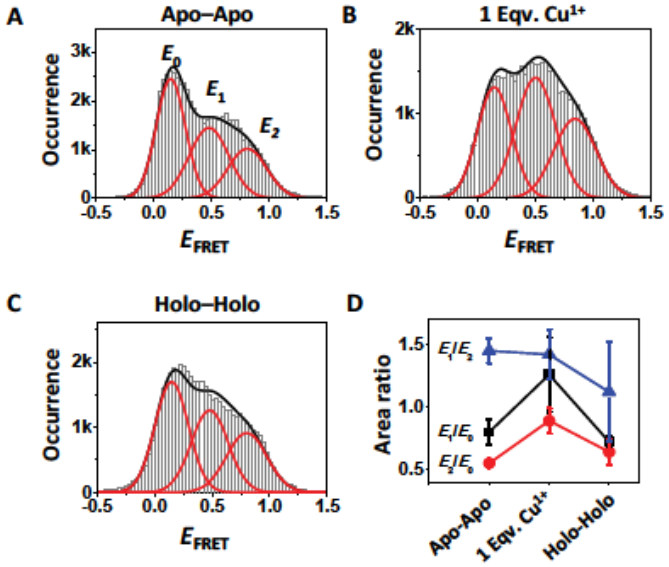

Figure 4.4. (A, B, C) Histograms of E_{FRET} trajectories of single-pair Hah1–MBD4 interactions in the absence (A), or in the presence of one equivalent (B), or four equivalents of Cu^{1+} (C). Data compiled from 309 (A), 420 (B), and 249 (C) Hah1–MBD4 interacting pairs. Each histogram is fitted with three Gaussian peaks, whose centers are set to the E_{FRET} values determined from Figure 4. (D) The area ratios of the Gaussian-resolved peaks from A, B, and C.

In contrast, in the presence of one equivalent of Cu^{1+}, significant changes are observed in the relative areas of the three peaks in the histogram of E_{FRET} trajectories, as compared with those of apo–apo Hah1–MBD4 interactions (Figure 4.4B versus 4A). Both the E_1 and the E_2 peak increase in their areas relative to that of the E_0 peak, indicating an increase in the stabilities of the two interaction complexes (Figure 4.4D). At one equivalent of Cu^{1+}, the Hah1–MBD4 pairs contain a mixture of apo–apo, apo–holo, and holo–holo forms. As each of the two complexes has similar stability in apo–apo and holo–holo Hah1–MBD4 interactions, the increase in the stabilities of the two complexes here must come from the contribution of apo–holo interactions. Therefore, apo–holo interactions between Hah1 and MBD4 also form two complexes, both of which are stabilized relative to those in the apo–apo interaction.

Interestingly, in the presence of one equivalent of Cu^{1+}, the E_1/E_2 peak area ratio stays essentially the same as that in the apo–apo interactions (Figure 4.4D). This

indicates that the two complexes are stabilized to a similar extent in apo–holo interactions, as compared with those in apo–apo interactions.

4.4.3. Hah1 mutation eliminates Cu^{1+}-induced stabilization of complexes.

To probe if the observed Cu^{1+} stabilization effects on apo–holo Hah1–MBD4 interactions are specific to their Cu^{1+} binding and transfer, we created a Hah1 mutant, mHah1, in which the two cysteines in the CXXC motif have been mutated to serines. Therefore, mHah1 cannot bind Cu^{1+} or accept Cu^{1+} from MBD4. Figure 4.5A shows the histogram of E_{FRET} trajectories of single-pair mHah1–MBD4 interactions in their apo-forms. Three E_{FERT} states are observed, corresponding to the dissociated state (E_0 ~0.2) and the two interaction complexes (E_1 ~0.5 and E_2 ~0.8). The relative areas of the three E_{FRET} peaks in the histogram are the same as those of apo–apo Hah1–MBD4 interactions, indicating that the cysteines in the CXXC motif of Hah1 are nonessential for the formation and the stability of apo–apo interaction complexes.

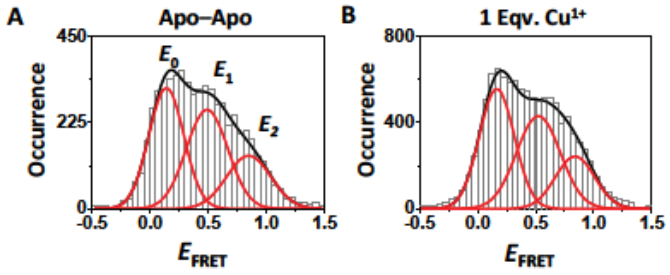

Figure 4.5. Histograms of E_{FRET} trajectories of single-pair mHah1–MBD4 interactions in the absence (A) and in the presence of one equivalent of Cu^{1+} (B). Each histogram is fitted with three Gaussian peaks, whose centers are set to the E_{FRET} values determined from the 2-dimensional E_{FRET} value analyses of the smFRET trajectories as in Figure 4.3.

In the presence of one equivalent of Cu^{1+}, MBD4 can bind Cu^{1+}, whereas mHah1 cannot. Thus, no Cu^{1+} transfer between mHah1 and MBD4 can occur. The histogram of E_{FRET} trajectories of their single-pair interactions still shows three states,

and no significant changes are observed in either the positions of the three peaks or their relative areas (Figure 4.5B). Therefore, the Cu^{1+}-binding by Hah1 and/or processes associated with Cu^{1+}-transfer between Hah1 and MBD4 are responsible for the Cu^{1+}-induced stabilization of E_1 and E_2 complexes in the apo–holo Hah1–MBD4 interactions.

4.5. Discussion

Using nanovesicle trapping combined with smFRET measurements, we have examined the dynamic interactions between single pairs of Hah1 and WDP MBD4 in the absence and the presence of Cu^{1+}. The apo–apo, apo–holo, and holo–holo interactions of Hah1 and MBD4 all lead to formation of two interaction complexes that interconvert dynamically. The stabilities of the two complexes do not change when both Hah1 and MBD4 are at their holo-forms, as compared with when both are in their apo-forms (Figure 4.4A, C). In contrast, when one protein is loaded with Cu^{1+}, i.e., in the apo–holo interactions, stabilization of both complexes is observed (Figure 4.4B). This stabilization is abolished when the Cu^{1+} binding ability (and thus the Cu^{1+} transfer ability) of Hah1 is eliminated by mutating the cysteines in its CXXC motif (Figure 4.5). Interestingly, the Cu^{1+} effects on the apo–holo Hah1–MBD4 interactions do not differentiate the two interaction complexes; both the E_1 and the E_2 complex are stabilized to a similar extent (Figure 4.4A, B).

Fundamentally, the Cu^{1+}-induced stabilization of protein complexes can be approximately divided into two types: one direct contribution, where the Cu^{1+} can bridge the two proteins at the interface via bonding with cysteines from both proteins; the other indirect contribution, where the Cu^{1+} binding to a protein causes changes in the protein's conformation, leading to better complex formation. The direct contribution is possible for apo–holo Hah1–MBD4 interactions, in which one Cu^{1+} is

coordinated by cysteine ligands from both interacting partners, as described in the thiol ligand exchange mechanism for copper chaperone mediated copper transfer.[5, 19, 43] This metal-bridging was directly supported by the crystal structure of a Cu^{1+}-bridged Hah1 dimer[20] and the NMR structure of a Cu^{1+}-bridged complex between Hah1 and a MBD of MNK protein (Figure 4.6),[50] as well as by computational studies.[51] This Cu^{1+} bridging is not applicable for holo–holo interactions, though, as both proteins here would have Cu^{1+} bound at their CXXC sites; consistently, no stabilization of protein complexes is observed in holo–holo Hah1–MBD4 interactions (Figure 4.4C).

The indirect contribution is likely not to play a significant role in stabilizing either Hah1–MBD4 complex. This comes from the results on holo–holo Hah1–MBD4 interactions, where only the indirect contribution is possible, but for which no stabilization of any protein complexes is observed (Figure 4.4C versus A).

Using the NMR structure of the Cu^{1+}-bridged Hah1–MBD complex (Figure 4.6)[50] and knowing that our Cy3–Cy5 pairs are located at the C-termini, the estimated Cy3–Cy5 distance in this complex is ~5 nm. Using an E_{FRET} versus distance calibration curve (unpublished results), this distance corresponds to an E_{FRET} of ~0.5, similar to E_1. Therefore, the E_1 complex between Hah1 and MBD4 could be associated with the interaction geometry shown by this NMR structure. In the E_2 complex, the Hah1 and MBD4 need to interact in a way that the distance between their C-termini is closer than that in the structure in Figure 4.6 to have a larger E_{FRET} value (~0.8). At the moment, we do not know the structural identity of the E_2 complex. SmFRET measurements only report structural differences along the coordinate of the donor–acceptor interdistance. Future smFRET studies, where Cy3–Cy5 are tagged at various locations on Hah1 and MBD4 to probe the structure of their complexes along multiple coordinates, may provide more information.

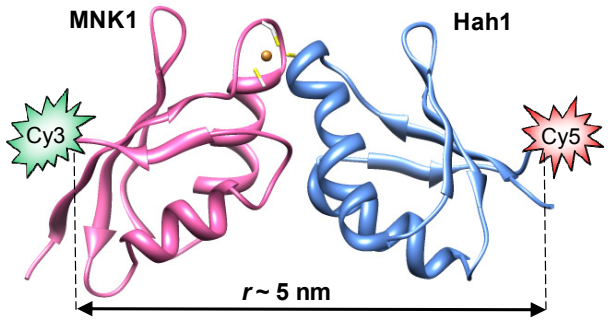

Figure 4.6. NMR structure (pdb code: 2K1R)[50] of a Cu^{1+}-bridged complex between Hah1 and the first MBD of MNK. The positions corresponding to where the Cy3 and Cy5 are labeled are indicated; the anchor-to-anchor distance between the two labels is ~5 nm.

4.6. Conclusion

Using a nanovesicle trapping scheme in combination with smFRET measurements, we have studied the weak, dynamic interactions between the copper chaperone Hah1 and the MBD4 of WDP in the absence and the presence of various equivalents of Cu^{1+}. We have visualized their interaction events in real time and identified their interaction complexes. Regardless of their metallation state, Hah1 and MBD4 can form two complexes that interconvert dynamically, an advantageous feature for their Cu^{1+}-transfer function. Within the limit of smFRET in resolving structural differences along the coordinate of the FRET donor-to-acceptor interdistance, the interaction geometries in these two complexes appear invariable. The stabilities of the two interaction complexes are dependent on the proteins' metallation state, though. When only one of the proteins has Cu^{1+} bound (i.e., apo–holo Hah1–MBD4 interactions), both complexes are stabilized relative to that observed in the apo–apo interactions. Cu^{1+}-bridging at the protein interface via

bonding to cysteines from both proteins is likely the cause of this stabilization. Consistently, this Cu^{1+}-induced stabilization of interaction complexes is undiscernible when the Cu^{1+}-binding cysteines in Hah1 are mutated to serines to eliminate its Cu^{1+} binding ability or when both proteins have Cu^{1+} bound (i.e., holo–holo Hah1–MBD4 interactions). Based on its E_{FRET} value, one of the complexes can be associated with a Hah1–MBD4 interaction complex where the CXXC motifs from the two proteins face each other to offer cysteine binding to a bridging Cu^{1+} ion. The structure of the other complex is not yet clear. These Cu^{1+}-induced effects on the Hah1–MBD4 interactions provide a step toward understanding how the dynamic protein interactions of copper chaperones are coupled with their metal transfer function.

4.7. Acknowledgements

Thanks are due to our collaborators Professors David L. Huffman from Western Michigan University, Liliya A. Yatsunyk from Swarthmore College and Amy C. Rosenzweig from Northwestern University. David L. Huffman's group provided the MBD4 expression plasmid and Liliya A. Yatsunyk provided the Hah1 expression plasmid during her postdoctoral work at Amy C. Rosenzweig's group. Thanks are also due to Feng Gao, from the Cornell University, for assistance in data processing using Igor programming. Thanks to Debashis Panda, from Cornell University, for sharing the results of dynamic light scatting measurements of nanovesicle size distributions. Aaron Keller contributed to the present work by assisting in mutagenesis experiments as well as assisting in protein purification and labeling of Hah1. We thank the National Institute of Health (GM082939), National Science Foundation (CHE0645392), Camille and Henry Dreyfus New Faculty Award, and Alfred F. Sloan Research Fellowship for funding our research. J.J.B. and A.M.K. were partially supported by National Institute of Health Molecular Biophysics Traineeships.

REFERENCES

1.Lippard, S. J.; Berg, J. M., *Principles of Bioinorganic Chemistry*. University Science Books: Mill Valley, 1994.

2.Waldron, K. J.; Rutherford, J. C.; Ford, D.; Robinson, N. J., Metalloproteins and Metal Sensing. *Nature* **2009,** *460*, 823-830.

3.Andrews, S. C.; Robinson, A. K.; Rodriguez-Quinones, F., Bacterial Iron Homeostasis. *FEMS Microbiol. Rev.* **2003,** *27*, 215-237.

4.Finney, L. A.; O'Halloran, T. V., Transition Metal Speciation in the Cell: Insights from the Chemistry of Metal Ion Receptors. *Science* **2003,** *300*, 931-936.

5.O'Halloran, T. V.; Culotta, V. C., Metallochaperones, An Intracellular Shuttle Service for Metal Ions. *J. Biol. Chem.* **2000,** *275*, 25057-25060.

6.Rosenzweig, A. C., Copper Delivery by Metallochaperone Proteins. *Acc. Chem. Res.* **2001,** *34*, 119-128.

7.Donnelly, P. S.; Xiao, Z.; Wedd, A. G., Copper and Alzheimer's disease. *Curr. Opin. Chem. Biol.* **2007,** *11*, 128-133.

8.Robinson, N. J.; Winge, D. R., Copper Metallochaperones. *Ann. Rev. Biochem.* **2010,** *79*, in press.

9.Huffman, D. L.; O'Halloran, T. V., Function, Structure, and Mechanism of Intracellular Copper Trafficking Proteins. *Ann. Rev. Biochem.* **2001,** *70*, 677-701.

10.Banci, L.; Rosato, A., Structural genomics of proteins involved in copper homeostasis. *Acc. Chem. Res.* **2003,** *36*, 215-221.

11.Bull, P. C.; Thomas, G. R.; Rommens, J. M.; Forbes, J. R.; Cox, D. W., The Wilson Disease Gene Is A Putative Copper Transporting ATPase Similar to the Menkes Gene. *Nature Genet.* **1993,** *5*, 327-337.

12.Hamza, I.; Schaefer, M.; Klomp, L. W. J.; Gitlin, J. D., Interaction of the Copper Chaperone Hah1 with the Wilson Disease Protein Is Essential for Copper Homeostasis. *Proc. Natl. Acad. Sci. U.S.A.* **1999,** *96*, 13363-13368.

13.Larin, D.; Mekios, C.; Das, K.; Ross, B.; Yang, A.-S.; Gilliam, T. C., Characterization of the Interaction between the Wilson and Menkes Disease Proteins and the Cytoplasmic Copper Chaperone, Hah1p. *J. Biol. Chem.* **1999,** *274*, 28497-28504.

14.Walker, J. M.; Tsivkovskii, R.; Lutsenko, S., Metallochaperone Atox1 Transfers Copper to the NH2-Terminal Domain of the Wilson's Disease Protein and Regulates Its Catalytic Activity. *J. Biol. Chem.* **2002,** *277*, 27953-27959.

15.Banci, L.; Bertini, I.; Cantini, F.; Massagni, C.; Migliardi, M.; Rosato, A., An NMR Study of the Interaction of N-terminal Cytoplasmic Tail of the Wilson Disease Protein with Copper(I)-Hah1. *J. Biol. Chem.* **2009,** *284*, 9354-9360.

16.Lutsenko, S.; Petrukhin, K.; Cooper, M. J.; Gilliam, T. C.; Kaplan, J. H., N-terminal Domains of Human Copper-transporting Adenosine Triphosphatases (the Wilson's and Menkes Disease Proteins) Bind Copper Selectively in vivo and in vitro with Stoichiometry of One Copper per Metal-Binding Repeat. *J. Biol. Chem.* **1997,** *272*, 18939-18944.

17.Banci, L.; Bertini, I.; Cantini, F.; Della-Malva, N.; Migliardi, M.; Rosato, A., The Different Intermolecular Interactions of the Soluble Copper-Binding Domains of the Menkes Protein, ATP7A. *J. Biol. Chem.* **2007,** *282*, 23140-23146.

18.Yamaguchi, Y.; Heiny, M. E.; Suzuki, M.; Gitlin, J. D., *Proc. Natl. Acad. Sci. U.S.A.* **1996,** *93*, 14030-14035.

19.Pufahl, R. A.; Singer, C. P.; Peariso, K. L.; Lin, S.-J.; Schmidt, P. J.; Fahrni, C. J.; Culotta, V. C.; Penner-Hahn, J. E.; O'Halloran, T. V., Metal Ion Chaperone Function of the Soluble Cu(I) Receptor Atx1. *Science* **1997,** *278*, 853-856.

20.Wernimont, A. K.; Huffman, D. L.; Lamb, A. L.; O'Halloran, T. V.; Rosenzweig, A. C., Structural Basis for Copper Transfer by the Metallochaperone for the Menkes/Wilson Disease Proteins. *Nat. Struct. Biol.* **2000,** *7*, 766-771.

21.Arnesano, F.; Banci, L.; Bertini, I.; Bonvin, M. J. J., A Docking Approach to the Study of Copper Trafficking Proteins: Interactions between Metallochaperones and Soluble Domains of Copper ATPases. *Structure* **2004,** *12*, 669-676.

22.Banci, L.; Bertini, I.; Cantini, F.; Chasapis, C. T.; Hadjiliadis, N.; Rosato, A., A NMR Study of the Interactions of a Three-Domain Construct of ATP7A with Copper(I) and Copper(I)-Hah1: The Interplay of Domains. *J. Biol. Chem.* **2005,** *280*, 38259-38263.

23.Achila, D.; Banci, L.; Bertini, I.; Bunce, J.; Ciofi-Baffoni, S.; Huffman, D. L., Structure of human Wilson protein domains 5 and 6 and their interplay with domain 4 and the copper chaperone HAH1 in copper uptake. *Proc. Natl. Acad. Sci. U.S.A.* **2006,** *103*, 5729-5734.

24.Huster, D.; Lutsenko, S., The Distinct Roles of the N-Terminal Copper-Binding Sites in Regulation of Catalytic Activity of the Wilson's Disease Protein. *J. Biol. Chem.* **2003,** *278*, 32212-32218.

25.Lutsenko, S.; LeShane, E. S.; Shinde, U., Biochemical Basis of Regulation of Human Copper-Transporting ATPase. *Arch. Biochem. Biophys.* **2007,** *463*, 134-148.

26.Walker, J. M.; Huster, D.; Ralle, M.; Morgan, C. T.; Blackburn, N. J.; Lutsenko, S., The N-Terminal Metal-Binding Site 2 of the Wilson's Disease Protein Play a Key Role in the Transfer of Copper from Atox1. *J. Biol. Chem.* **2004,** *279*, 15376-15384.

27.Yatsunyk, L. A.; Rosenzweig, A. C., Copper(I) Binding and Transfer by the N-terminus of the Wilson Disease Protein. *J. Biol. Chem.* **2007,** *282*, 8622-8631.

28.van Dongen, E. M. W. M.; Klomp, L. W. J.; Merkx, M., Copper-Dependent Protein-Protein Interactions Studied by Yeast Two-Hybrid Analysis. *Biochem. Biophys. Res. Commun.* **2004,** *323*, 789-795.

29.Hung, I. H.; Casareno, R. L. B.; Gilles, L.; Mathews, F. S.; Gitlin, J. D., Hah1 Is A Copper-Binding Protein with Distinct Amino acid Residues Mediating Copper Homeostasis and Antioxidant Defense. *J. Biol. Chem.* **1998,** *273*, 1749-1754.

30.Strausak, D.; Howies, M. K.; Firth, S. D.; Schlicksupp, A.; Pipkorn, R.; Multhaup, G.; Mercer, J. F. B., Kinetic Analysis of the Interaction of the Copper Chaperone Atox1 with the Metal Binding Sites of the Menkes Protein. *J. Biol. Chem.* **2003,** *278*, 20821-20827.

31.Strausak, D.; Fontaine, S. L.; Hill, J.; Firth, S. D.; Lockhart, P. J.; Mercer, J. F. B., The Role of GMXCXXC Metal Binding Sites in the Copper-induced Redistribution of the Menkes Protein. *J. Biol. Chem.* **1999,** *274*, 11170-11177.

32.Voskoboinik, I.; Strausak, D.; Greenough, M.; Brooks, H.; Petris, M.; Smith, S.; Mercer, J. F.; Camakaris, J., Functional Analysis of the N-terminal CXXC Metal-binding Motifs in the Human Menkes Copper-transporting P-type ATPase Expressed in Cultured Mammalian Cells. *J. Biol. Chem.* **1999,** *274*, 22008-22012.

33.Huffman, D. L.; O'Halloran, T. V., Energetics of Copper Trafficking between the Atx1 Metallochaperone and the Intracellular Copper Transporter Ccc2. *J. Biol. Chem.* **2000,** *275*, 18611-18614.

34.Banci, L.; Bertini, I.; Del Conte, R.; D'Onofrio, M.; Rosato, A., Solution Structure and backbone Dynamics of the Cu(I) and Apo Forms of the Second Metal-Binding Domain of the Menkes Protein ATP7A. *Biochemistry* **2004,** *43*, 3396-3403.

35.Banci, L.; Bertini, I.; Cantini, F.; Migliardi, M.; Rosato, A.; Wang, S., An Atomic-level Investigation of the Disease-causing A629P Mutant of the Menkes Protein, ATP7A. *J. Mol. Biol.* **2005,** *352*, 409-417.

36.Chen, P.; Andoy, N. M.; Benitez, J. J.; Keller, A. M.; Panda, D.; Gao, F., Tackling Metal Regulation and Transport at the Single-Molecule Level. *Nat. Prod. Rep.* **2010**, DOI:10.1039/B906691H.

37.Benitez, J. J.; Keller, A. M.; Ochieng, P.; Yatsunyk, L. A.; Huffman, D. L.; Rosenzweig, A. C.; Chen, P., Probing Real-time Transient Metallochaperone-Target Protein Interactions at the Single-Molecule Level with Nanovesicle Trapping. *J. Am. Chem. Soc.* **2008,** *130*, 2446-2447.

38.Benitez, J. J.; Keller, A. M.; Ochieng, P.; Yatsunyk, L. A.; Huffman, D. L.; Rosenzweig, A. C.; Chen, P., Correction/Addition: Probing Real-time Transient Metallochaperone-Target Protein Interactions at the Single-Molecule Level with Nanovesicle Trapping. *J. Am. Chem. Soc.* **2009,** *131*, 871.

39.Benitez, J. J.; Keller, A. M.; Chen, P., Nanovesicle Trapping for Studying Weak Protein Interactions by Single-Molecule FRET. *Meth. Enzymol.* **2010**, in press.

40.Chiu, D. T.; Wilson, C. F.; Karlsson, A.; Danielsson, A.; Lundqvist, A.; Strömberg, A.; Ryttsén, F.; Davidson, M.; Nordholm, S.; Orwar, O.; Zare, R. N., Manipulating the biochemical nanoenvironment around single molecules contained within vesicles. *Chem. Phys.* **1999,** *247*, 133-139.

41.Boukobza, E.; Sonnenfeld, A.; Haran, G., Immobilization in Surface-Tethered Lipid Vesicles as a New Tool for Single Biomolecule Spectroscopy. *J. Phys. Chem. B.* **2001,** *105*, 12165-12170.

42.Okumus, B.; Wilson, T. J.; Lilley, D. M. J.; Ha, T., Vesicle Encapsulation Studies Reveal that Single Molecule Ribozyme Heterogeneities Are Intrinsic. *Biophys. J.* **2004,** *87*, 2798-2806.

43.Boal, A. K.; Rosenzweig, A. C., Structural Biology of Copper Trafficking. *Chem. Rev.* **2009,** *109*, 4760–4779.

44.Benitez, J. J.; Keller, A. M.; Chen, P., Nanovesicle Trapping for Studying Weak Protein Interactions by Single-Molecule FRET. *Meth. Enzymol.* **2009**, accepted.

45.Brenner, A. J.; Harris, E. D., A quantitative test for copper using bicinchoninic acid. *Anal. Biochem.* **1995,** *226*, 80-84.

46.Cremer, P. S.; Boxer, S. G., Formation and spreading of lipid bilayers on planar glass supports. *J. Phys. Chem. B* **1999,** *103*, 2554-2559.

47.Sarkar, S. K.; Andoy, N. M.; Benitez, J. J.; Chen, P. R.; Kong, J. S.; He, C.; Chen, P., Engineered Holliday Junctions as Single-Molecule Reporters for Protein-DNA Interactions with Application to a MerR-Family Regulator. *J. Am. Chem. Soc.* **2007,** *129*, 12461-12467.

48.Ha, T., Single-Molecule Fluorescence Resonance Energy Transfer. *Methods* **2001,** *25*, 78-86.

49.Rasnik, I.; McKinney, S. A.; Ha, T., Nonblinking and Long-lasting Single Molecule Fluorescence Imaging. *Nature Methods* **2006,** *3*, 891-893.

50.Banci, L.; Bertini, I.; Calderone, V.; Della-Malva, N.; Felli, I. C.; Neri, S.; Pavelkova, A.; Rosato, A., Copper(I)-mediated protein-protein interactions result from suboptimal interaction surfaces. *Biochem. J.* **2009,** *422*, 37-42.

51.Rodriguez-Granillo, A.; Crespo, A.; Estrin, D. A.; Wittung-Stafshede, P., Copper-Transfer Mechanism from the Human Chaperone Atox1 to a Metal-Binding Domain of Wilson Disease Protein. *J. Phys. Chem. B* **2010,** *114*, 3698–3706.

CHAPTER 5

Concluding Remarks

5.1. Research summary

In this thesis, the interaction dynamics between the copper chaperone Hah1 and a single metal binding domain (MBD4) of the Wilson disease protein were studied at the single-molecule level using single-molecule fluorescence resonance energy transfer (smFRET). Since these interactions are relatively weak ($K_D \sim 10^{-6}$ M), they represent a challenge to study with single-molecule fluorescence techniques. The challenge resides in the requirement to have low fluorophore concentrations for spatial separation of individual molecules, thereby permitting single molecule optical detection. For a weakly interacting protein pair, concentrations must be high enough to allow for facile detection of the interaction complex. To overcome this challenge a nanovesicle trapping strategy was adapted to confine individual protein pairs to a reduced volume, effectively increasing their concentration. Furthermore, the overall number of vesicles can be kept low enough to allow for single-pair optical detection. Nanovesicle trapping has indeed resulted in a viable strategy to study relatively weak protein interactions and flexible enough to allow for different concentration regimes as well as experimental conditions by changing either the vesicle size or the lipid composition. In chapter 2, the details for the nanovesicle trapping approach and the single-molecule kinetic analysis of bimolecular interactions involving three states were presented. Both the experimental approach and the theoretical analysis are generally applicable for studying many other biological processes at the single-molecule level.

Using nanovesicle trapping, the interaction dynamics of Hah1 and MBD4 were characterized first in the absence of Cu^+. These two proteins can bind to each other in two distinct geometries which can interconvert dynamically. From the analysis of dwell-time distributions and the E_{FRET} histogram, the interaction kinetics and thermodynamics were quantified. Functionally, the presence of two interaction

geometries increases the probability of complex formation when the two proteins encounter in the cell by diffusion. Also, having two interaction geometries suggests that either Hah1 or MBD4 might interact with multiple domains simultaneously. The study exemplifies the ability of nanovesicle trapping in combination with smFRET for studying weak protein interactions and provides insight into how Hah1 and WDP may collaborate to mediate Cu^{+} transfer inside cells. This study represents the first evidence that Hah1 and MBD4 can interact in the absence of Cu^{+} and that they do so in two different interaction geometries.

To determine the Cu^{+}-dependent interaction dynamics of Hah1 and MBD4, a set of experiments with different equivalents of Cu^{+} in the solution were performed. Regardless of the proteins' metallation state, we observe multiple, interconverting interaction complexes between Hah1 and MBD4. Within our experimental limit, the overall interaction geometries of these complexes appear invariable, but their stabilities are dependent on the proteins' metallation state. In apo–holo Hah1–MBD4 interactions, the complexes are stabilized relative to that observed in the apo–apo interactions. This stabilization is undiscernible when Hah1's Cu^{+}-binding is eliminated or when both proteins have Cu^{+} loaded. The results suggest that apo-holo interactions are stabilized due to metal bridging, presumably during Cu^{+} transfer. The observation that both interaction geometries are stabilized also suggests that both might be productive Cu^{+} transfer complexes. The structural identity of the E_1 interaction geometry can be correlated to available structures of Hah1-MBD heterocomplexes. Yet, the identity of the second interaction geometry, E_2, is unclear at the moment. Nevertheless, these Cu^{1+}-induced effects on the Hah1–MBD4 interactions provide a step toward understanding how the dynamic protein interactions of copper chaperones are coupled with their metal transfer function.

5.2. Further research

Further analyses and experiments are necessary in order to scrutinize the Cu^+ transfer process and dynamic behaviors of Hah1 and MBD4. To extract more detailed information on the apo-holo interaction processes, we need to extract the relevant information from the experiments in the presence of 1 equivalent Cu^+, in which a mixture of apo–apo, apo–holo, and holo–holo interactions exist. We can also label Hah1 or MBD4 at alternative sites to probe the geometries of the interaction complexes. Furthermore, to assess the copper transfer process we can design different protein mutants that can mimic the 3-coordinate copper transfer intermediate. Finally, once the copper dependent behavior is better understood we can probe the metal-dependent behavior by performing experiments in the presence of different metals.

5.2.1. The 1 eqv. Cu^+ mixture problem

In chapter 4 we explain that experiments in the presence of one equivalent of Cu^+ actually represent a mixture of conditions upon trapping in a nanovesicle. Some vesicles will contain a pair of apo proteins, some will have a pair of holo proteins and still some will contain an apo-holo combination. The fraction of vesicles containing any combination of proteins will depend on the concentrations of each species in solution, assuming equal entrapment probability. As an initial approximation, we can assume that in the solution there is only one chemical equilibrium:

$$\textbf{Hah1-Cu + MBD4} \underset{}{\overset{\mathbf{K_{Exchange}}}{\rightleftharpoons}} \textbf{Hah1 + MBD4-Cu}$$

where there are only four different protein species: Hah1-Cu, Hah1, MBD4-Cu, and MBD4. Using the equilibrium constant for copper exchange ($K_{Exchange}$) and the total protein and copper concentrations, the individual concentrations of each protein

species can be readily calculated. Using the individual concentrations we can calculate the probability of finding any particular protein species in solution. It then follows that the joint probability of obtaining any protein pair is easily calculated (Figure 5.1). For this approximation we assume equal entrapment probability and that all copper is bound to protein. Due to the high copper binding affinity of Hah1 and MBD4 ($K_{Cu} \sim 10^{-10}$ M) assuming that all the copper is protein-bound is not unreasonable.

Once the contribution of each type of trapped protein pair is determined, the pure apo-holo contribution can be extracted. For either E_{FRET} or dwell-time distribution, the data represents a weighted linear combination of each contribution (i.e. apo-apo, apo-holo, and holo-holo). This strategy only works if we know the behavior for pure apo-apo and holo-holo interactions.

Upon further inspection of this type of analysis we can formulate many additional processes occurring in solution that will affect the concentrations for each one of the proteins. We can include Hah1 dimerisation[1] and MBD4 dimerisation, both in the presence and absence of Cu^{+} (i.e. apo-apo, holo-holo and apo-holo homo-dimers). We should also take into consideration the different hetero-complexes that can form in solution and be trapped as a single body, such as Hah1-MBD4 complexes of the three types: apo-apo, apo-holo and holo-holo.

These considerations complicate the analytical expressions for determining the probability of finding any specific protein pair, and some of the equilibrium constants, such as those for dimer formation, are not yet known. Therefore, further experiments are necessary to determine these constants. Also further analysis is necessary to determine to what extent the additional parameters affect the final determination of the probability of finding any particular protein pair in the nanovesicle.

Once we can resolve the apo-holo contributions in the 1 equivalent Cu^{+} condition, we can analyze in more detail the contributions from Cu^{+} transfer and extract detailed kinetic information regarding the Cu^{+} transfer process itself.

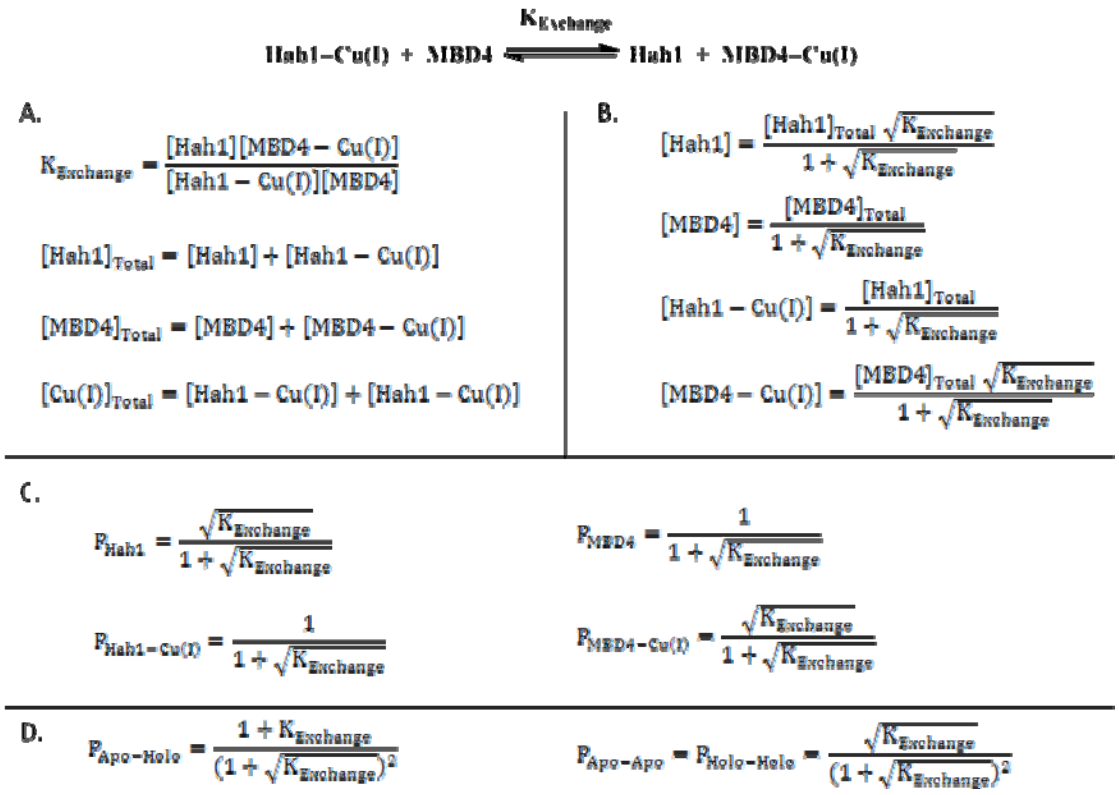

Figure 5.1. Trapping probability equations for simplest scheme. A. Initial set of equations. B. Individual protein concentrations in solution prior to trapping. C. Probability of finding each protein species. D. Joint probabilities for apo-apo, apo-holo and holo-holo. In this model we assume all Cu^{+} to be protein-bound.

5.2.2. Alternative labeling schemes

To investigate the structural identity of the E_2 complex we propose in chapter 4 that alternative labeling schemes could be used in combination with the available structural data from the literature to map out the interaction geometries. At the moment all experiments were done with the fluorescent label at the C-termini. An alternative labeling position could be closer to the metal binding motif of either

protein thus making the E_1 state a higher E_{FRET} state and see how E_2 is affected (Figure 5.3). In this fashion we can map out the different interaction geometries by systematically changing either protein's labeling position.

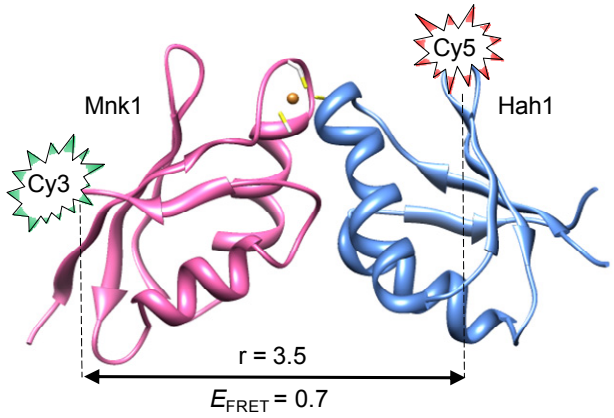

Figure 5.3. NMR structure (pdb code: 2K1R)[2] of a Cu^{1+}-bridged complex between Hah1 and the first MBD of MNK. The positions corresponding to where the Cy3 and Cy5 may be labeled are indicated; the anchor-to-anchor distance between the two labels would be ~3.5 nm. The expected E_{FRET} is approximately 0.7.

5.2.3. Assessing the 3-coordinate Cu^+ *transfer intermediate*

O'Halloran and others[3-7] have proposed that Cu^+ transfer between Hah1 and the MBDs of WDP occurs via a thiol exchange mechanism through a 3-coordinate Cu^+ intermediate (Figure 5.2).

In order to probe this interaction intermediate, a mutant of Hah1 will be prepared in which one of the metal binding cysteine residues is mutated to alanine, specifically Cys15. From the two cysteine residues that coordinate copper in Hah1, cysteine 12 is the most solvent exposed and is proposed to be the first cysteine residue to bind copper during the transfer process.[2, 5, 7]

This type of experiment provides two major advantages. First, all interactions observed will most likely be apo-holo interactions, as the binding affinity for copper is very high ($K_{Cu} \sim 10^{-10}$ M) and only one protein can bind Cu^+, thereby eliminating the

mixture problem in the 1 equivalent Cu^+ experiment. Second, we will be able to probe this initial 3-coordinate interaction intermediate involved in the Cu^+ transfer process.

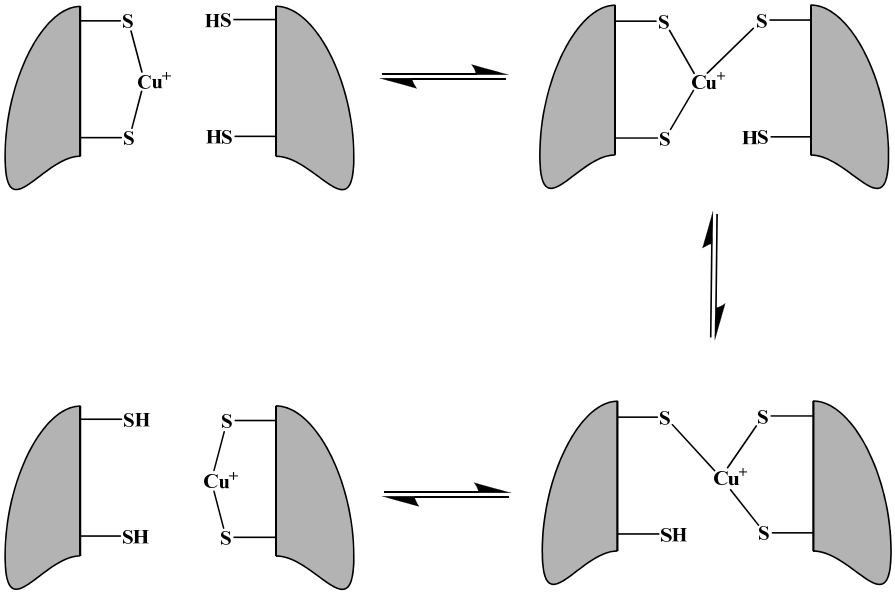

Figure 5.2. The ligand exchange mechanism of Cu^+ transfer through a 3-coordinate intermediate between Hah1 and a MBD domain of WDP.

5.2.4. Metal dependence of interactions

Up to now we have probed interactions in the presence of varying equivalents of Cu^+, which is the biologically relevant metal. Other studies suggest that the interactions and metal transfer between Hah1 and the MBDs of WDP, although functionally geared for Cu^+, can also occur in the presence of Hg^{2+}.[8] Up to now, various structures have been solved for Hah1 and the MBDs in the presence of different transition metals such as Cu^+, Cd^{2+}, and Hg^{2+}.[3] Next we can perform experiments in the presence of different metal ions to probe the metal-dependent behavior of Hah1 and MBD4 interactions. We have performed preliminary experiments in the presence of 1 equivalent Hg^{2+}. The results are similar to those observed in the presence of Cu^+ (Figure 5.4). Hg^{2+} dependent experiments are necessary to fully assess the effect of Hg^{2+} on the interaction dynamics.

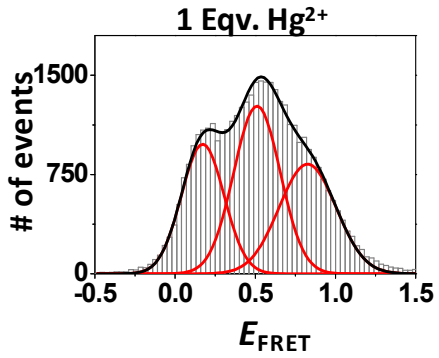

Figure 5.4. E_{FRET} histogram of Hah1–MBD4 interactions in the presence of 1 equivalent of Hg^{2+} (250 molecules).

5.3. Research outlook

The single domain study represents the simplest system available to scrutinize the interactions between the copper chaperone Hah1 and the MBDs of WDP. It provides the fundamental interaction dynamics applicable to either Hah1-MBD or MBD-MBD interactions. We can probe the fundamental interaction dynamics, Cu^{+} transfer intermediates, and metal dependence of interactions. This system represents a stepping stone to increase system complexity. It is essential to fully scrutinize this system in order to better understand the more complex interaction dynamics of a multi-domain system, such as Hah1's interactions with the full 6-domain construct of the metal binding domains of WDP, or even MBD-MBD interactions within WDP.

Overall, we have contributed to a better understanding of the fundamental interaction dynamics of Hah1 and MBD4 in the presence and absence of Cu^{+} as well as provided structural insight on the interaction process for metal transfer. It is clear that there are still many studies that can be performed with this system, ensuring long lasting continuation of the project.

REFERENCES

1.Tanchou, V.; Gas, F.; Urvoas, A.; Cougouluègne, F.; Ruat, S.; Averseng, O.; Quéméneur, E., Copper-mediated homo-dimerisation for the HAH1 metallochaperone. *Biochemical and Biophysical Research Communications* **2004,** *325*, 388-394.

2.Banci, L.; Bertini, I.; Calderone, V.; Della-Malva, N.; Felli, I. C.; Neri, S.; Pavelkova, A.; Rosato, A., Copper(I)-mediated protein-protein interactions result from suboptimal interaction surfaces. *Biochem. J.* **2009,** *422*, 37-42.

3.Boal, A. K.; Rosenzweig, A. C., Structural Biology of Copper Trafficking. *Chem. Rev.* **2009,** *109*, 4760–4779.

4.Pufahl, R. A.; Singer, C. P.; Peariso, K. L.; Lin, S.-J.; Schmidt, P. J.; Fahrni, C. J.; Culotta, V. C.; Penner-Hahn, J. E.; O'Halloran, T. V., Metal Ion Chaperone Function of the Soluble Cu(I) Receptor Atx1. *Science* **1997,** *278*, 853-856.

5.Wernimont, A. K.; Huffman, D. L.; Lamb, A. L.; O'Halloran, T. V.; Rosenzweig, A. C., Structural Basis for Copper Transfer by the Metallochaperone for the Menkes/Wilson Disease Proteins. *Nat. Struct. Biol.* **2000,** *7*, 766-771.

6.Wernimont, A. K.; Yatsunyk, L. A.; Rosenzweig, A. C., Binding of Copper(I) by the Wilson Disease Protein and Its Copper Chaperone. *J. Biol. Chem.* **2004,** *279*, 12269-12276.

7.Rodriguez-Granillo, A.; Crespo, A.; Estrin, D. A.; Wittung-Stafshede, P., Copper-Transfer Mechanism from the Human Chaperone Atox1 to a Metal-Binding Domain of Wilson Disease Protein. *J. Phys. Chem. B.* **2010,** *114*, 3698-3706.

8.Larin, D.; Mekios, C.; Das, K.; Ross, B.; Yang, A.-S.; Gilliam, T. C., Characterization of the Interaction between the Wilson and Menkes Disease Proteins and the Cytoplasmic Copper Chaperone, Hah1p. *J. Biol. Chem.* **1999,** *274*, 28497-28504.